QA:NA

Civilian Radioactive Waste Management System
Management and Operating Contractor

Evaluation of flow and transport models of Yucca Mountain, based on chlorine-36 and chloride studies for FY98

Revision 00

BA0000000-01717-5700-00007

September 15, 1998

Prepared for:

U.S. Department of Energy
Yucca Mountain Site Characterization Office
P.O. Box 30307
North Las Vegas, Nevada 89036-0307

Prepared by:

TRW Environmental Safety Systems Inc.
1261 Town Center Drive
Las Vegas, NV 89134

Authors:
J.T. Fabryka-Martin, A.V. Wolfsberg, S.S. Levy, K. Campbell,
P. Tseng, J.L. Roach, L.E. Wolfsberg
Los Alamos National Laboratory, Los Alamos NM 87545

Civilian Radioactive Waste Management System
Management and Operating Contractor

Evaluation of flow and transport models of Yucca Mountain, based on chlorine-36 and chloride studies for FY98

Revision 00

BA0000000-01717-5700-00007

September 15, 1998

Prepared by: Thomas J. Hirons for J. T. Fabryka-Martin, LANL — Date: 9-15-98

Check Review by: Thomas J. Hirons for C. Harrington, LANL — Date: 9-15-98

Reviewed by: R E Smith for W. B. Scott, Technical Lead for UZ Hydrology & Climate — Date: 9-15-98

Approved by: R E Smith R. E. Smith, Ambient Testing & Regulatory Support Office Manager — Date: 9-15-98

Approved by: Andrew L. Leigh for LRH L. R. Hayes, Natural Environment Program Operations Manager — Date: 9/15/98

PREFACE

This report has been prepared as part of the Yucca Mountain Site Characterization Program Level 3 Milestone SP32D5M3.

Data acquired as part of this activity and presented in this report were developed under Yucca Mountain Project (YMP) quality assurance (QA) procedures; their Q status and traceability to Data Tracking Numbers (DTN) are indicated in Appendix B.

TABLE OF CONTENTS

LIST OF FIGURES

LIST OF TABLES

ABSTRACT

The objective of the Water Movement Test activity is to acquire geochemical and isotopic data relevant to the development and test of conceptual and numerical flow and transport models of the unsaturated zone at Yucca Mountain. This report updates the Yucca Mountain data base for porewater Cl concentrations and $^{36}Cl/Cl$. The expanded data base of porewater Cl concentrations is consistent with data collected earlier, particularly in verifying a trend of higher concentrations in the South Ramp samples than in the samples from the North Ramp and Main Drift of the ESF. These differences translate into infiltration rates that are lower in the southern ESF. Geochemistry and $^{36}Cl/Cl$ data are presented for 22 samples from local and regional wells and for regional springs. All of the groundwater samples from the Yucca Mountain area have $^{36}Cl/Cl$ ratios close to present-day meteoric background, suggesting ages less than 10,000 years.

The compositions of extracted porewaters and salts were evaluated for evidence of contamination by LiBr-tagged construction water. The Br/Cl ratios of salts in samples from holes that were angle-drilled into the floor of the ESF provide evidence of construction-water migration only 2 m downward within the relatively high-porosity, unfractured Tptpul unit. Penetration of construction water to the 3-m total depth of a hole was detected with the more highly fractured Tptpmn unit.

New $^{36}Cl/Cl$ analyses of samples from the ESF South Ramp confirm that the southern part of the ESF has lower $^{36}Cl/Cl$ values than the northern part. None of the samples from beyond Station 45+00 have ratios above the bomb-pulse threshold value of 1250×10^{-15}. Bomb-pulse levels of ^{36}Cl were detected in samples from Niche 3566 and from the Sundance and Ghost Dance faults in Alcove 6.

Chlorine-36 was analyzed in surface soils and surface runoff at Yucca Mountain to test whether bomb-pulse ^{36}Cl still resides at the surface and to characterize the isotopic composition of waters infiltrating into the bedrock at present. The data confirm that water entering the bedrock today will still contain bomb-pulse ^{36}Cl and that bomb-pulse ^{36}Cl has not yet been completely removed from the soil profile.

A statistical analysis framework was developed to quantitatively assess 2) whether measured $^{36}Cl/Cl$ ratios include the presence of bomb-pulse ^{36}Cl, b) the correlation between bomb-pulse observations and geologic- and hydrologic-system attributes (covariates), and c) the spatially varying trend of the background $^{36}Cl/Cl$ ratio distribution. The two background distributions correlate well with the thinning of the PTn from north to south and support the hypothesis that background $^{36}Cl/Cl$ ratio should be higher where the PTn is thicker due to travel times that exceed 10,000 years. One of the key capabilities associated with this statistical approach is a method for assigning the probability that each observation contains a bomb-pulse component. Analysis of the correlation between the system attributes (covariates) and the probability that a sample contains bomb-pulse improves the interpretative power of the data analysis. Bomb-pulse measurements correlate well with TS w samples from intersecting joints and PTn samples at

stratigraphic contacts.

Predictive numerical simulations of ^{36}Cl and chloride migration from the ground surface to the ESF and the East-West Cross Drift (EWCD) were performed using the YMP Performance Assessment radionuclide transport model. The numerical simulations were compared to measured values and to predictions based on conceptual models of infiltration, percolation, and isotopic variations over time. The model simulations of chloride concentrations n the ESF North Ramp and Main Drift porewaters are in general accord with the measured values whereas the simulated concentrations in the South Ramp are well below the measured values. This indicates that the estimated infiltration rates used in the flow model for the vicinity of the South Ramp may require reassessment.

The simulations in this report focus on the site-scale transport of ^{36}Cl away from faults. Based on the conceptual model and its support from the statistical analysis, the modeling serves to test whether the integrated site-scale model is consistent with the data interpretation. The integrated site-scale model includes the surface infiltration model which feeds the site-scale flow model which, in turn, feeds the site-scale transport mode. In this analysis, travel times from the surface to the ESF stations is used for the interpretation. The data and their statistical interpretation show background signals greater than present day background in the northern ESF and approximated present day background in the southern ESF. Therefore, the model was used to test whether simulated travel times greater than 10,000 years to the ESF were more prominent in the northern ESF than in the South.

Simulations of ground-water travel times in portions of the rock mass that are away from faults do not support certain elements of the conceptual model of solute travel times to the ESF. Specifically, simulated travel times do not show a significant relationship with thickness of the PTn unit, but do reflect the influence of spatially varying infiltration rates. The infiltration rates vary significantly over distances less than 100m but do not have a specific trend with distance through the ESF. Similarly, simulated travel times vary on the same scale as the infiltration map, but do not reflect strongly the trend of thinning PTn to the south. Changing the magnitude of the infiltration rates directly affects the simulated travel times, but will only lead to a trend in the simulated travel times if a specific trend is built into a modification of the existing infiltration map. However, such a trend may evolve if the discrepancy between simulated and observed porewater chloride leads to adjustments to the infiltration map only in the south. Another adjustment that may be warranted based on this analysis is a modification of hydrologic properties to incorporate more lateral flow. This would help corroborate the low porewater chloride measurements found in the northern ESF below regions with very low estimated infiltration rates (hence expected high chloride concentrations).

The geologic samples from the ESF main drift within several hundred meters north and south of the Sundance fault, an interval that includes many bomb-pulse sites (but only north of the fault), are distinguished by the common presence of thick clay coatings on fracture walls and translocated particulates in the fractures. The presence of clay and particulate deposits attests to particularly well-connected fractures favorable for particulate transport and, perhaps, for lateral

dispersion of fast flow moving through the fault zone.

1. INTRODUCTION

Defining the spatial distribution and timing of subsurface fluid percolation is one of the most important factors determining long-term performance of the potential high-level radioactive waste repository at Yucca Mountain, Nevada. The potential repository would be constructed at a depth of about 250 m below the surface within rocks of the Miocene (12.8-12.7 Ma) Paintbrush Group. This sequence of volcanic rocks is greater than 460 m thick and consists of two regionally extensive, densely welded, fractured pyroclastic flows that are separated by an interval of generally nonwelded, bedded pyroclastic deposits. The nonwelded interval of the Paintbrush Group (PTn), which overlies most of the potential repository, has high matrix porosities and permeabilities and is mostly unfractured.

The Exploratory Studies Facility (ESF) is a tunnel, 8km in length and 7.6m in diameter, excavated beneath Yucca Mountain to the level of the potential repository horizon to access the stratigraphic level of the potential repository along its eastern margin (Figure 1-1). In the vicinity of the ESF, thicknesses of the nonwelded PTn unit vary from about 20 to over 70 meters. A second tunnel (1.8km in length), the East-West Cross Drift (EWCD, or Cross Drift), was started in 1998 to provide a southwesterly transect across the potential repository horizon. An extensive program of geologic and hydrologic investigations is being carried out within these tunnels to characterize hydrologic, geologic and material properties of the potential repository horizon beneath Yucca Mountain.

Rapid fracture flow of water is expected to be pervasive both in the welded Tiva Canyon (TCw) hydrologic unit above the PTn as well as in the welded Topopah Spring (TSw) hydrologic unit below the PTn. This expectation is supported by various geochemical, isotopic and other lines of evidence. In contrast, the higher porosity and low degree of fracturing of PTn rocks would be expected to result in matrix flow with very low vertical velocities throughout most of this unit and travel times on the order of several thousand years. However, several samples collected within the ESF have measured chlorine-36-to-chloride ($^{36}Cl/Cl$) ratios indicative of anthropogenic ^{36}Cl (bomb-pulse ^{36}Cl). Such data imply that at least some fraction of the water has traversed the overlying PTn in 40 years or less and that flow is not confined to the matrix of that unit. The presence of a fast path transmitting bomb-pulse ^{36}Cl to depth appears to require the simultaneous presence of a structure (such as a fault) cutting the PTn and sufficiently high magnitude of surface infiltration to initiate and sustain at least a small component of fracture flow along the connected fracture path associated with the structure.

A previous report (Fabryka-Martin et al., 1997a) summarized available data about the subsurface distribution of ^{36}Cl and porewater chloride (Cl) and assessed alternative conceptual models about flow and transport through the unsaturated zone at Yucca Mountain based on model consistency with the subsurface distribution of environmental tracers. Chloride and ^{36}Cl data were simulated with a site-scale flow and transport model using the FEHM code to establish bounds on

infiltration rates at the site and to provide greater confidence in our understanding of unsaturated flow processes at the site—including fast transport paths—by showing consistency between the

observed and simulated data sets. The present report updates the data base for Yucca Mountain with respect to porewater Cl concentrations and $^{36}Cl/Cl$ ratios at the site and discusses the extent to which these new data are consistent with the earlier report. In addition, the report presents data illustrating the applicability of bromide-to-chloride (Br/Cl) ratios for tracing construction water and applied infiltration.

2.0 CHLORIDE DISTRIBUTION IN THE UNSATURATED ZONE

2.1 Chloride as a hydrologic tracer

Chloride porewater concentrations obtained from unsaturated core samples serve several purposes within the Yucca Mountain investigation:

- *Infiltration estimates.* Cl concentrations provide independent corroboration of surface infiltration rates estimated by modeling. The Cl mass balance (CMB) method estimates infiltration as a proportion of precipitation based upon the enrichment of Cl in porewater relative to its concentration in precipitation (Figure 2-1(a)). This approach is based on the premise that the flux of Cl deposited at the surface equals the flux of Cl carried beneath the root zone by infiltrating water. With increasing depth, as water is extracted by evapotranspiration, Cl concentrations increase and apparent infiltration rates decrease. Net infiltration is the flux of water moving below the zone of evapotranspiration, at which depth Cl concentrations remain relatively constant.

- *Perched water origin.* The origin and age of perched water bodies underlying Yucca Mountain have been problematic because their Cl concentrations (4-10 mg/L) are generally considerably lower than those of porewaters from the unsaturated zone above the bodies. Expanding the spatial coverage of the porewater data will help constrain the various hypotheses on the derivation of the perched water.

- *Mixing of waters.* Cl, Br, and sulfate (SO_4) porewater concentrations indicate the extent to which water geochemistry is homogenized as it percolates through the nonwelded Paintbrush unit. Fracture-dominated flow in the overlying low-permeability, highly fractured TCw unit is expected to transition to matrix-dominated flow in the high-permeability, comparatively unfractured PTn. The transition process from fracture to matrix flow in the PTn, as well as the transition from low to high matrix storage capacity, could damp out most of the seasonal, decadal, and secular variability in surface infiltration. This process could also result in the homogenization of the variable geochemical and isotopic characteristics of porewater entering the top of the PTn. In contrast, fault zones that provide continuous fracture pathways through the PTn may damp climatic and geochemical variability only slightly and may provide fast paths from the surface to the sampled depths, whether within the PTn or in underlying welded tuffs. If this concept can be validated, then it would suggest that repository design and performance assessment efforts can be based on fluxes that are uniform in time, except near fault zones.

- *Lateral diversion.* Variability in Cl, Br, and SO_4 porewater concentrations can be used to assess the extent to which water may be laterally diverted due to contrasting hydrologic properties of the various stratigraphic units above the potential repository horizon.

- *Total dissolved solids.* Porewater compositions above and within the potential repository horizon are significant because they represent the types of water that could enter the near field of the potential repository. Extraction of sufficient porewater from these rocks for full

geochemical analysis is difficult. However, Cl concentrations can serve as a surrogate measure of the total dissolved solid contents of these waters for constraining models of rock/water interactions under different thermal scenarios.

- *Model calibration.* To the extent that the Cl porewater data base can be extended to a wide spatial and stratigraphic coverage, it is an increasingly valuable data set for site-scale modelers to use in calibrating flow and transport models of Yucca Mountain.

2.2 Previous work

2.2.1 Numerical model of surface infiltration

A numerical model of the spatial distribution of net infiltration for the Yucca Mountain site area describes the effect that observed processes of precipitation, runoff, evapotranspiration, and redistribution of water in the shallow unsaturated zone have on net infiltration (Flint et al., 1996). The model combines surface elevation, bedrock geology, thickness of surficial material, and hydraulic properties of both the soil and the underlying bedrock to spatially distribute estimated net infiltration within the over 250,000 30-m grid cells in the model area as a function of spatially and temporally variable precipitation (Flint et al., 1996). The numerical model for infiltration is based upon the results of detailed mapping of surface soils, bedrock, and precipitation (Flint et al., 1996). Detailed field and laboratory measurements of soil and rock properties are used to develop the necessary spatially distributed model properties (Flint, 1998a). The measured properties were used to define the average property for each surface map unit, both surficial material and underlying bedrock (Flint et al., 1996). For precipitation during an average year (~170 mm), net infiltration estimates range from zero for a soil thickness of 6 m or more to over 50 mm/yr for a thin soil on north-facing slopes and at high elevations overlying highly permeable bedrock (Flint et al., 1996). Infiltration averages 3.8 mm/yr in the vicinity of the potential repository area and approximately 6 mm/yr for the study area shown in Figure 1-1.

Although the numerical infiltration model captures most of the spatial variability in these properties, there is some concern about missing the surface runoff events and subsurface (down-slope) flow. In determining average annual net infiltration, surface runoff is accounted for by adding approximately 10 mm/yr to the calculated infiltration in the channels, which is consistent with neutron probe data collected after runoff events (Flint and Flint, 1995). Accounting for subsurface flow is more difficult. However, the 30-m spacing used for the grid squares in the model is generally large enough so that lateral flow is self-contained. The one-dimensional assumption for infiltration, therefore, would only cause slight errors and only at the base of slopes. For the first approximation of spatially distributed infiltration, these errors are assumed to be minimal.

2.2.2 Choride porewater concentrations

An extensive data base of porewater chemistry for the nonwelded PTn unit and for the mostly nonwelded Calico Hills (CHn) hydrologic unit (which underlies the TSw unit) has been developed from surface-based boreholes (Yang et al., 1988, 1990, 1996, 1998). The lowest Cl

concentration in PTn porewaters in data published for Yucca Mountain is 32 mg/L, and the average value is 72 mg/L. These data were summarized by Fabryka-Martin et al. (1997a), who estimated infiltration rates from them using the CMB method and concluded that the rates were consistent with those predicted for these locations by the numerical infiltration model of Flint et al. (1996).

More recently, Cl concentrations have been measured in porewaters extracted from ESF drillholes, thereby expanding the spatial coverage of the subsurface distribution of this anion (Fabryka-Martin et al., 1998a). Concentrations ranged from 10 mg/L to 129 mg/L. The average concentration for samples from the North Ramp (20 mg/L) was about half that for those from the South Ramp (42 mg/L), corresponding to surface infiltration rates of 5.3 mm/yr for the north set and 2.5 mm/yr for the south set by the CMB method. This trend was qualitatively consistent with that predicted by the site-scale numerical infiltration model described in section 2.2.1 insofar as the model predicts higher infiltration rates along the North Ramp than along the South Ramp. However, the Cl data indicated that the infiltration model might overestimate the rates for the southern portion.

The present report extends the Cl porewater data set for the ESF and evaluates the reproducibility of the data.

2.3 Methods

About 60 drillholes, each approximately 2m in length and 0.15m in diameter, were dry-drilled horizontally into rocks in the north ramp of the Exploratory Studies Facility (ESF) at Yucca Mountain along a 0.3-km section between Stations 7+27 and 10+69 and in the southern half of the ESF along a 1.7-km section between Stations 59+65 and 76+33, where the notation for stations indicates the distance in meters from the North Portal entrance). The boreholes penetrated mainly the PTn, as well as units above and below it. Ten horizontal drillholes were also drilled at roughly 200-m intervals in the ESF main drift between Stations 39+50 and 58+00. Finally, samples were made available for this effort from three drillholes in Niche 3566 (also called Niche #1) at ESF Station 35+66. Two of the Niche 3566 drillholes were drilled prior to niche excavation, parallel to its axis, and about 2 m apart (ESF-MD-NICHE3566#1 and ESF-MD-NICHE3566#2). The third hole was drilled laterally from the niche to intersect the Sundance fault (ESF-MD-NICHE3566LT#1).

Samples were sealed in Lexan Protecore in the field and stored under cool conditions until ready for analysis. Porewater was extracted from the unsaturated drillcore using ultracentrifuges capable of operating at 10,000 to 16,000 rpm by running in a vacuum chamber. Typical yields were 0.2 to 2 mL for samples with masses of 35 to 160 g after an extraction period of about 24 hours. Solutions were analyzed for Cl, Br, and SO_4 using ion chromatography.

2.4 Results

Average Cl, Br, and SO_4 concentrations are listed in Table 2-1 for 53 of the above ESF drillholes. The absence of significant contamination of these samples by construction water is indicated by Cl/Br ratios that fall generally well within the range expected for meteoric water (50

to 250). Mine construction water is traced with LiBr to a Cl/Br of 0.4, and none of the samples approach this low value. The low Br/Cl ratio (17) for porewater extracted from ESF-NR-MOISTSTDY-#9 at Station 8+73 indicates that this sample may contain a very small component of construction water but not enough to be significant. This sample has the lowest Cl concentration (5.7 mg/L) reported to-date for PTn porewaters, lower even than that of the construction water (7.0 mg/L). Nineteen meters away, drillhole ESF-NR-MOISTSTDY#11 (Station 8+92) has a similarly low Cl concentration (6.7 mg/L) with no indication of any construction water.

The welded sample from ESF-SR-MOISTSTDY#18r has a high Cl/Br ratio (>300) which may indicate the presence of a small amount of Cl from rock fluid inclusions. For this reason, the measured Cl concentration (45 mg/L) should be considered an upper limit for infiltrating water at this location.

The average concentrations reported in Table 2-1 are calculated from multiple analyses of porewaters from a given drillhole. Each individual porewater sample is analyzed at least twice, and the coefficient of variation of the ion chromatography data is always less than 10% and usually less than 5%. In addition, in many cases, two or more porewaters have been extracted from a given sample at different centrifuge times, from different aliquots of the same sample processed separately, or from different samples from the same drillhole. This approach is illustrated by data shown for four drillholes in Table 2-2. For example, porewater has been extracted from samples from four depth intervals of ESF-NR-MOISTSTDY#3 (EDC014, EDC015, EDC016 and EDC017). Two separate aliquots of one interval were processed (EDC015-1 and EDC015-2), and porewater was extracted from one of these drillcore aliquots (EDC015-2) at two different times (20 hours and 48 hours) during the centrifuging. Averages reported in Table 2-1 are then calculated by weighting individual results by the associated porewater volumes.

Evaluation of the full data base indicates that the reproducibility of the porewater data is fairly good provided the moisture content is at least 4% by weight. Below this moisture content, results can be highly variable or otherwise questionable. Open questions are the extent to which porewater chemistry may vary with pore size when pore diameters extend down to the range in which ions may be interacting with charged mineral surfaces, or how the chemistry of pore fluids is affected when a significant proportion of the porewater is structurally bound (e.g., by clays or zeolites).

2.5 Discussion

The Cl porewater concentrations in Table 2-1 range from 6 to 150 mg/L. Nearly half (24) of the 53 samples are less than 30 mg/L. In general, they are lower than those reported for PTn porewaters by Yang et al. (1988, 1990, 1996, 1998). These earlier samples, which were extracted from drillcore from surface-based boreholes, may be spatially biased because they were sited in locations in channels and terraces, which tend to be zones of lower infiltration (and hence higher Cl concentrations) due to higher evapotranspiration losses.

Cl porewater concentrations for the North and South Ramp samples are plotted as a function of stratigraphic depth in Figure 2-2. The South Ramp samples have been plotted separately for two stretches of the tunnel because the topography and surface geology overlying this area is quite variable such that infiltration rates may also be expected to differ dramatically over short distances here. In that figure, Cl concentrations are observed to be fairly homogeneous throughout the PTn, particularly for the North Ramp samples and the South Ramp samples between Stations 66+41 to 68+26. Cl concentrations in the fractured welded units above and below the PTn show more variability and extend to higher concentrations than do the data for the PTn. This trend may reflect the effectiveness of the PTn in damping the geochemical variability of the infiltrating waters entering it and in homogenizing the fluid chemistry. Such a trend would not be apparent if the South Ramp samples had not been plotted separately from one another, indicating that lateral diversion of water in this area is not on the order of hundreds of meter and, most likely, is limited to less than 200 m.

Another useful way to view the Cl data is in terms of the corresponding infiltration rates. Table 2-1 shows infiltration rates calculated from the measured Cl concentrations using the CMB method. In this method, infiltration, I, in mm yr^{-1} is calculated from $I = (P\ C_0)/C_p$, where P is average annual precipitation at Yucca Mountain (~170 mm yr^{-1}, Hevesi et al., 1992), C_0 is average Cl concentration in precipitation (0.62 mg L^{-1}, Fabyrka-Martin et al., 1993) including the contribution from dry fallout, and C_p is the measured Cl concentration in porewater (mg L^{-1}). This relationship is plotted in Figure 2-1(b). The CMB method assumes one-dimensional, downward piston flow, constant average annual precipitation rate, constant average annual Cl deposition rate, no run-on or run-off, no Cl source other than precipitation (e.g., it is assumed that the concentrations of Cl brought in by surface runoff and Cl released from weathering of surface rocks are negligible), and no Cl sink (e.g., it is assumed that removal of Cl through the formation of halite is negligible). Conditions under which these assumptions may not be valid at Yucca Mountain are discussed by Fabryka-Martin et al. (1997a, section 6.3).

The CMB infiltration rates are plotted as a function of stratigraphic depth in Figure 2-3. From this figure, one would conclude that the infiltration rates for the North Ramp samples, which average 6 mm/yr, are two to three times higher than those from the South Ramp. Despite the variable Cl concentrations in the easternmost South Ramp samples, the corresponding infiltration rates cover a narrow range, 1 to 3 mm/yr, because of the insensitivity of the CMB method to concentrations above about 20 mg/L (Figure 2-1(b)).

Figure 2-4 plots the measured Cl concentrations as a function of distance along the ESF, comparing them to the Cl concentrations corresponding to the numerical surface infiltration model of Flint et al. (1996). Cl porewater concentrations for the North Ramp sample set (geometric average, 18 mg/L) and Main Drift (19 mg/L) are about a third of the average value for the South Ramp set (56 mg/L), corresponding to surface infiltration rates of 5.7 mm/yr in the north, 5.3 mm/yr along the Main Drift, and 1.9 mm/yr in the south by the CMB method. The agreement between measured and modeled concentrations is fairly good for the North Ramp and Main Drift samples, but many of the South Ramp samples have considerably higher Cl concentrations than the numerical infiltration model would predict. Figure 2-5 is based on the same data, this time plotting the infiltration rates for the measurement porewater samples against

those of the numerical infiltration model. The data for samples around Station 75+00 indicate that the numerical model may over-estimate infiltration in this area.

An effort is underway to revise the numerical infiltration model of Flint et al. (1996). For example, a more recent geologic map (Day et al., 1998) is being used to define the spatial distribution of permeability, which exerts a dominant control on the modeled infiltration rates. This change is expected to lead to closer agreement between the modeled rates and those calculated by the CMB method in the south part of the study area.

These geochemical data are being used to test alternative conceptual models of flow and transport in the unsaturated zone at Yucca Mountain and to establish bounding fluxes for the site-scale flow model, as illustrated by recent numerical model simulations of Cl transport (Robinson et al., 1997; Fabryka-Martin et al., 1997a; Sonnenthal and Bodvarsson, 1998; TRW Environmental Safety Systems Inc., 1998, pages 38-46). For example, a site-scale solute transport model using the FEHM code was used to predict the distribution of Cl concentrations in ESF porewaters, with the Flint et al. (1996) numerical model defining the surface boundary condition. The results of this modeling exercise are shown in Figure 2-6, in which nearly all of the measured Cl porewater concentrations in the South Ramp area exceed the predicted porewater concentrations. This discrepancy emphasizes the need to revise the numerical infiltration model. Applicability of these data to flow and transport modeling is discussed in more detail in section 5.

3. CHLORINE-36 DISTRIBUTION IN THE UNSATURATED ZONE

3.1 Chlorine-36 as a hydrologic tracer

Development and testing of conceptual flow and transport models for hydrologic systems are strengthened when natural environmental tracers are incorporated into the process. One such tracer is chlorine-36 (^{36}Cl, half-life, 301,000 years), a radioactive isotope produced in the atmosphere and carried underground with percolating groundwater. High concentrations of this isotope were also added to meteoric water during a period of global fallout from atmospheric testing of nuclear devices, primarily in the 1950s. This bomb-pulse signal has been used to test for the presence of fast transport paths in the unsaturated zone at Yucca Mountain and to provide the basis for a conceptual model for their distribution (Fabryka-Martin et al., 1997a, 1997b, 1998b; Wolfsberg et al., 1998). Under wetter climatic conditions, fast flow pathways will respond quickly to increases in infiltration and have the potential to become seeps in the tunnel drifts. The ^{36}Cl data are also being used in numerical flow and transport models to establish lower bounds on infiltration rates, estimate groundwater ages, and establish bounding values for hydrologic flow parameters governing fracture transport.

3.2 Previous work

Chlorine-36 analyses for over 250 ESF samples were summarized in Fabryka-Martin et al. (1997a). These included systematic samples collected at fixed intervals along the tunnel and feature-based samples that targeted specific features such as damp zones, faults, fractures, or stratigraphic unit contacts. The goal of this sampling scheme was to address key aspects of flow variability and permeability differences and to test conceptual models of subsurface percolation. The following trends were noted in that report:

- The majority of the samples (77%) have $^{36}Cl/Cl$ ratios ranging between 350×10^{-15} and 1000×10^{-15}, or 0.7 to 2 times the present-day background value of 500×10^{-15}. These results fall well within the range over which the atmospheric $^{36}Cl/Cl$ signal has varied during the past 30,000 years or more, based on analyses of fossil packrat urine (Plummer et al., 1997).
- A small number of samples in the southern portion of the ESF have $^{36}Cl/Cl$ ratios that lie significantly below the range of meteoric background values (i.e., these samples have $^{36}Cl/Cl$ ratios less than 350×10^{-15}). These low values may provide evidence for stagnant zones with travel times sufficiently long for radioactive decay of meteoric ^{36}Cl to have occurred (i.e., water ages on the order of 10^5 years). Alternatively, they may indicate dilution of the meteoric signal by a component of "dead" rock Cl released when the rock samples are crushed before leaching.

- At a few locations, ratios extend well above the range of background values to a maximum of 4100×10^{-15}. These high ratios are interpreted as indicating the presence of a component of bomb-pulse ^{36}Cl at these locations, a clear indication that some fraction of the water at the ESF level arrived there during the past 50 years. Based on statistical analyses, samples with ratios above 1250×10^{-15} are considered to contain a component of bomb-pulse ^{36}Cl.

This interpretation is supported to some extent by measurements of bomb-pulse tritium and carbon-14 in borehole samples from other parts of Yucca Mountain (Yang et al., 1996, 1998).

- The ^{36}Cl signals in the northern part of the ESF are highly variable and elevated above present background levels. In contrast, signals in the south part of the ESF are nearly constant.

Detailed characterization of the structural settings of the ^{36}Cl sample locations and of their relationships to structural features and infiltration rates provided the basis for a proposed conceptual model for fast pathways at Yucca Mountain (Fabryka-Martin et al., 1997a). The conceptual model states that three conditions must be present to transmit bomb-pulse ^{36}Cl to the sampled depth within 50 years:

- A continuous fracture path must extend from the surface to the sampled depth. This condition is necessary because travel times through the matrix of unfractured rock is expected to exceed 50 years. The condition of a continuous fracture path is easily satisfied in most of the welded portions of the Tiva Canyon and Topopah Spring units. The limiting hydrologic unit for controlling transport rates is the nonwelded PTn unit, which is usually relatively unfractured. Hence, satisfying the condition of a continuous fracture pathway requires the presence of faults that cut the PTn unit and increase its fracture conductivity.
- Surface infiltration rates must be sufficiently high to initiate and sustain at least a small component of fracture flow along the connected fracture path. Transport simulations indicate that the threshold rate may be on the order of 1-2 mm/yr.
- The residence time of water in the soil cover must be less than 50 years, i.e., the soil thickness must be less than 3 meters.

A qualitative case-by-case examination of the ESF data against the model's prediction of the presence or absence of bomb-pulse ^{36}Cl showed that the model was generally successful in predicting the presence of bomb-pulse ^{36}Cl. However, in some cases, the conceptual model did not adequately account for the observed ^{36}Cl data. For example, in the southern part of the ESF, faults are encountered at locations where the modeled infiltration rates exceed 2 mm/yr but, nonetheless, bomb-pulse ^{36}Cl has not been detected to the extent that it is present in the northern part.

The apparent lack of bomb-pulse ^{36}Cl in most ESF samples suggests that the PTn, at least away from fault zones, significantly delays the timing and damps the magnitude of episodic fluxes (Fabryka-Martin et al., 1997a; Wolfsberg et al., 1998). If this concept holds true through further analysis, then it would suggest that repository design and performance-assessment efforts can be based on fluxes that are uniform in time except near fault zones. Although the ^{36}Cl data cannot be used to quantify fluxes directly, they do at least identify the type of fast path for which it may not be acceptable to assume damping of high fluxes.

3.3 Methods

Chlorine-36 analyses contained in this report have been conducted on a variety of sample matrices for this study, including soils, drillcore, rocks collected by hand from ESF tunnel walls, and surface and subsurface waters at the site. Sample preparation involves leaching of soil and

rock samples with deionized water to extract soluble salts or direct extraction of pore fluids from drill core by high-speed centrifugation. Mass spectrometry is used to measure $^{36}Cl/Cl$ ratios for these samples, and ion chromatography is used to measure the anion concentrations. Details of the processing and analytical methods and of the various quality-control measures are discussed in Fabryka-Martin et al. (1997a).

Based on Br/Cl ratios in the salts leached from the rocks, measured $^{36}Cl/Cl$ ratios are adjusted for the presence of Cl from construction water. The proportion of Cl contributed by construction water is estimated using a two-component mixing equation and estimated Br/Cl ratios of the construction water and percolating waters (Fabryka-Martin et al., 1997a, 1998b). It is important to note that the $^{36}Cl/Cl$ ratio of the construction water (500×10^{-15}) is equal to the atmospheric background $^{36}Cl/Cl$ level, such that any ^{36}Cl levels above background cannot be attributed to this source.

3.4 Results

3.4.1 Analytical reproducibility

A standard quality-control measure involves re-analysis of environmental samples starting from the raw material and independently processing different aliquots of the same sample. Additional analyses obtained during the past year confirm the earlier finding—signals measured in Cl extracted from homogeneous samples such as waters, soils, and bedded tuffs are reproducible but signals measured for fractured rock samples are often difficult to reproduce, presumably because of variable degrees of dilution of the meteoric component by other sources of Cl (Table 3-1). The data in that table show that differences in $^{36}Cl/Cl$ ratios for replicate samples of fractured rock are particularly large—by as much as a factor of two—if bomb-pulse ^{36}Cl is present in the sample.

3.4.2 Chlorine-36 in the ESF

Table 3-2 reports ^{36}Cl data for ESF rock samples analyzed between August 1997 and September 1998. These include samples from the South Ramp, Niche 3566, Alcove 6 and Alcove 7. In addition, $^{36}Cl/Cl$ ratios were measured in porewater extracted from ESF drillcore from 2-m horizontal boreholes along the North and South Ramps and from boreholes drilled in Niche 3566 (see section 2.3 for drillhole locations).

The South Ramp, Niche 3566 and ESF porewater data are plotted as a function of ESF station in Figure 3-1, together with other ESF data reported in Fabryka-Martin et al. (1997a). Consistent with the trends shown by earlier data (Fabryka-Martin et al., 1997a), $^{36}Cl/Cl$ ratios for the new South Ramp rock samples are lower than those measured previously for the northern half. Eighty-four of the 132 ESF samples beyond Station 45+00 have $^{36}Cl/Cl$ ratios near the background meteoric ratio, between 400×10^{-15} and 600×10^{-15}. Nine of the South Ramp samples have $^{36}Cl/Cl$ ratios below 300×10^{-15}. Such low values are not observed in the northern half of the ESF. Only four samples beyond Station 45+00 have ratios above 800×10^{-15}, and none of these ratios lie above the threshold (1250×10^{-15}, Fabryka-Martin et al., 1997a) that indicates the unambiguous presence of bomb-pulse ^{36}Cl. The highest four values measured in the

south part are: 1117 x 10^{-15} at Station 56+93 near the Ghost Dance fault, 1003 x 10^{-15} for a porewater sample from Station 74+53, 983 x 10^{-15} for a rock sample from station 78+50, and 942 x 10^{-15} for a rock sample from Station 51+33.

Several large faults are present in the portion of the ESF beyond station 45+00. The block-bounding Dune Wash fault and the large intrablock fault exposed in the ESF around Station 70+56 have vertical separations that are greater than the thickness of the PTn unit (thickness less than 30 m along the South Ramp of the ESF; Moyer et al., 1996) and thus create a discontinuity in the PTn (Day et al., 1998). The other faults (including the Ghost Dance fault) are intrablock faults with less than 20 m of offset (Day et al., 1998). These faults do not completely offset the PTn by an amount greater than the thickness of the PTn. The lack of elevated levels of ^{36}Cl in these faulted areas indicates that the presence of faults is not the only controlling factor in the distribution of ^{36}Cl in the ESF. The distribution of ^{36}Cl in the ESF depends upon multiple interrelated controls; the presence of faults does not result in bomb-pulse ^{36}Cl in the ESF without sufficient net infiltration and sufficiently fast travel times through the alluvial cover.

The elevated $^{36}Cl/Cl$ ratios measured for the Niche 3566 drillcore samples (Table 3-4) confirm the widespread presence of bomb-pulse ^{36}Cl in this area near the Sundance fault. The Sundance fault is the only structure mapped in this vicinity (Potter et al., 1995; Day et al., 1998) that could serve as the pathway through rocks equivalent to the PTn hydrogeologic unit. The broad zone of elevated $^{36}Cl/Cl$ values north of the fault thus appears to represent lateral flow away from the plane of the fault and implies a connection between the fault and other structures, either small subsidiary faults or interconnected joints, in the rock mass surrounding the fault. Bomb-pulse ^{36}Cl was not present in the rock samples collected manually as damp breccia filling a cooling joint in the back of Niche 3566. Lack of elevated ^{36}Cl here may indicate that flow in this feature is through the matrix and, hence, its travel time may be too slow to conduct bomb-pulse ^{36}Cl to this depth. No bomb-pulse ^{36}Cl was measured in the rock sample collected manually from the niche wall, but this sample was also found to have been contaminated significantly by construction water (E336-1, Table 3-2).

Profiles of $^{36}Cl/Cl$ ratios are plotted along the lengths of Alcoves 6 and 7 in Figure 3-2. Bomb-pulse ^{36}Cl is observed in several of the samples from Alcove 6 (the Northern Ghost Dance fault alcove) but not in the samples from Alcove 7 (the Southern Ghost Dance fault alcove). A key question that has not been determined is the dip of the fault in these alcoves and, hence, where it would break through the PTn. According to the conceptual model for fast paths summarized in section 3.2, bomb-pulse ^{36}Cl is expected in a zone that is vertically beneath the location in which faults break the nonwelded unit.

3.4.3 Chlorine-36 in Soils and Surface Runoff

Chlorine-36 was analyzed in surface soils and surface runoff at Yucca Mountain to characterize the isotopic composition of waters presently infiltrating into the bedrock. Soil samples were collected above the ESF South Ramp, between stations 67+00 and 78+00 (Table 3-5). Surface runoff was collected from three washes in February 1998, augmenting the 7 samples that had been collected in 1995 (Table 3-6). All of these soil and water samples had $^{36}Cl/Cl$ ratios elevated above natural (pre-nuclear) background, ranging from 1010 x 10^{-15} at a depth of 0.75 m

below the channel in Dune Wash, to 3660 x 10^{-15} for soil from the eastern sideslope of Boundary Ridge. A comparison of the 1998 runoff sample data to those for the 1995 samples (excluding the two snowmelt samples) shows a downward trend from an average $^{36}Cl/Cl$ ratio of 3030 x 10^{-15} to an average ratio of 2010 x 10^{-15} in 1998, as would be expected as the bomb-pulse ^{36}Cl is gradually washed out of the surface soil into the deeper soil. These data confirm that water entering the bedrock today will still contain bomb-pulse ^{36}Cl and that bomb-pulse ^{36}Cl has not yet been completely removed from the soil profile.

4. STATISTICAL ANALYSIS OF $^{36}Cl/Cl$ RATIO DATA

4.1 Overview

Multiple processes and system attributes may affect the $^{36}Cl/Cl$ ratios observed in the ESF. These include infiltration rates, overlying PTn thickness, material in which the sample is collected, overlying soil thickness, and sample distance from faults. Each of these is referred to as a covariate in this preliminary statistical analysis. This analysis develops a framework and provides preliminary results for correlating the observations to covariates and assessing the influence of the various covariates on bomb-pulse and background signals. The analysis also provides a quantitative method for assessing the probability that any observed ratio contains a bomb-pulse signal. As the background signal varies spatially, this method is particularly useful in separating the background signal from the bomb-pulse signal.

The results presented here are preliminary because the sample classification scheme requires further refinement and an updated infiltration model needs to be incorporated. The mixing model will have to be expanded to include a component for radioactive decay of ^{36}Cl in the samples, and additional modifications will be to the entire analysis Preliminary statistical correlations between the $^{36}Cl/Cl$ ratio data and various covariates lead to the following results:

1. The $^{36}Cl/Cl$ ratios in ESF samples which do not appear to contain bomb pulse are spatially varying. This variation appears to be best correlated with the thickness of the overlying PTn unit and is consistent with a background signal coming from one of two distinct background distributions (Wolfsberg et al., 1998; also section 5 of this report). For ESF samples above which the PTn exists (after Station 10+00), the two distributions are representative of ESF samples before and after Station 41+00, where the PTn thickness drops below 29m.

2. Table 4-1 provides a breakdown of the sample analysis with respect to sample location and characteristic. Within the TSw unit, 88% of the bomb-pulse ^{36}Cl observations are associated with structural features: joints, fault rocks within 30m of a PTn-cutting fault or wall rock within 10-m of such faults, and stratigraphic contacts. About 35% of the samples from these categories exhibit a component of bomb-pulse ^{36}Cl, compared with 14% of the samples from the remaining categories.

3. Within the PTn unit, 82% of the bomb-pulse ^{36}Cl observations are associated with stratigraphic contacts, and the remainder are from joints within 10m of faults. Approximately 40% of the PTn samples in these categories exhibit a component of bomb-pulse ^{36}Cl.

Infiltration rate and alluvial thickness are not correlated with either background levels or with the presence of bomb-pulse ^{36}Cl.

4.2 Development of the statistical analysis framework

A plot of the $^{36}Cl/Cl$ ratio data vs. distance in the ESF suggests that underlying the obvious "bomb pulse" spikes is a varying baseline or background $^{36}Cl/Cl$ level. This association is

OFFICE OF CIVILIAN RADIOACTIVE WASTE MANAGEMENT
TRANSMITTAL/RECEIPT ACKNOWLEDGEMENT

QA: N

Page: 1 of: 1

1. Record Date	2. Title/Description	3. No. of Pages
11/03/98	DELIVERABLE ID #SP32D5M3, TRANSPORT MODELS OF YUCCA MOUNTAIN, BASED ON	
	CI-36 AND CHLORIDE STUDIES FOR FY98, DI #BA0000000-01717-5700-00007, REV 00,	
	WBS #1.2.3.3.1.2.2, YDAR #20024	163
11/03/98	DELIVERABLE ID #SSH13NM3, SUMMARY MONITORING THROUGH CALENDAR YEAR 1997	
	WBS #1.2.8.4.9, YDAR #20017	136

4. Comments

5. Sender	6. Organization	7. Mailstop	8. Date
Marina Blackwell	M&O - DCC	423	11/03/98

9. Recipient	10. Date

11. RPC Acceptance	12. Date

particularly striking when the plot is produced on a logarithmic scale (Figure 4-1) which compresses the spikes and spreads out the lower part of the range (below approximately $1000x10^{-15}$) that is occupied by the background signal. This varying background must be accounted for before the presence/absence or magnitude of the bomb pulse component can be reliably estimated. The background level may also be a function of one or more of the covariates, such as PTn thickness.

The main focus of this statistical analysis is the association of the bomb pulse component with structural features and other covariates listed below. The problem of adjusting for background is handled in two ways:

1. In Section 4.3, the raw $^{36}Cl/Cl$ ratio data are divided into subsets from the north and south halves of the ESF. The division between north and south of the ESF is made 4100m from the north end of the tunnel, based on the analysis of the spatially variable background signal discussed in Appendix A. Statistical analysis of the bomb pulse component in Section 4.3 is exploratory and largely qualitative, but some possible correlations are suggested.

2. In Section 4.4, the $^{36}Cl/Cl$ ratio data are transformed into estimates of the probability that each sample contains a bomb pulse component, using a method discussed in detail in Appendix A that simultaneously models the background component for each sample. The standardizing effect of this transformation—the "data" become numbers between 0 and 1—improves the performance of formal statistical hypothesis tests of the association between bomb pulse and covariates.

Some of the covariates available for the analysis of the $^{36}Cl/Cl$ ratio data are plotted in Figure 4-2. These include:

- thickness of the overlying PTn unit (Clayton et al., 1997) (Figure 4-2(a)),
- average and maximum infiltration rates for an area of 35m radius overlying the sample location (Flint et al., 1996) (Figure 4-2(b)),
- soil thickness (Figure 4-2(c)), and
- mean travel time as modeled using FEHM (Figure 4-2(d)) (interpolated from data from Section 5).

Other covariates are categorical, including

- classification of sampled locations by type of feature such as faults, joints, and stratigraphic contacts (Table 4-2), and
- classification of sampled locations by proximity to a fault or (in the TSw) to the projected location of a fault inferred to cut through the PTn (Table 4-3).

The technical details of the probability transformation that underlies the analysis in Section 4.4 and also the summary tabulation in Table 4-1 are relegated to Appendix A. This transformation

is based on mixture modeling of the data. In particular, the background component appears to be a mixture of two distributions, and the bomb pulse component may also be stronger in the north half of the ESF than in the south half. Section 4.3 uses the results of Appendix A only to separate the ESF into a northern and a southern half.

4.3 Correlation of observations with covariates

Plots of the $^{36}Cl/Cl$ ratio magnitude vs. the individual covariates uncover only a limited number of promising correlations. Figures 4-3(a-e) show the distributions of the observations with respect to classifications by type of feature, proximity to faults, thickness of overlying alluvium, thickness of overlying PTn, and average infiltration rate at each location.. Trends can be assessed to some extent by following the median line through the several groups in each subplot, but the numbers of samples and the upper tails of each group also need to be considered.

The following observations can be made based on in Figures 4-3(a-e).

- Figure 4-3(a) plots the distribution of the $^{36}Cl/Cl$ ratio magnitude for the categories of Table 4-1. Active and inactive intersections have been combined into a single category in this plot, labeled "Intersection", and all other joints—active, inactive and gently dipping—have been combined in the category labeled "Joint". There is some indication in Figure 4-3(a) that steeply dipping joints that intersect gently dipping joints in the TSw in the north end of the ESF are associated with bomb-pulse ^{36}Cl. Also, within the PTn, observations from stratigraphic contacts are most likely to exhibit bomb-pulse ^{36}Cl. Otherwise, the feature classification is not (by itself) a particularly good predictor for the observation of bomb-pulse ^{36}Cl.

- Proximity to a PTn-cutting fault has some predictive power for observations in the TSw in the north end of the tunnel (Figure 4-3(b)).

- Thicker alluvium may be associated with bomb-pulse ^{36}Cl in the TSw in the north end of the tunnel (Figure 4-3(c)). This association could be attributed to infiltration at the bases of sideslopes.

- The median trends that appear on the "All" subplots of Figure 4-3(d), showing $^{36}Cl/Cl$ ratio magnitude as a function of the thickness of the overlying PTn, do not appear to hold up for the north and south halves separately.

- Finally, the average infiltration rate does not seem to have any predictive power (Figure 4-3(e)). However, such a correlation was not expected from the conceptual model for fast paths (section 3.2).

Potentially more relevant are compound hypotheses involving two or more covariates. Two are considered in this section:

1. Hypothesis 1: The occurrence of bomb-pulse ^{36}Cl (particularly in the TSw) is associated *with* the combination of proximity to a fault known or inferred to cut the PTn, together with the

sample coming from either the fault rocks themselves (the first classification in Table 4-2) or from a joint.

2. Hypothesis 2: The occurrence of bomb-pulse ^{36}Cl is associated with a combination of proximity to a fault, adequate infiltration, and thin alluvial overburden.

The first of these hypotheses is moderately successful for TSw samples from the north half of the ESF (Figure 4-4(a)), and also for TCw samples from the south half. In the TSw, however, Hypothesis 1 leaves in the "other" category joints that are more than 30m from a PTn-cutting fault and also wall rock within 10m of such faults, both of which also include a number of bomb-pulse ^{36}Cl observations. In the PTn, Hypothesis 1 leaves out stratigraphic contacts, which account for the majority of bomb-pulse observations in the PTn.

The second hypothesis appears somewhat successful for the TSw samples overall (Figure 4-4(b)), but not for either the north or south halves separately, which suggests that this result may not be real. In view of the fact that neither infiltration nor thin alluvial overburden by themselves seem to be associated with bomb-pulse ^{36}Cl, this result is not unexpected.

4.4 Correlation of probability of bomb-pulse ^{36}Cl with covariates

Translating the raw data into estimates of the probability that a component of bomb-pulse ^{36}Cl has been observed has two potential advantages. First, it may exaggerate the differences between background and bomb-pulse samples by sorting the observations into a set of numbers near zero and a set of numbers near 1. In fact, the method described in Appendix A does this very well, as shown in Figure 4-5. (The lower peak is near 0.2 rather than zero for reasons described in the Appendix.) Secondly, standardizing all of the data to lie between zero and one makes the data more homogeneous and increases the power of statistical tests, particularly if the varying background has been adequately accounted for prior to estimating the probability of the presence of bomb-pulse ^{36}Cl.

The estimation procedure used in Appendix A makes use of the apparent correlation between the background level (Figure 4-1) and the thickness of the overlying PTn (Figure 4-2(a)). Figure 4-6 illustrates the probability with which each observation is estimated to contain a component of bomb-pulse ^{36}Cl, and the band of small symbols (corresponding to low probability) shifts from its upper level to its lower level at points that correspond approximately to a PTn thickness of 29m.

Figures 4-7 and 4-8 are analogous to the plots shown in Figures 4-3 and 4-4 and show the estimated probabilities that bomb-pulse ^{36}Cl has been detected vs. the covariates.. Also reported are the results of a non parametric analysis of variance test, the Kruskal-Wallis (KW) statistic. Analysis of variance is used to test the hypothesis that each of several groups of observations comes from the same distribution. Rejection of this hypothesis is indicated by a small value (less than 0.1, say) of the KW statistic, but rejection of the hypothesis does not by itself indicate which of the groups is different if more than two groups are being compared.

- Figure 4-7(a) confirms the association of bomb-pulse ^{36}Cl in the north TSw with intersecting joints. The overall KW statistic is less than 0.1, and examination of the plot shows that this

is almost certainly due to the "Intersection" group. This can be verified by repeating the test without the "Intersection" group, and in fact the resulting KW statistic is almost 1. That is, the samples sizes of the other groups with high medians are too small to produce a significant result.

- Figure 4-7(a) confirms the association of bomb-pulse ^{36}Cl with stratigraphic contacts in the PTn.

- Proximity to PTn-cutting faults appears to be statistically significant in both the north TSw and the north PTn (Figure 4-7(b)).

- There is now a suggestion in Figure 4-7(c), absent from Figure 4-3(c), that thin alluvial overburden is associated with bomb-pulse ^{36}Cl in the PTn and TCw. By contrast, the result that was significant in Figure 4-3(c) (for thick alluvial overburden in the north TSw) is seen to be statistically insignificant in Figure 4-7(c).

- The trend of increasing bomb-pulse component with increasing thickness of the PTn appears to be significant in the north PTn. However, this result actually represents a confounding of the "contact" feature with PTn thickness, because most of the stratigraphic contact samples are between the PTn and the TSw, at the bottom of the PTn.

- There may be a significant correlation between the highest average infiltration rate and bomb-pulse ^{36}Cl in the TCw in Figure 4-7(e), but the sample sizes are small.

- Figure 4-8(a) is similar to Figure 4-4(a). In particular, Hypothesis 1 appears to have significant explanatory power in the north TSw

- Hypothesis 2 is seen to have no statistical significance in Figure 4-8(b).

The proposed Hypotheses 1 and 2 were suggested before the data were looked at closely. Table 4-1 shows the number of samples identified as containing a component of bomb-pulse ^{36}Cl, cross-classified using the categories listed Tables 4-2 and 4-3. For this table, a sample is identified as containing bomb-pulse ^{36}Cl if the estimated probability of bomb-pulse exceeds 0.5. Table 4-3 suggests some alternative hypotheses. Within the PTn, for example, the bomb pulse component is strongly associated with fault zones, but stratigraphic contacts appear to provide lateral pathways away from such zones. Similarly, in the TSw, the bomb pulse component is found in fault rocks in fault zones and wall rock immediately adjacent to such faults, but again steeply dipping joints allow migration away from these zones, particularly joints that are known to intersect other, more gently dipping joints.

The few bomb-pulse ^{36}Cl samples that are not associated with structural features (i.e., classified as "Bedrock" or "Broken") are listed in Table 4-4, along with samples omitted from Table 4-3 because they were incompletely classified (either feature or distance from fault was missing) and one lithophysal cavity sample. The two exceptional samples from Alcove 6 might have been considered fault rocks (being broken rocks within 10 and 30m of a major fault). The two samples from station 11+00 are two of three aliquots of sample E027, which span almost the

entire range of reported $^{36}Cl/Cl$ ratios from $236x10^{-15}$ to the highest reported value of $5620x10^{-15}$, a data set which is not entirely understood.

The five samples for which distance to faults were not recorded include two TCw joint samples, neither of which contained bomb-pulse ^{36}Cl, and three PTn contact samples, all of which contained bomb-pulse ^{36}Cl. The two samples from Niche 3566 (Niche 1) (feature classified as "unknown", but more than 30m from the nearest fault) appear not to contain bomb-pulse ^{36}Cl, and the lithophysal cavity sample contains only a minor component, if any.

4.5 Porewater samples

Another question of interest is whether the $^{36}Cl/Cl$ ratios of ESF porewater samples (Table 3-3) differ significantly from those of the bulk of leached ESF rock samples. Only a handful of ESF porewater samples have been analyzed, all from the PTn and TCw units. Figure 4-9 suggests that they have a higher probability of containing a bomb-pulse signal than do the ESF rock samples, but the observations are neither numerous nor randomly selected, so caution is needed in interpreting these statistical results.

5. APPLICABILITY OF DATA TO SITE-SCALE FLOW AND TRANSPORT MODELS

5.1 Introduction

The effect of the PTn on unsaturated-zone hydrologic processes in the TSw and CHn is important for both repository design and performance assessment. If the PTn damps episodic infiltration events, yielding a relatively constant flux to the deeper units, then time scales on the order of storms or even seasons do not need to be considered in the modeling-associated design and performance assessment. As the ESF is mostly below the PTn, very few direct observations of flow and transport in the PTn can be made. However, measurements made at the surface and in the TSw, below the PTn, provide boundaries for understanding PTn flow and transport processes.

Predictive simulations of ^{36}Cl and chloride migration from the ground surface to the ESF and the East-West Cross Drift (EWCD) were performed using the YMP Performance Assessment radionuclide transport model. For these simulations, three-dimensional flow solutions by Wu et al. (1997) are used as input to the Los Alamos three-dimensional site-scale transport model. These transport simulations integrate the infiltration model for Flint et al. (1996), the geologic model of Clayton et al. (1997), the hydrologic properties and flow model of Wu et al. (1997), the transient historic $^{36}Cl/Cl$ ratios over the last 500,000 years estimated by Plummer et al. (1997), and the chloride concentration in infiltrating water estimated by Fabryka-Martin et al. (1997a, 1997b, section 2.5 of this report). These simulations are then compared with measured porewater chloride concentrations and $^{36}Cl/Cl$ ratios to evaluate the parameters of the different components of the model as well to help interpret the data. The model is also used to make predictions at locations in the EWCD where samples have not yet been analyzed.

The transport model uses a dual-permeability particle-tracking formulation in which input source concentration can vary both spatially and temporally (Robinson et al., 1997). In terms of travel time from the ground surface to the ESF and EWCD, the most important effects captured with this model are those due to spatial variability in both the estimated infiltration rate and PTn thickness.

5.2 Summary of previous studies

Over the past three years, Fabryka-Martin et al. (1997a, 1997b, 1998a, 1998b) and Robinson et al. (1995, 1996, 1997) have presented studies coupling the modeling of chloride and chlorine-36 transport with the observations of those species from the ESF. In those reports, the conceptual model that a fault through the PTn is a necessary condition for bomb-pulse ^{36}Cl to travel from the ground surface to ESF sample locations in the TSw is developed. This restriction, of course, applies only to ESF locations above which the PTn exists. That conceptual model is tested with numerical models in which PTn fracture permeability is greater in faults than away from faults.

The data and modeling of fault-zone processes have received significant attention within the Yucca Mountain Project because they address bomb-pulse signatures at depth in Yucca Mountain. However, because through-going faults are relatively sparse, particularly in the

potential repository-block region, the data and modeling away from fault zones play an equally if not more important role in evaluating the overall hydrologic system as well as the site-scale numerical infiltration model, the hydrologic properties data set, and the hydrologic flow model.

One of the primary roles served by the coupled ^{36}Cl data analysis and transport modeling in the past has been an independent evaluation of the current hydrologic flow model. The flow model has matured over the years from one that considered low infiltration rates with an equivalent continuum formulation (Wittwer et al., 1995; Bodvarsson et al., 1996) to one that considered the higher infiltration rates of Flint et al. (1996) with a dual-permeability formulation (Bodvarsson et al., 1997). The models before 1997 led to very long solute travel times from ground surface to the repository horizon due to predominant transport in the matrix of all materials. The modeled travel times are so long that decay of ^{36}Cl occurs and predicted $^{36}Cl/Cl$ ratios are all lower than those measured in the ESF. The Bodvarsson et al. (1997) model properties lead to fracture flow in all units, including some in the PTn. This feature results in some solute travel times of less than 50 years to ESF stations even away from fault zones. Modification of those properties by Wu et al. (1997) leads to a very similar flow field with the exception that fracture flow is generally not sustained in the PTn away from fault zones. The model predicts fracture flow throughout most of the TCw and TSw but mostly matrix flow in the PTn. This outcome results in travel times to the ESF being controlled by the PTn matrix hydrologic and transport characteristics (in and away from faults) as well as by the local infiltration rate.

5.3 Purpose of this study

Just as previous modeling studies of chlorine-36 and chloride transport have served to evaluate current Project hydrologic models as well as interpret the data, this study uses and evaluates the Project's most recent infiltration model, unsaturated-zone flow and transport models, and solute concentration data sets. The study includes an evaluation of the consistency of the solute tracer data with respect to the hydrologic properties, fracture-matrix interactions, flow paths and solute transport rates in the welded and nonwelded units, and the structural controls on flow paths. The modeling exercise starts with a conceptual model of chloride and chlorine-36 transport processes and then examines it with respect to the observed chloride concentrations and $^{36}Cl/Cl$ ratios in samples.

5.4 Conceptual model

The data described earlier in this report support a conceptual model for fast paths linking faults to observations of bomb-pulse $^{36}Cl/Cl$ ratios in the ESF. Away from fault zones, $^{36}Cl/Cl$ ratios greater than present-day background but less than ratios found near faults represent either water that entered the system more than 10,000 years ago when such ratios were higher (Plummer et al., 1997) or the dilution of water containing bomb-pulse ^{36}Cl with older water. Considering the latter hypothesis, there is a discrepancy between where the data would support such a model and where the process is most likely to occur. Higher than present-day ratios are found in the north part of the ESF where the PTn is thick but not in the south part where this unit is only half as thick. If bomb-pulse ^{36}Cl were to penetrate the PTn away from faults, it would be more likely to do so where the PTn is thin. Thus, a more plausible interpretation is that the higher-than-present-day ratios away from fault zones in the north are due to longer-than-10,000-year travel times

through the 40- to 60-m thick PTn matrix. In the south, where the PTn is about 30-m thick, modeled travel times are generally less than 10,000 years except in the few locations where infiltration rates are near zero. Under those locations, there is little lateral flow to bring younger water to the east, so the travel times are tens to hundreds of thousands of years, leading to the observed decay of the $^{36}Cl/Cl$ ratio. As part of the assessment of infiltration rates, porewater chloride should be lower in zones of higher flux and higher in zones of lower flux.

5.5 Summary of model simulations

Chloride Concentration: In the North Ramp, Main Drift, and Main Drift alcoves, the simulated chloride porewater concentrations match the measurements well considering the scale difference between the model (50 m) and samples (<1 m). On the other hand, the simulated porewater chloride concentrations in the South Ramp are generally well below the measurements. The model simulates predominantly vertical flow in the region, ruling out significant simulated mixing with dilute water from the west. Thus, these results indicate that the infiltration model may overestimate the percolation flux in this region, leading to overly dilute chloride concentrations.

Simulations of porewater chloride concentrations in the EWCD, where samples have not yet been analyzed for this constituent, provide an opportunity to test the models in regions with higher estimated infiltration rates than the ESF. As the EWCD has stations directly below Yucca Crest, estimated infiltration rates (Flint et al., 1996) are as high as 20 mm/yr leading to lower porewater chloride concentrations than are found in the ESF. Once the samples are collected and analyzed, they will be used in conjunction with the predictions to assess the infiltration model.

Faults and Bomb-Pulse Chlorine-36: The role faults play on the migration of bomb-pulse tracers has been studied extensively with past modeling efforts (Fabryka-Martin et al., 1997a, 1997b, 1998b). Those efforts develop and support the hypothesis that faults through the PTn create a pathway through which some solutes can travel quickly, bypassing the PTn matrix in which velocities are slower. Such models are consistent with the limited PTn fault-zone properties that have been developed with field-scale testing. Namely, air permeability measurements indicate that PTn bulk permeabilities increase one to two orders of magnitude in fault zones. That increase is incorporated into the models as increased fracture permeability and leads to simulations in which some solutes reach the ESF in less than 50 years, consistent with the measured bomb-pulse signatures. With the current flow models, the only other locations in which bomb-pulse signals reach the ESF and EWCD are those for which there is no overlying PTn. One exception may be Station 22+00 in the EWCD. However, this is very near the location where the PTn ceases to exist on the west slope of Yucca Crest. Additionally, Fabryka-Martin et al. (1997b) have used models to study whether episodic infiltration events are damped in and away from fault zones. Their findings indicate that in fault zones, storm-related infiltration events may not be completely damped, leading to partially damped transient fluxes at the potential repository.

Chlorine-36 Away from Faults: Away from fault zones, the $^{36}Cl/Cl$ ratios at the ESF are used to evaluate the site-scale model, which involves primarily matrix flow and transport in the PTn. The solute travel time to the ESF is an integrated function of the infiltration rate, the PTn

thickness, and solute pathway, which may involve residence in the fracture and matrix domains of each of the units. Thus, a solute analysis from a sample at the ESF represents a distribution of travel times to the sample location. Whereas some of the solutes in any given sample may have traveled predominantly in fractures of all units, other solutes in that same sample may have traveled predominantly in the matrix material of all units. The travel times for these contributors are significantly different due to the difference in velocities between fractures and matrix. However, because most of the flow is expected to occur in the fractures of the TCw and TSw and in the matrix of the PTn, those domains control the majority of travel times to the ESF. Simulated travel time distributions at ESF locations show this to be the case. Most solutes have similar travel times controlled by the PTn matrix. Yet, long tails to the transport time distribution represent the additional time for the few solutes that migrate in the matrix of the welded tuff as well as the PTn matrix.

Predictive simulations at EWCD locations (Fabryka-Martin et al., 1998a) indicate that the higher infiltration rates to the west of the ESF should lead to shorter travel times and, hence, to $^{36}Cl/Cl$ ratios similar to present-day background. However, due to varying fracture-matrix interactions with depth in the TSw, the $^{36}Cl/Cl$ ratio in TSw matrix material will also vary with depth.

5.6 Calculation details

Chloride Concentration: Porewater chloride concentrations are simulated with the steady-state, three-dimensional performance assessment transport model. Flow fields from Wu et al. (1997) are used as input to the transport models. Simulated chloride concentrations at ESF and EWCD locations are then extracted from the model and compared with measurements or used for predictions. Previously in this report, the simulated chloride porewater chloride concentrations were compared with ESF measurements and with estimates derived from the local infiltration rate estimates above the ESF (see Section 2.4). Predictions of porewater chloride concentrations in the EWCD are shown in Figure 5-1.

Chlorine-36 Away from Faults: Excluding the measured $^{36}Cl/Cl$ ratios that represent unambiguous bomb-pulse, the remainder of the samples show higher ratios in the northern ESF than in the southern ESF (see Section 3.2 and Figure 3-1). Because $^{36}Cl/Cl$ ratios in infiltrating water more than 10,000 years ago were higher than they have been for the past 10,000 years (Plummer et al., 1997), the data are consistent with the conceptual model of longer travel times where the PTn is thicker. The data indicate that in the north where the PTn is thicker, travel times greater than 10,000 years contribute to the higher than present-day background ratio. On the other hand, in the south where the PTn is thinner, the data indicate $^{36}Cl/Cl$ ratios more similar to the present-day background, hence less than 10,000-year travel times.

In the three-dimensional transport model, simulated travel times from ground surface to the ESF are dependent on the local infiltration rate, the PTn thickness, and the hydrologic properties of the TCw, PTn, and TSw. A distribution of travel times from ground surface to the ESF is simulated, even when only advective processes are considered, because there are different pathways with different residence times in the matrix and fracture material of each unit between the ground surface and the ESF station. The youngest ages, or earliest arrivals, contributing to a sample represent pathways primarily through fractures, whereas the oldest ages, or late arrivals,

represent pathways mostly through matrix material. Simulations of age distributions or travel times to ESF stations spaced every 100 m were performed and compared with anticipated travel times. Figure 5-2 shows the simulated cumulative age distributions for several northern and southern ESF stations. As most of the flow is in the fractures of the TCw and TSw and in the matrix of the PTn, the distributions show that between 70% and 99%of the ages at any station are about the same. The tails of the distribution represent pathways involving either more fracture flow in the PTn or more matrix flow in the welded units.

The mean travel time to each station is plotted in conjunction with the PTn thickness in Figure 5-3 and with the infiltration rate in Figure 5-4. The anticipated correlation linking travel time to PTn thickness is not particularly obvious. This result is due to the spatially variable infiltration rate above the ESF. As the PTn thins to the south, the infiltration rate also tends to diminish but is still highly variable. Thus, a dominating effect of PTn thickness can not be directly correlated with the mean travel time to the ESF. However, there is a fairly strong relationship between the magnitude of the local infiltration rate and the mean travel time. Figure 5-4 shows a relatively noisy infiltration-rate distribution along the surface trace of the ESF. As infiltration rates increase, mean simulated travel times tend to decrease, and as infiltration rates decrease, mean simulated travel times increase. Figure 5-5 shows that in the southern ESF, where the PTn is thinner, the mean travel times associated with peaks in the infiltration rate tend to be lower than in the north for approximately the same infiltration rate. Because the travel time should be proportional to the PTn thickness and inversely proportional (or at least related) to the local infiltration rate, some form of the ratio between the two may lead to an indicator of mean travel time.

Although the data support a conceptual model of longer travel times to the northern ESF stations than to the southern stations, the simulated mean travel times do not strongly support such a model. Except where the infiltration rate is very small or even zero (near Stations 20+00, 58+00, and 68+00), the simulated mean travel times to the ESF are all less than 10,000 years. If the measured $^{36}Cl/Cl$ ratios are representative of mean travel times, then we must consider which model parameters should be adjusted to lead to longer travel times to the ESF in the north. The two sets of parameters that will have the greatest impact on the simulated travel times are infiltration rates and PTn hydrologic properties.

For this sensitivity study, only the infiltration model is varied for three reasons. First, it has greater uncertainty than the PTn matrix hydrologic properties. Second, because we use the performance-assessment model that requires flow fields developed by Lawrence Berkeley National Laboratory (LBNL), we do not have ready access to a flow model in which physical parameters can be modified and tested easily. And third, we do have access to several flow-field simulations that use different scaled versions of the infiltration model of Flint et al. (1996). Of particular interest is the flow field in which all infiltration rates across the top of the domain are uniformly scaled down by a factor of three. Figures 5-6 and 5-7 show the simulated mean travel time to ESF stations compared with PTn thickness and infiltration rate for the three-dimensional model in which all infiltration rates are scaled down by a factor of three. Whereas the base-case model is referred to as the I infiltration map, this scaled version is referred to as the I/3 infiltration map.

With the I/3 infiltration map, simulated mean travel times start to increase above 10,000 years at stations where the infiltration is not at or near zero. Also, we start to see some correlation between PTn thickness, infiltration rate, and the mean travel time. In the north, where the PTn is thicker, travel times of 10,000 or more are simulated for infiltration rates as large as 0.3 mm/yr. In the south, however, where the PTn is thinner, 10,000-year or more travel times are only simulated for infiltration rates up to about 0.1 mm/yr.

Comparing the results for simulations using the I and I/3 infiltration maps shows that the simulated mean travel time is somewhat proportional to the magnitude of the local infiltration rate above an ESF station. Also, the simulated mean travel times reflect the local variations of the infiltration models. Both are oscillating signals that can change over an order of magnitude in less than 100 m. In fact, if the simulations were performed at a resolution greater than every 100 m, they would probably reflect the same frequency as the infiltration model (Figures 5-4 and 5-7). This process may be partially responsible for the observed variation in $^{36}Cl/Cl$ ratios over very short separation distances (Figure 3-1). However, because the site-scale simulations do not strive to resolve the individual fracture-matrix interactions and small-scale phenomena responsible for each measurement, the general trends are the most useful guide in evaluating the models and assessing potential modifications to consider.

The data indicate a likelihood of longer travel times to the ESF at the northern stations. With the current infiltration model, the thicker PTn alone does not lead to simulations completely consistent with that interpretation of the data. Therefore, one model modification that may be considered is a modification of infiltration rates such that mean travel times to the northern ESF stations are 3 to 5 times greater than those simulated with the base-case model. Regardless of how the infiltration map is scaled, simulated travel times to the ESF near Stations 20+00, 58+00, and 68+00 are tens of thousands of years due to the near zero infiltration rates. In comparing these locations with the measured $^{36}Cl/Cl$ ratios, we see that near the latter two stations, ratios significantly less than present-day background are found, indicating very long travel times. Near Station 20+00, however, $^{36}Cl/Cl$ ratios remain at or above present-day background. The probable reason for this observation is that Station 20+00 is nearer to regions of much higher infiltration (see Figure 5-4). A small degree of lateral flow below Drillhole Wash will bring younger water to Station 20+00, diluting any signals representing slow transport associated with near-zero infiltration rates. This observation leads to a suggestion that not enough lateral flow is simulated above the ESF near Station 20+00. In fact, with the current flow model, flow and transport are almost entirely vertical at all ESF stations. In considering whether PTn hydrologic properties need to be modified to yield more lateral flow, they may also need to be evaluated for simulated velocities in the matrix. Although PTn matrix properties are not varied in this sensitivity analysis, reevaluation may be warranted to examine whether reasonable variation leads to slower velocities and increased solute travel times to the ESF. This reevaluation could be done to corroborate the conceptual model that elevated ratios in the northern ESF are due to 10,000-year or longer travel times.

6. MINERALOGIC AND TEXTURAL STUDIES

6.1 Issues addressed by mineralogic and textural studies

The secondary mineralogy, especially in the fractures, of Yucca Mountain ESF samples reflects the hydrologic, geochemical, structural, and thermal processes that have been in effect at various times during the past 12.7 million years. All of these processes have contributed to the evolution of the present subsurface hydrogeochemical system. The goal of mineralogic and textural studies is to help establish whether there are distinctive mineralogic associations of fast pathways and what they reveal about the development and distribution of such pathways. It is hypothesized that the first-order structural control on the locations of fast pathways is usually the presence of a fault cutting the PTn hydrogeologic unit, but local structures such as fracture networks may influence the lateral distribution of fast flow at the ESF level. Some associations of mineralogy and fast paths may help identify and establish the origins of local distributary features. The applicability of previously identified associations as predictors of fast flow will be tested in the E-W Cross Drift (TRW Environmental Safety Systems Inc., 1998).

Beyond its direct application to isotopic studies of percolation, the mineralogic information reported here is the only data base of fracture mineralogy for the entire ESF that is based on microscopic examination. This data base has been used to update the conceptual model of fracture mineralogy in the unsaturated zone, as incorporated in the site description that will support a license application. The data have also been used to help distinguish between natural alteration and the products of *in situ* thermal tests in the ESF (Levy et al., 1998).

6.2 Previous work

The results reported here build upon mineralogic and textural studies of chlorine-36 geologic samples summarized in Fabryka-Martin et al. (1997a) and TRW Environmental Safety Systems Inc. (1998). The data set in existence when those reports were prepared included mostly samples from the ESF North Ramp and Main Drift. Interpretations of that data set were heavily influenced by the relatively common occurrence of fast paths. Extension of the data set to the southern ESF, where no unambiguous fast flow has been detected, allows this report to present a more balanced assessment of the associations between hydrologic behavior and secondary mineralogy.

6.3 Methods and results

6.3.1 Methods

From each rock sample collected for chlorine-36 analysis, a separate aliquot was reserved for examination by binocular microscopy (magnification up to 400×) and under short-wavelength ultraviolet (UV) illumination. The basic sample characterization included a description of rock textural attributes (e.g., degree of welding, vitric or devitrified condition, presence of brecciation) and an identification of the secondary minerals present on the fracture surfaces (or in the matrix of nonwelded tuffs). The presence of translocated particulates on fracture surfaces or in other void spaces was also noted. The mineralogic information for aliquots that has been examined so

far is summarized in Table 6-1.

6.3.2 Distributions of secondary minerals in the ESF

Calcite

Examination of the subset of analyzed samples for which mineralogic data are available shows that calcite is present at slightly more than half of the sample sites that have received infiltration during the last 50 years (Table 6-1) with 15 of 28 bomb-pulse values obtained for samples associated with calcite. In comparison, calcite is present in 44 of the 126 samples in which a bomb-pulse signal is not unmistakably present. Between Stations 17+00 and 36+00 (an interval in which flow is influenced by the Drill Hole Wash, Diabolus Ridge, and Sundance faults), calcite is present at 19 of the 27 feature-based sample sites, 13 of which are bomb-pulse sites. Intervals of common calcite occurrence but without bomb-pulse sites also exist. A notable example is the interval from Station 63+30 to Station 66+40, which approximately corresponds in stratigraphic position to the Station 17+00 to Station 36+00 interval.

The data set, taken as a whole, indicates that bomb-pulse sites may be slightly more likely to contain calcite than sites without unmistakable bomb-pulse signals. This relationship essentially owes its existence to the zone of abundant calcite and bomb-pulse signals between Stations 17+00 and 36+00. Calcite is clearly an indication that percolating water reached a site where the mineral occurs, but its presence need not be directly related to the hydrologic and structural factors responsible for fast-path behavior. Where these favorable factors exist, the presence of calcite may be taken as an additional but minor predictor of fast flow.

Opal

Amorphous opal (opal-A) is much less common than calcite in the samples and is associated with only one of the bomb-pulse samples from the Bow Ridge fault zone (E011). There are three main modes of occurrence for opal-A in the ESF samples. Opal-A spherules, where present, generally occur only with calcite (Whelan et al., 1996) and, like the calcite, are derived from percolating groundwater. Opal with a drip-like texture is an attribute of alteration localized at and below the Tpcplnc/Tpcpv2 transition in the southern ESF, and may be a product of alteration during the cooling of the host tuff (Levy and Chipera, 1997). This type of occurrence is commonly associated with fractures or breccia zones that cut across the Tpcplnc/Tpcpv2 stratigraphic boundary corresponding to the TCw/PTn hydrogeologic boundary. The potential role of such transmissive features as fast paths has not been confirmed because the features lie below areas of net infiltration too low to sustain fast flow.

The third mode of opal-A occurrence is one in which the identity of the silica as opal-A is uncertain and is queried in Table 6-1. Thin sheets of silica-rich material with a glassy opaline appearance are present on broken-rock surfaces in the vicinities of breccia zones in the southern ESF. In addition to the textural differences, this material differs from the other opal occurrences by an absence of fluorescence in short-wavelength UV light. The two occurrences *(E260, E290)* are in aliquots of samples from the south ramp with values of $^{36}Cl/Cl$ ratios below 350×10^{-15}. It remains an open question whether either the occurrence or survival of this material is linked in

some way to the local deformational history and/or hydrologic environment.

Clays

The expanded data set examined for this report is compatible with earlier observations and interpretations of clay occurrences (Fabryka-Martin et al., 1997a). The mineralogic data set, taken as a whole, does not indicate an association between fast paths (defined by the presence of bomb-pulse ^{36}Cl) and the presence of clay/mordenite. However, in the interval from Station 34+28 to Station 35+93 (Sundance fault), there is a high incidence of both bomb-pulse $^{36}Cl/Cl$ values and clay/mordenite. When the thicknesses of the clay coatings on fractures are taken into account, the coatings in this interval stand out as tending to be thicker than elsewhere.

Occurrences of two or more visually distinctive clay deposits are predominantly associated with the Tptpmn (Topopah Spring middle nonlithophysal) subunit, and are most common in the interval from Station 35+00 to Station 38+00. The existence of multiple clay deposits was originally included as a parameter in the sample description for its potential as an indicator of long-range fine-particulate transport. However, the occurrences of such deposits mostly *within* the Tptpmn suggest that they may be indicators of *local* transport only.

Transported Particulates

For particulates larger than clay particles, it is possible in many cases to determine whether they are different from the local bedrock and have, therefore, been transported to their present location from elsewhere in the geologic section. It is relatively easy to recognize samples in which the fine particulates are highly enriched in vapor-phase or hydrothermal minerals relative to their abundance in the local bedrock, and this enrichment is a good preliminary criterion for documenting evidence of particulate transport. Vapor-phase particulates are typically mixtures of very well formed < 1-mm crystals of tridymite, cristobalite, alkali feldspar, quartz, biotite, Fe-Ti oxides, and hematite. An overall white color is also common for vapor-phase particulates. The presence of translocated particulates within a flow path attests to the existence of connected pore spaces with apertures large enough to permit the passage of the particulates.

Two zones containing multiple samples with transported particulates exist in the ESF. Rock fragments in breccia samples from the Bow Ridge fault, a fast path identified by the presence of bomb-pulse ^{36}Cl signals, are thickly coated by vapor-phase particulates probably derived from overlying rocks rich in vapor-phase material. A second, more extensive interval with common translocated particulates in fractures and breccias exists between Stations 34+32 and 37+68 (including the Sundance fault exposure in Alcove 6). This interval includes eight bomb-pulse sites thought to be related to the Sundance fault (Fabryka-Martin et al., 1997a). Particulate transport in this interval may have been associated in some way with faulting. For example, the faulting process may have caused vapor-phase deposits higher in the stratigraphic section to be pulverized and loosened from fracture surfaces and eventually transported downward through the fracture network.

Manganese minerals

The transition from uncommon to nearly ubiquitous manganese minerals corresponding approximately to the Tptpul/Tptpmn boundary was observed in data collected from the North Ramp. New data for the South Ramp barely mirror this trend because manganese minerals are commonly present on fractures even in the Tptpul. The differences in the North Ramp were attributed to variations in fracture smoothness such that manganese minerals were especially abundant on smooth-surfaced cooling joints that are best developed in the Tptpmn (Fabryka-Martin et al., 1997a). Smooth surfaces might have promoted the transport of manganese within fluid films that could exist more stably on such surfaces than on rougher surfaces. If this interpretation is correct, the similarity of manganese-mineral occurrence between the two subunits in the south ramp may reflect greater similarities of fracture-surface texture.

6.4 Applicability of data to site characterization and performance issues

These data support the conceptual models of infiltration and percolation that are the basis for numerical modeling of the chlorine-36 isotopic data. Numerical modeling of these hydrologic processes, in turn, provides input to site-scale performance-assessment simulations. In addition, as described above, the mineralogic database is the only source of information suitable for updating a site description that supports the draft license application. Through the application to interpretation of thermal-test results, these data also support the characterization of the near-field environment and repository-design issues.

Chlorine-36 isotopic studies of groundwater percolation in the East-West Cross Drift at Yucca Mountain will continue the investigations begun in the ESF. Basic mineralogic and textural characterization has been conducted on samples collected for ^{36}Cl isotopic study of groundwater percolation in the rock mass above the ESF. The mineralogic and textural data collected so far have not defined generally applicable, distinctive characteristics of either fast-path or long water-residence sites in the ESF. These special percolation cases apparently represent relatively minor variations in the hydrologic and geochemical environment of the unsaturated zone, especially when the effects of infiltration, as represented by the mineralogy, are averaged over very long periods of time. However, the distribution of fast flow away from the primary transmissive structure can be a function of local structural development, documented by distinctive mineral deposits, alteration, or textural modification. Specific examples of fast-path systems, in particular, may be distinguished by characteristic differences in mineral abundances and assemblages or textural development that influences hydrologic properties. The Sundance fault and associated subsidiary flow paths constitute the best example of distinctive mineralogy (this report) and flow-path textures (Fabryka-Martin et al., 1997a; TRW Environmental Safety Systems Inc., 1998).

7. MONITORING CONSTRUCTION WATER PLUME MIGRATION

7.1 Construction water issues

A primary objective for monitoring the movement of construction water in the underground drifts at Yucca Mountain is to evaluate the fate, distribution, and effects of construction water and surfactants used during construction. Construction water is used for numerous routine operations in the drifts, including wetting the Tunnel Boring Machine cutter head, wet-drilling for installation of rock bolts, providing dust control on the muck belt, and spraying tunnel ribs to facilitate fracture mapping. This water is subsequently removed from the tunnel by ventilation, imbibition into the walls followed by removal due to dry out, and downward percolation. It is important to determine the fate of the water in order to bound its potential effect on waste isolation.

7.2 Methods and results

7.2.1 Characterization of construction water

Water supplied for the construction of the tunnels at Yucca Mountain is prepared from UE25 J#13 wellwater traced with lithium bromide (LiBr), thereby increasing the Br/Cl ratio to values higher by more than two orders of magnitude than those found in natural porewaters. Construction water has been sampled periodically from 1995 to 1998 from the mixing tank where the LiBr tracer is added, as well as from multiple water outlets within the ESF and Cross Drift. Cl, Br, SO_4, and $^{36}Cl/Cl$ analyses of these samples are summarized in Table 7-1 and plotted in Figure 7-1. Based on 36 samples, these data confirm that the construction water is usually traced with appropriate precision and accuracy to a Br concentration of 19 ± 2 mg/L. The Cl concentration in these samples varies slightly with an average value of 7.0 ± 0.5 mg/L. The Br/Cl ratio has an average value of 2.8 ± 0.3, compared to a value of 0.01 in natural infiltrating porewaters (Fabryka-Martin et al., 1997a). Hence, construction water is assumed to be present in a given porewater sample extracted from ESF drillcore if its Br/Cl ratio is greater than 0.01. In the subsections that follow, more precise thresholds are estimated by statistical analyses of the data using Chauvenet's criterion to identify outliers from a background population (Fabryka-Martin et al., 1997a).

7.2.2 ESF construction water (CWAT) slant holes

Three slanted boreholes (CWAT#1, CWAT#2, and CWAT#3) were drilled downward from the ESF along the main drift to examine the penetration of construction waters in the Topopah Spring Tuff. CWAT#1 and CWAT#2 were drilled in the low-conductivity, highly fractured middle nonlithophysal zone (Tptpmn) near Alcove 6 at Station 37+37 and near Alcove 7 at Station 50+64, respectively. CWAT#3 was drilled at Station 63+92 in the upper lithophysal zone (Tptpul) of the Topopah Spring Tuff. This stratigraphic unit has a higher porosity, larger matrix conductivity, and lower degree of fracturing than the underlying middle nonlithophysal zone (Tptpmn), which in CWAT#3 is found at a depth of 5.2 m.

Porewater salts were extracted from CWAT drillcore for analysis by leaching about 100 grams of rock with an equal mass of deionized water for 48 hours. Samples were gently crushed to 1- to 2-cm size fragments prior to leaching to increase the efficiency of extracting porewater salts. The leached solutions were then analyzed for Cl and Br by ion chromatography. Analytical data are plotted as borehole profiles in Figure 7-2.

Chauvenet's criterion for identifying outliers is the basis of the statistical test used to establish the cutoff Br/Cl ratio above which a sample result is considered to be elevated over natural background (Bevington and Robinson, 1992), i.e., the minimum Br/Cl ratio that would indictate the presence of construction water in a sample. The approach taken in this report is to rank the 65 CWAT data points from lowest to highest value and to calculate a cumulative average and standard deviation for each step of the ranking. One then calculates the number of standard deviations that the highest-value data point lies above the mean as each new data point is included in the cumulative average. These standard deviations are plotted in Figure 7-3, in which they are compared against Chauvenet's criterion for identifying outliers (solid line) as a function of ranking. This criterion states that a data point is an outlier of a Gaussian (normal) distribution if the probability of such a value being that far from the cumulative mean of the ranked data set is less than 0.5% (Bevington and Robinson, 1992). The plot of sample standard deviations versus sample rank (Figure 7-3) varies smoothly within the region of background values but shows an abrupt increase between samples ranked 36 and 37, with Br/Cl ratios of 0.0083 and 0.010. For the latter sample, the calculated number of standard deviations (2.7) exceeds Chauvenet's criterion for identifying statistical outliers for a population of this size. Hence, all values above 0.009 are considered to lie clearly outside the range of the population of background samples.

The apparent penetration depth of the construction water based on analysis of Br/Cl ratios varies considerably with location and shows an irregular profile with multiple concentration peaks (Figure 7-2). Based on analyses of Br/Cl ratios, the shallowest depth of penetration was in CWAT#3, in which construction water was detected only in the top 2 m. This finding substantiates the expectation that water entering the Tptpul unit is initially more likely to be held in the relatively high-porosity, unfractured matrix than to flow deeper through the fracture network. The deepest penetration was in CWAT#2, in which construction water had penetrated to the bottom of the hole (30 m). In CWAT#1, construction water was detected in all samples to a depth of 2.4 m and in isolated occurrences at depths of 6.7 m and 8.5 m, indicating fracture flow in the Tptpmn.

Differences in migration distances are most likely related to differences in water application rates as well as in hydraulic characteristics of the geologic units at each location (Finsterle et al., 1998). For example, prior to drilling of CWAT#2, local flooding occurred at Alcove 7 when over 38,000 liters (10,000 gallons) were accidentally released as a result of a broken water hose.

Typical daily water use in Alcove 7 is on the order of 400 to 800 liters (100 to 200 gallons). It is likely that some of this water entered the upper part of the fractured flow system intercepted by CWAT#2. A comparison between boreholes CWAT#1 and CWAT#3 is more instructive. The more limited migration observed in CWAT#3 is probably because the top 5 m of this hole is in

the upper lithophysal zone (Tptpul) of the Topopah Spring Tuff. CWAT#1 and CWAT#2 are both located in the Tptpmn zone. Br/Cl ratios for the upper part of CWAT#3 are significantly larger than those for the same interval in CWAT#1, suggesting that a larger proportion of construction water may have been retained in the Tptpul matrix in CWAT#3 as compared to the Tptpmn matrix in CWAT#1, in which water flowed deeper through the fracture system.

These observations provide a minimum estimate for the depth of penetration of the construction water. It is possible that the water may have migrated considerably farther through the fracture network than indicated by these data, particularly where the water was applied directly onto the Tptpmn as in the case of CWAT#1 and CWAT#2 (Finsterle et al., 1998).

7.2.3 North Ramp Moisture-Study holes

As part of the USGS PTn Lateral Diversion study, 21 two-m boreholes were dry-drilled horizontally into rocks in the north ramp of the ESF, 18 directly into the right rib and 3 into the right rib of Alcove #4 (the Lower Paintbrush Contact Alcove, LPCA). Samples collected from these holes were from the vapor-phase welded Tpcplnc at the base of the Tiva Canyon Tuff, stratigraphically through the nonwelded and bedded tuffs of the PTn, and into the upper vitrophyre of the Topopah Spring Tuff. Core samples were collected and analyzed for construction water using Br/Cl ratios. Chauvenet's criterion for identifying outliers was used to establish the cutoff ratio above which a sample result is considered to be elevated over natural background; the cutoff value was 0.015 for these samples. Twelve of the 29 samples had ratios above this threshold.

Br/Cl ratios are plotted as a function of distance from the tunnel wall for the samples in Figure 7-4. For the majority of the holes in the PTn bedded and nonwelded tuffs and from the Pah Canyon and Yucca Mountain members, construction water penetrated less than 0.4 m (Figure 7-4(a) and (b)). In the Pah Canyon and Yucca Mountain samples, high Br/Cl ratios indicate most of the construction water stayed in the outermost 10 to 20 cm. The exception to this overall trend was drillhole NR#9 (Tpbt3), in which construction water penetrated to at least 0.9 m.

Only one of the samples from the welded Tiva Canyon and Topopah Spring units (Figure 7-4(c)) shows a slight indication of construction water. However, it is possible that the construction water penetrated to greater distances in these locations than suggested by the data if the water stayed in the fractures and did not have enough contact time to imbibe significantly into the rock matrix.

7.2.4 Cross Drift 2-m holes

Horizontal coreholes are drilled every 50 m in the Cross Drift as soon as possible after mining by the TBM. The holes are cored to a depth of approximately 2 m. Core samples are collected and analyzed for construction water using Br/Cl ratios. Thus far, samples have only been received and processed from the first two 2-m holes at stations 0+50 and 1+00. Br/Cl analyses conducted for samples from these two boreholes shows evidence of construction water only in the outermost sample of the first borehole, indicating a penetration depth of a few cm or less.

7.2.5 Surfactant and water test zones

During construction of the East-West Cross Drift, two test zones were established to evaluate, in detail, the use of water and surfactant as a dust control agent. Test zone 1 started in the Cross Drift at Station 2+38 and ended at Station 2+88. Construction water used in this zone contained only the lithium bromide (LiBr) tracer. Three boreholes were drilled in this test zone at Station 2+53 (Table 7-2). One hole was drilled vertically to a depth of 10 meters, the next hole was drilled at an angle of 45 degrees from vertical about 6 m in depth, and the third hole was a 2m horizontal borehole. The second test zone began at Station 2+88 and ended at Station 3+38. Construction water in this zone contained the surfactant as well as the LiBr tracer. The same array of three boreholes was drilled at Station 3+00 (Table 7-2). All of these borehole arrays were drilled as soon as possible after mining was completed by the TBM. A fourth vertical hole, 15-m deep, was drilled in each test zone between 7 and 10 days after the first 10m hole to evaluate further migration of construction water.

Core from these holes was analyzed for construction water by measuring Br/Cl ratios in soluble salts leached from coarsely crushed drillcore. Application of Chauvent's criterion to the evaluation of these data indicated that samples with Br/Cl ratios greater than 0.009 contained a component of construction water. Table 7-2 summarizes the Br/Cl results for these 8 boreholes and indicates those intervals containing construction water based on this criterion.

- In test zone 1, tracer was observed throughout the 2m horizontal hole and in the topmost few cm of the two vertical holes but not in the top portion of the 6m slant hole. A local isolated peak of construction water salts was present at 0.8 m in the slant hole and at 5.3 m in the 10m vertical hole. These isolated peaks might be attributed to fracture flow.
- In test zone 2, tracer was observed in the outermost meter of the 2m horizontal hole, the top 0.5 m of the slant hole, and throughout the 10m vertical hole, but only in the top 0.3 m of the 15m vertical hole.

Based on the quantity of Br leached from the samples as well as Br/Cl ratios, considerably higher concentrations of Br were present in the uppermost 0.3 m of the slant and vertical holes in test zone 2 than in these holes in test zone 1. No systematic trend with regard to degree of enrichment was observed for the horizontal holes in the two test zones.

7.3 Conclusions

Using data from the CWAT holes, it is apparent that water from TBM operations is lost to the formation through fracture flow. The Br tracer used in the construction water in the ESF main drift was detected to depths exceeding 30 m in the middle non-lithophysal zone of the Topopah Spring Tuff but appeared to be limited to 2 m in the upper lithophysal zone. Two test zones in the Cross Drift were used to verify the depth of penetration of the construction water in the upper lithophysal zone. Construction water in the Cross Drift penetrated less than one meter in two 5m slant holes and two 15m vertical holes, similar to its limited penetration in nonwelded and bedded tuffs in the North Ramp horizontal drillholes. However, it was observed throughout one of the 10m vertical holes, with an isolated occurrence at 5.3 m in the other 10m vertical hole.

8. SEEPAGE IN ALCOVE 1

Alcove 1 is shallow to the surface (37 m) and highly fractured and thus provides excellent conditions to test the hypothesis that, given a sufficiently high flux, water will flow into emplacement drifts. An active infiltration experiment at the surface directly above the end of Alcove 1 was initiated by the USGS on March 9, 1998, by applying a continuous source of water for a long period of time. The amount of water applied was monitored by the USGS to allow calculation of the surface flux. During and following the water application, collectors were used by the USGS to detect seepage into the alcove. The role of Los Alamos was to analyze seepage samples for Cl and Br. These data are reported here.

The drip irrigation system used traced water from the Baker Tank at the North Portal. This same source supplies the construction water used in underground excavations at Yucca Mountain. Table 7-1 shows that 11 samples collected between March and June 1998 had average concentrations of 18.0 ± 0.9 mg/L for Br and 7.0 ± 0.3 for Cl with an average Br/Cl ratio of 2.6 ± 0.2. The above-ground surface area over which the water is applied is 50-ft x 50-ft, with the application rate on the order of 1 to 2 cm day^{-1}. A plastic liner ensures controlled boundary conditions for flux and initial concentrations by reducing evaporative water losses. The low application rate is set to prevent loss of water downslope from the controlled area.

Collection trays in the alcove ceiling were laid out in a grid pattern with each collector corresponding to a ceiling surface area of one ft^2 (Figure 8-1). Two isolated drips of water were detected in the alcove collector for grid location R21 soon after water application began. These appeared to be associated with a rock bolt. However, very low Cl, Br, and SO_4 concentrations indicated that these drips were clearly not construction water and probably resulted from increases in relative humidity in the alcove after the bulkhead doors were installed (Table 8-1, samples W173 and W180).

Water began dripping into the alcove collectors between May 2 and May 5, 1998. Thus far, 138 seep samples have been analyzed out of 816 samples that had been submitted to Los Alamos as of early June 1998. Br concentrations ranged from 9 to 38 mg/L, Cl concentrations ranged from 207 to 1346 mg/L, and SO_4 concentrations ranged from 272 to 1308 mg/L. These concentrations are considerably higher than *in-situ* porewater concentrations measured in ESF and surface-based drillcore samples (sections 2.2 and 2.4). Low Br/Cl ratios confirm that Cl in the seeps does not derive from the construction water applied at the surface. The high Cl concentrations most likely indicate that the construction water is washing out salts accumulated in the overburden for hundreds to thousands of years under low infiltration conditions. In support of this hypothesis, $^{36}Cl/Cl$ ratios for the seeps are all close to the background meteoric ratio, ranging from 483 x 10^{-15} to 610 x 10^{-15} (Table 8-1). A large proportion of the Br in the seeps is likewise probably from natural sources, somewhat obscuring the presence of the construction water tracer. For example, typical Br/Cl ratios for natural porewaters at Yucca Mountain range from 0.005 to 0.02. A sample with a Cl concentration of 500 mg/L would be expected to have a Br concentration between 2.5 and 10 mg/L. One implication of this data set is that it illustrates how salt concentrations in infiltrating porewaters might temporarily increase following an increase in the

natural infiltration rate at a site with low infiltration at the present time until the salts stored in the soil were flushed out. Such an increase might occur due to climate changes or to changes in the site's topographic setting (e.g., rerouting of the channel in a wash).

Figure 8-2 plots Cl and Br concentrations of seeps collected at three locations over a 30-day period. Cl concentrations decrease by almost a factor of two during this time. Br concentrations show a very slight increase throughout the period for which data are available, and Br/Cl ratios show a greater increase with time mostly attributable to the decreasing Cl concentrations.

To evaluate the influence of the shotcrete on the geochemical composition of the seeps, soluble salts were extracted from a sample of shotcrete using two techniques (data in DTN LAJF83122AN98.016). First, leaching shotcrete in deionized water removed about 20 mg Cl kg^{-1}, 0.6 mg Br kg^{-1}, and highly variable quantities of SO_4 ranging from 13 to 200 mg kg^{-1}. Second, the shotcrete was saturated with deionized water, and then the water was extracted using an ultracentrifuge. The extracted water had average concentrations of 27 mg/L as Cl, 0.8 mg/L as Br, and 185 mg/L SO_4. Cl/Br ratios for both techniques averaged 35, and SO_4/Cl ratios ranged from 0.8 to 7.4. The conclusion from these data is that Cl and Br concentrations of the seeps will not change by percolation during shotcrete although the shotcrete may possibly increase SO_4 concentrations depending upon contact time and the concentration in the infiltrating water as it enters the shotcrete.

9. REGIONAL DISTRIBUTION OF CHLORINE-36, CHLORIDE, BROMIDE, AND SULFATE

9.1 Local groundwater

Concentrations of Cl, Br, and SO_4 and $^{36}Cl/Cl$ ratios are reported for a number of local boreholes and wells in Table 9-1. With a few exceptions, one striking pattern in the Cl concentrations and $^{36}Cl/Cl$ ratios is the uniformity of values. Most of the $^{36}Cl/Cl$ ratios lie within the narrow range of 457×10^{-15} to 583×10^{-15}, implying groundwater ages less than 10,000 years. These 22 samples average $523 (\pm 33) \times 10^{-15}$, indistinguishable from present-day meteoric background. This constancy holds true for samples collected from different depths within a given well (e.g., USW G-2 and USW UZ-14) as well as for samples collected over time from the same well. Exceptions to this trend—which were not included in the average reported above—are easily explained:

- UE-29 a#1 and UE-29 a#2 are situated adjacent to Fortymile Wash and thus receive recharge of water containing bomb-pulse ^{36}Cl, resulting in high $^{36}Cl/Cl$ ratios.
- Drilling fluid lost in USW G-1 is believed to be the mechanism for having introduced bomb-pulse ^{36}Cl into nearby USW UZ-1.
- Among the samples with low $^{36}Cl/Cl$ ratios, UE#25 p1 taps the carbonate aquifer and the atmospheric signal in this groundwater has been diluted by Cl leached from the aquifer; this hypothesis is supported by the high Cl/Br ratio.
- Water in UE-25 UZ#16 was contaminated with salt used during water-level measurements, resulting in high Cl/Br ratios and a low $^{36}Cl/Cl$ ratio (42×10^{-15}). The salt used for these measurements has a $^{36}Cl/Cl$ ratio of 30×10^{-15} and no detectable Br.
- Low Cl/Br ratios also indicate the presence of traced water in many of the UE-25 c#3 samples, as well as the samples from USW WT-24 (see section 9.2) and UE-25 WT#17. Because the traced water is prepared from J-13 water, its $^{36}Cl/Cl$ ratio is indistinguishable from the local background.

Cl concentrations for 29 uncontaminated samples listed in Table 9-1 range from 6.0 to 7.9 mg/L and average 6.7 ± 0.5 mg/L. Samples excluded from this average are the following:

- wells contaminated with traced or untraced construction water (UE-25 c#3, 1996-97 samples; UE-25 WT#17, USW WT-24, USW UZ-1),
- a well contaminated with tape salt (UE-25 UZ#16),
- wells receiving recharge from Fortymile Wash (UE-29 a#1 and UE-29 a#2),
- a well tapping an aquifer below the water-table aquifer (UE#25 p1), and
- a sample not collected under an approved quality assurance protocol (USW VH-1).

9.2 Sample contamination in USW WT-24

USW WT-24 is approximately 1.5 km north of USW UZ-14. Water was perched above either the moderately welded base of the Topopah Spring Tuff (Tptpv2, depth to top of unit is 512 m) or the basal vitrophyre of the Topopah Spring Tuff (Tptpv3, depth to top of unit is 524.5 m) (Flint, 1998b). The perching layer was difficult to determine with more precision because of inadequate core preservation for moisture analyses. The regional water table was encountered at a depth of 670 m. Coring began in lithostratigraphic unit Tptpv3 and extended downward through Tptpv2, the nonwelded base of the Topopah Spring Tuff (Tptpv1), the pre-Topopah Spring bedded tuff (Tpbt1), and the nonwelded and zeolitized Calico Hills formation (Tac).

Some of the samples from the Tptpv2 and Tptpv3 units were analyzed for Br/Cl ratios to assess the extent to which measured saturation and geochemical data were representative of natural conditions. J-13 water traced with lithium bromide was accidentally released into the WT-24 wellbore when the check valve on the Moyno pump was opened while the pump was being primed for the purpose of sampling perched water from the well. Subsequently, a cement plug was installed, and the borehole was deepened to below the water table after drilling through this plug. Elevated Br/Cl ratios for core samples from the depth interval 515 to 529 m (Tptpv3 and Tptpv2) clearly show the presence of construction water in the pores of these units (Table 9-2). Its presence in groundwater from the aquifer is clearly shown by the low Br/Cl ratio (Table 9-1). n issue needing evaluation is the extent to which the contaminated perched water may have migrated into the pores of the unsaturated zone as well, thereby influencing the moisture analyses of the drillcore.

9.3 Regional wells and springs

Concentrations of Cl, Br, and SO_4 and $^{36}Cl/Cl$ ratios are reported for a number of regional wells and springs in Table 9-3. The wells, which are on Pahute Mesa and approximately up-gradient of Yucca Mountain, have $^{36}Cl/Cl$ ratios within the range calculated for the local groundwaters in section 9.1. Three of the Cl concentrations also fall within the range calculated for the local groundwaters, but two other samples have the highest concentrations among the data set of uncontaminated groundwaters (11 to 12 mg/L).

Chemical and isotopic characteristics of regional spring samples are highly variable (Table 9-3). These range from low salt concentrations and high $^{36}Cl/Cl$ ratios measured for springs discharging young water containing bomb-pulse ^{36}Cl (e.g., Water Pipe Butte Spring), to high salt concentrations and low $^{36}Cl/Cl$ ratios for springs discharging water with a long subsurface residence time. The latter waters have had time to interact with the rocks. In these cases, Cl leached from the formation increases the Cl/Br ratio and dilutes the $^{36}Cl/Cl$ ratio (e.g., Tecopa Hot Springs).

10. CONCLUSIONS

10.1 Geochemical and isotopic data

This report updates the Yucca Mountain data base for porewater Cl concentrations and $^{36}Cl/Cl$ ratios. The expanded data base of porewater Cl concentrations is consistent with data collected earlier, particularly in verifying a trend of higher concentrations in the ESF South Ramp samples than in the samples from the North Ramp and Main Drift of the ESF. These differences translate into indicating infiltration rates that are lower in the southern ESF than in the north. Infiltration rates for the North Ramp and Main Drift, based on porewater Cl concentrations, are in reasonable agreement with rates based on a numerical model of infiltration (Flint et al., 1996), but the rates for the South Ramp are lower than the predictions of the numerical model. On this basis results, it is recommended that the numerical infiltration model be modified to allow lower infiltration above the South Ramp.

New $^{36}Cl/Cl$ analyses of samples from the ESF South Ramp confirm that the southern part of the ESF has lower $^{36}Cl/Cl$ values than the northern part. None of the samples from beyond Station 45+00 have ratios above the bomb-pulse threshold value of 1250×10^{-15}. The South Ramp data confirm that the existence of major faults offsetting the PTn unit is by itself insufficient for fast flow to occur; the additional requirements of adequate net infiltration and fast travel times through the alluvial cover must also be satisfied.

The detection of bomb-pulse ^{36}Cl in drillcore from Niche 3566 (Niche 1) confirms the previously observed lateral migration of fast flow northward away from the fault zone proper. Bomb-pulse levels of ^{36}Cl were detected in samples from the Sundance and Ghost Dance faults in Alcove 6. Without information about the dip of the faults in the alcove, the conceptual model of fast-path flow can not be fully tested for this location. The dip determines where the fault would break the PTn unit above the alcove, and the conceptual model predicts that bomb-pulse ^{36}Cl should occur in a zone vertically below the break in the PTn.

Chlorine-36 was analyzed in surface soils and surface runoff at Yucca Mountain to test whether bomb-pulse ^{36}Cl still resides at the surface and to characterize the isotopic composition of waters infiltrating into the bedrock at present. The data confirm that water entering the bedrock today will still contain bomb-pulse ^{36}Cl and that bomb-pulse ^{36}Cl has not yet been completely removed from the soil profile. A comparison of 1998 runoff data with data collected for 1995 runoff does, however, reveal a downward trend of $^{36}Cl/Cl$ from 1995 to 1998.

10.2 Statistical analyses of ESF chlorine-36 data

A statistical analysis framework was developed to quantitatively assess a) whether measured $^{36}Cl/Cl$ ratios indicate the presence of bomb-pulse ^{36}Cl, b) the correlation between bomb-pulse observations and geologic-system attributes (covariates) such as sample location characteristics, proximity to faults, and overlying alluvial thickness, and c) the spatially varying trend of the background $^{36}Cl/Cl$ ratio distribution. The analysis leads to a mixture distribution which explains the observations very well. One or more components of the mixture distribution

represent the bomb-pulse signal while two components are needed to represent the background. The two background distributions correlate well with the thinning of the PTn from north to south. They also support the hypothesis that background $^{36}Cl/Cl$ ratios should be higher where the PTn is thicker due to travel times that exceed 10,000 years.

One of the key capabilities associated with this statistical approach is a method for assigning the probability that each observation contains a bomb-pulse component. This also results in a visual description of the background trend through the ESF. Analysis of the correlation between the system attributes (covariates) and the probability that a sample contains bomb-pulse yields significant interpretative power to the data analysis. Bomb-pulse measurements correlate well with TSw samples from intersecting joints and PTn samples at stratigraphic contacts. The analysis also indicates that there is a significant correlation between the highest infiltration rates and bomb-pulse in the TCw, while there is a significant correlation between samples from faults or joints near faults and bomb pulse in the lower PTn and TCw units. Although the statistical analysis is preliminary, it is a valuable quantitative tool to test the ^{36}Cl data for the presence of bomb-pulse as well as for correlations between structural and hydrologic system controls on the observed and predicted ratios. Within the PTn, for example, the bomb pulse component is strongly associated with fault zones, but stratigraphic contacts appear to provide lateral pathways away from such zones. Similarly, in the TSw, the bomb pulse component is found in fault rocks in fault zones and wall rock immediately adjacent to such faults, but again steeply dipping joints allow migration away from these zones, particularly joints that are known to intersect other, more gently dipping joints.

10.3 Site-scale flow and transport models

Predictive numerical simulations of ^{36}Cl and chloride migration from the ground surface to the ESF and the East-West Cross Drift (EWCD) were performed using the YMP Performance Assessment radionuclide transport model. The numerical simulations were compared to measured values and to predictions based on conceptual models of infiltration, percolation, and isotopic variations over time. The model simulations of chloride concentrations in the ESF North Ramp and Main Drift porewaters are in general accord with the measured values whereas the simulated concentrations in the South Ramp are well below the measured values. This provides an indication that, in the vicinity of the south ramp, the estimated infiltration rates used in the flow model may require reassessment.

The simulations in this report focus on the site-scale transport of ^{36}Cl away from faults. Based on the conceptual model and its support from the statistical analysis, the modeling serves to test whether the integrated site-scale model is consistent with the data interpretation. The integrated site-scale model includes the surface infiltration model which feeds the site-scale flow model which, in turn, feeds the site-scale transport model. In this analysis, travel times from the surface to the ESF stations is used for the interpretation. The data and their statistical interpretation show background signals greater than present day background in the northern ESF and approximated present day background in the southern ESF. Therefore, the model was used to test whether simulated travel times greater than 10,000 years to the ESF were more prominent in the northern ESF than in the south.

Simulations of ground-water travel times in portions of the rock mass that are away from faults do not support certain elements of the conceptual model of solute travel times to the ESF. Specifically, simulated travel times do not show a significant relationship with thickness of the PTn unit, but do reflect the influence of spatially varying infiltration rates. The infiltration rates vary significantly over distances less than 100m but do not have a specific trend with distance through the ESF. Similarly, simulated travel times vary on the same scale as the infiltration map, but do not reflect strongly the trend of thinning PTn to the south. Changing the magnitude of the infiltration rates directly affects the simulated travel times, but will only lead to a trend in the simulated travel times if a specific trend is built into a modification of the existing infiltration map. However, such a trend may evolve if the discrepancy between simulated and observed porewater chloride leads to adjustments to the infiltration map only in the south. Another adjustment that may be warranted based on this analysis is a modification of hydrologic properties to incorporate more lateral flow. This would help corroborate the low porewater chloride measurements found in the northern ESF below regions with very low estimated infiltration rates (hence expected high chloride concentrations).

10.4 Mineralogic and textural analyses of ESF samples

Mineralogic and textural characterization was undertaken for a subset of the samples analyzed for $^{36}Cl/Cl$, in part to identify associations between fast paths (as identified by the presence of bomb-pulse ^{36}Cl) and the mineralogic or textural settings of the sample sites. The samples from the ESF main drift within several hundred meters north and south of the Sundance fault, an interval that includes many bomb-pulse sites (but only north of the fault), are distinguished by the common presence of calcite, thick clay coatings on fracture walls, and translocated particulates in the fractures. The common calcite may be simply a function of the stratigraphic level at which the ESF crosses the fault, unrelated to the existence of fast paths associated with the fault. The presence of clay and particulate deposits attests to particularly well-connected fractures favorable for particulate transport and, perhaps, for lateral dispersion of fast flow moving through the fault zone.

10.5 Construction water migration

In order to help bound the potential effect of migrating construction water on waste isolation, the compositions of extracted porewaters and salts were evaluated for evidence of contamination by construction water tagged with lithium bromide. The observed range of Cl/Br values indicates that analyzed porewater samples from the ESF horizontal boreholes are almost all contamination-free, with construction water having traveled no more than 10 to 20 cm. The Br/Cl ratios of salts in samples from the CWAT holes angle-drilled into the floor of the ESF provide evidence of construction-water migration only 2 m downward within the upper lithophysal unit of the Topopah Spring Tuff (Tptpul). This finding supports the expectation that water entering the Tptpul unit is initially held in the relatively high-porosity, unfractured matrix. In comparison, penetration of construction water to the 30-m total depth of a hole was detected within the more highly fractured middle nonlithophysal unit of the Topopah Spring Tuff (Tptpmn). Penetration rates, beside depending on the fracture characteristics of the rock, probably depend on the rate

and amount of construction water released at a given location.

ACKNOWLEDGMENTS

This work was supported and managed by the U.S. Department of Energy, Yucca Mountain Site Characterization Office (YMP) as part of the Civilian Radioactive Waste Management Program. Data acquired as part of this activity and presented in this report were developed under YMP quality assurance procedures; their QA status and traceability to data tracking numbers are given in Appendix B.

The YMP Test Coordination Office, particularly A. Mitchell, supported field sample collection in the ESF tunnel. We are grateful for extensive sampling guidance and advice on geologic and hydrologic aspects from D.S. Sweetkind and A. Flint. Numerous colleagues and students assisted with the sampling and sample processing activity during the period covered by this report, including W. Guertal, D. Hudson, Q. Snead, K. Tripp, S. Winters, and J. Hildebrand. D. Elmore, P. Sharma, and T. Miller at PRIME Laboratory worked assiduously to ensure timely and accurate isotopic analyses. R. Eckhardt provided welcome editorial assistance. A technical review by C. Harrington is also appreciated.

11. REFERENCES

Best, N.G., Spiegelhalter, D.J. , Thomas, A., and Brayne, C.E.G. 1996. Baysian analysis of realistically complex models. *J. Royal Statistical Society A* 159: 323-342.

Bevington, P.R., and Robinson, D.K. 1992. *Data Reduction and Error Analysis for the Physical Sciences*, p. 328. McGraw-Hill, Inc., New York.

Bodvarsson, G.S., and Bandurraga, T.M., editors. 1996. Development and calibration of the three-dimensional site-scale unsaturated zone model of Yucca Mountain, NV. Lawrence Berkeley National Laboratory Technical Report LBNL-39315. (MOL.19970211.0176)

Bodvarsson, G.S., Bandurraga, T.M., and Wu, Y.S. 1997. The site-scale unsaturated zone model of Yucca Mountain, Nevada, for the Viability Assessment. Lawrence Berkeley National Laboratory Technical Report LBNL-40378. (MOL.19971014.0232)

Buesch, D.C., Spengler, R.W., Moyer, T.C., and Geslin, J.K. 1996. Proposed stratigraphic nomenclature and macroscopic identification of lithostratigraphic units of the Paintbrush Group exposed at Yucca Mountain, Nevada. U.S. Geol. Surv. Open File Rep. 94-469, p. 52. (MOL.19970205.0059)

Carlin, B.P., and Louis, T.A. 1996. *Bayes and Empirical Bayes Methods for Data Analysis.* Chapman & Hall, London, xvi+399 pp.

Clayton, R.W., Zelinski, W.P., and Rautman, C.A. 1997. ISM2.0: A 3-D geological framework and integrated site model of Yucca Mountain, ID B0000000-01717-5700-00004 Rev 0. Civilian Radioactive Waste Management System Management and Operating Contractor, February 1997. (MOL.19970122.0053)

Day, W.C., Potter, C.J., Sweetkind, D.S., Dickerson, R.P., and San Juan, C.J. 1998. Bedrock geologic map of the central block area, Yucca Mountain, Nye County, Nevada. U.S. Geol. Surv. Misc. Invest. Ser. I-2601, 1:6000 scale, 2 plates with text. (DTN GS6-708314221.001; TIC Catalog No. 233245)

Fabryka-Martin, J.T., Roach, J.L., Winters, S.T., and Wolfsberg, L.E. 1998a. Using chloride to trace water movement in the unsaturated zone at Yucca Mountain. *Proceedings, 1998 8th Annual International High-Level Radioactive Waste Management Conference*, pp 264-268. American Nuclear Society, La Grange Park, IL.

Fabryka-Martin, J.T, Wolfsberg, A.V., Levy, S.S., Roach, J.L., Winters, S.T., Wolfsberg, L.E., Elmore, D., and Sharma, P. 1998b. Distribution of fast hydrologic paths in the unsaturated zone at Yucca Mountain. *Proceedings, 1998 8th Annual International High-Level Radioactive Waste*

Management Conference, pp 93-96. American Nuclear Society, La Grange Park, IL..

Fabryka-Martin, J.T., Wolfsberg, A.V., Dixon, P.R., Levy, S.S., Musgrave, J., and Turin, H.J. 1997b. Summary report of chlorine-36 studies: systematic sampling for chlorine-36 in the Exploratory Studies Facility. Los Alamos National Lab. Report LA-13352-MS, Yucca Mountain Project Milestone Report 3783M. (MOL.19970211.0036)

Fabryka-Martin, J.T., Flint, A.L., Sweetkind, D.S., Wolfsberg, A.V., Levy, S.S., Roemer, G.J.C., Roach, J.L., Wolfsberg, L.E., and Duff, M.C. 1997a. Evaluation of flow and transport models of Yucca Mountain, based on chlorine-36 studies for FY97. Los Alamos National Laboratory Yucca Mountain Project Milestone report SP2224M3. (MOL.1998024.0916)

Fabryka-Martin, J.T., Wightman, S.J., Murphy, W.J., Wickham, M.P., Caffee, M.W., Nimz, G.J., Southon, J.R., and Sharma, P. 1993. Distribution of chlorine-36 in the unsaturated zone at Yucca Mountain: An indicator of fast transport paths. In *Proc., FOCUS '93: Site Characterization and Model Validation*, pp. 58-68. Amer. Nucl. Soc., La Grange Park, IL. (NNA19940614.0063)

Finsterle, S., James, A.L., Wang, J.S.Y., Fabryka-Martin, J.T., Wolfsberg, L.E., Flint, A.L., and Guertal, W.R. 1998. Model prediction of local plume migration from the Cross Drift. Lawrence Berkeley National Laboratory Milestone SP33S3M4.

Flint, L.E., and Flint, A.L. 1995. Shallow infiltration processes at Yucca Mountain, Nevada - neutron logging data 1984-93. U.S. Geol. Surv. Water Resource Invest. Rept. 95-4035, 46 pp. (MOL.19960924.0577)

Flint, A.L., Hevesi, J.A., and Flint, L.E. 1996. Conceptual and numerical model of infiltration for the Yucca Mountain Area, Nevada. U.S. Geol. Surv. Yucca Mountain Project Milestone Rep. 3GUI623M, U.S. Geol. Surv. Water Resour. Invest. Rep. (USGS report number pending USGS Director's approval), DOE Milestone 3GUI623M. (MOL.19970409.0087; DTN GS960908312211.003)

Flint, L.E. 1998a. Characterization of hydrogeologic units using matrix properties, Yucca Mountain, Nevada. U.S. Geological Survey Water Resources Investigation Report 97-4243, Denver, CO. (MOL.19980429.0512)

Flint, L.E. 1998b. Milestone SPG33UM4. U.S. Geological Survey memorandum submitted to Robert Craig on July 1, 1998.

Hevesi J.A., Flint, A.L., and Istok, J.D. 1992. Precipitation estimation in mountainous terrain using multivariate statistics: Part II. Isohyetal maps. *J. Appl. Meteor.* 31: 677-688. (NNA.19930427.0167)

Levy, S.S., and Chipera, S.J. 1997. Updated mineralogic and hydrologic analysis of the PTn hydrogeologic unit, Yucca Mountain, Nevada, as a barrier to flow. Los Alamos National Laboratory YMP milestone report SP321DM4, 49 pp. (DTN LASL831322AQ97.001)

Levy, S.S., Chipera, S.J., and Snow, M. 1998. Mineralogic products of the ESF single heater test. Los Alamos National Laboratory Yucca Mountain Project report SP1410M4. (DTN LASL831151AQ98.001)

Moyer, T.C., Geslin, J.K., and Flint, L.E. 1996. Stratigraphic relations and hydrologic properties of the Paintbrush Tuff nonwelded (PTn) hydrologic unit, Yucca Mountain, Nevada. U.S. Geol. Surv. Open File Rep. 95-397, 151 pp. (MOL.19970204.0216)

Murphy, W.M. 1998. Commentary on studies of ^{36}Cl in the Exploratory Studies Facility at Yucca Mountain, Nevada. In *Scientific Basis for Nuclear Waste Management XXI*, I. G. McKinley and C. McCombie, editors. *Materials Research Society Symposium Proceedings* 506: 407-414.

Plummer, M.A., Phillips, F.M., Fabryka-Martin, J.T., Turin, H.J., Wigand, P.E., and Sharma, P. 1997. Chlorine-36 in fossil rat urine: An archive of cosmogenic nuclide deposition during the past 40,000 years. *Science* 277: 538-541. (MOL.19980213.0010)

Potter, C.J., Dickerson, R.P., and Day, W.C. 1995. Nature and continuity of the Sundance fault, Yucca Mountain, Nevada. U.S. Geological Survey unpublished administrative report (Denver, CO). (MOL.19960403.0161)

Robinson, B.A., Wolfsberg, A.V., Viswanathan, H.S., Gable, W., Zyvoloski, G. A., and Turin, H.J. 1996. Modeling of flow, radionuclide migration, and environmental isotope distributions at Yucca Mountain. Los Alamos National Laboratory YMP Milestone 3672. (MOL.19970103.0042)

Robinson, B.A., Wolfsberg, A.V., Zyvoloski, G.A., and Gable, C.W. 1995. An unsaturated-zone flow and transport model of Yucca Mountain. Los Alamos National Laboratory YMP Milestone 3468. (MOL.19980213.0091)

Robinson, B.A., Wolfsberg, A.V., Viswanathan, H.S., Bussod, G.Y., Gable, C.W., and Meijer, A. 1997. The site-scale unsaturated-zone transport model of Yucca Mountain. Los Alamos National Lab. Yucca Mountain Project Milestone SP25BM3. (MOL.19980203.0570)

Sonnenthal, E.L., and Bodvarsson, G.S. 1998. Percolation flux estimates from geochemical and thermal modeling. *Proceedings, 1998 8th Annual International High-Level Radioactive Waste Management Conference*, pp 130-132. American Nuclear Society, La Grange Park, IL.

Spiegelhalter, D.J., Thomas, A., Best, N.G., and Gilks, W.R. 1995. BUGS: Bayesian inference using Gibbs sampling, Version 0.50. MRC Biostatistics Unit, Cambridge (see also http://www.mrc-bsu.cam.ac.uk/bugs/mainpage.html).

Titterington, D.M., Smith, A.F.M., and Makov, U.E. 1985. *Statistical Analysis of Finite Mixture Distributions*. John Wiley and Sons, Chichester, x+243 pp.

TRW Environmental Safety Systems Inc. 1998. Predictions of hydrologic, geochemical, and microbiological properties and conditions in the East-West Cross Drift (EWCD). BABEA0000-01717-5705-00003, Rev. 0, 82 pp.

Whelan, J.F., Moscati, R.J.,. Allerton, S.B.M., and Marshall, B.D. 1996. Applications of isotope geochemistry to the reconstruction of Yucca Mountain paleohydrology. U.S. Geological Survey milestone report 3GQH257M to DOE-YMPSCO. (MOL.19980205.0693)

Wittwer, C., Chen, G., Bodvarsson, G.S., Chornack, M., Flint, A., Flint, L., Kwicklis, E., and Spengler, R. 1995. Preliminary development of the LBL/USGS three-dimensional site-scale model of Yucca Mountain, Nevada. Lawrence Berkeley National Laboratory Technical Report LBL-37356/UC-814. (TIC Catalog No. 221218)

Wolfsberg, A.V., Robinson, B.A., Roemer, G.J.C., and Fabryka-Martin, J.T. 1998. Modeling flow and transport pathways to the potential repository horizon at Yucca Mountain. *Proceedings, 1998 8th Annual International High-Level Radioactive Waste Management Conference*, pp 81-84. American Nuclear Society, La Grange Park, IL.

Wu, Y.S., Ritcey, A.C., Ahlers, C.F., Mishra, A.K., Hinds, J.J., and Bodvarsson, G.S. 1997. Providing base-case flow fields for TSPA-VA: Evaluation of uncertainty of present day infiltration rates using DKM/base-case and DKM/weeps parameter sets. Lawrence Berkeley National Laboratory Yucca Mountain Project Milestone SLX01LB2. (MOL.19980501.0461)

Yang, I.C., Turner, A.K., Sayer, T.M., and Montazer, P. 1988. Triaxial-compression extraction of pore water from unsaturated tuff, Yucca Mountain, Nevada. U.S. Geol. Surv. Water Resour. Invest. Rep. 88-4189. (NNA.19890309.0161)

Yang, I.C., Davis, G.S., and Sayer, T.M. 1990. Comparison of pore-water extraction by triaxial compression and high-speed centrifugation method. In *Minimizing Risk to the Hydrologic Environment*, pp. 250-259. Dubuque, Iowa, Kendall/Hunt Publ. Co. (NNA.199009170051)

Yang, I.C., Rattray, G.W., and Yu, P. 1996. Interpretations of chemical and isotopic data from boreholes in the unsaturated zone at Yucca Mountain, Nevada. U.S. Geol. Surv. Water Resour. Invest. Rep. 96-4058. (TIC Catalog No. 236260)

BA0000000-01717-5700-00007
Milestone SP32D5M3

Yang, I.C., Yu, P., Rattray, G.W., and Thorstenson, D.C. 1998. Hydrogeochemical investigations and geochemical modeling in characterizing the unsaturated zone at Yucca Mountain, Nevada. U.S. Geol. Surv., Water Resour. Invest. Rep. (in press).

Table 2-1. Weighted-average chloride, bromide, and sulfate concentrations measured for ESF porewater samples

Borehole ID	ESF station[1]	Hydro-geologic unit[2]	Lithologic unit[2]	# samples included in average	Pore-water vol. (mL)	Average concentration (mg/L)			Cl/Br	SO_4 /Cl	Infil. (mm /yr)
						Cl	Br	SO_4			
North Ramp											
ESF-NR-MOISTSTDY#1a	7+27	TCw	Tpcplnc	6	67.1	19.7	0.163	24.0	121	1.2	5.4
ESF-NR-MOISTSTDY#2	7+50	TCw	Tpcplnc/mw	4	73.8	18.4	0.171	26.6	108	1.5	5.7
ESF-NR-MOISTSTDY#3	7+70	TCw	Tpcplnc/mw	7	48.5	40.3	0.237	51.9	170	1.3	2.6
ESF-NR-MOISTSTDY#4	7+72	PTn	Tpcpv2	2	26.5	47.1	0.287	59.4	164	1.3	2.2
ESF-NR-MOISTSTDY#5	7+83	PTn	Tpcpv2	2	0.6	27.9	0.207	31.2	135	1.1	3.8
ESF-NR-MOISTSTDY#6	8+21	PTn	Tpcpv1	1	0.5	69.2	0.706	92.5	98	1.3	1.5
ESF-NR-MOISTSTDY#7	8+67	PTn	Tpbt4	2	16.4	15.1	0.137	24.1	110	1.6	7.0
ESF-NR-MOISTSTDY#8	8+70	PTn	Tpy	2	5.6	15.7	0.186	24.0	85	1.5	6.7
ESF-NR-MOISTSTDY#9	8+73	PTn	Tpbt3	1	0.3	5.7	0.343	8.1	17	1.4	18.6
ESF-NR-MOISTSTDY#10	8+80	PTn	Tpbt3	3	4.2	15.0	0.152	27.9	98	1.9	7.0
ESF-NR-MOISTSTDY#11	8+92	PTn	Tpp	1	1.3	6.7	0.056	11.0	119	1.6	15.7
ESF-NR-MOISTSTDY#13	10+08	PTn	Tpbt2	4	74.1	12.0	0.116	21.0	103	1.8	8.8
ESF-LPCA-MOISTSTDY#2	Alcove 4	PTn	Tpbt2 arg	1	0.8	17.7	0.251	35.7	71	2.0	6.0
ESF-LPCA-MOISTSTDY#3	Alcove 4	PTn	Tpbt2	4	44.4	17.5	0.239	41.8	73	2.4	6.0
ESF-NR-MOISTSTDY#15	10+54	PTn	Tptrv3/rv2	1	1.1	20.8	0.169	37.1	123	1.8	5.1
ESF-NR-MOISTSTDY#16	10+69	PTn	Tptrv2	2	5.5	12.9	0.124	23.9	104	1.8	8.2
Main Drift											
ESF-MD-NICHE3566#1	Niche 3566	TSw	Tptpmn	2	0.3	16.6	0.190	21.0	88	1.3	6.3
ESF-MD-NICHE3566#2	Niche 3566	TSw	Tptpmn	2	0.1	23.3	0.240	18	97	0.8	4.5
ESF-MD-NICHE3566LT#1	Niche 3566	TSw	Tptpmn	1	0.1	26.8	NA	17.8	NC	0.7	3.9
ESF-MD-WATMOVE#9	39+50	TSw	Tptpmn	1	0.1	14.5	NA	11.7	NC	0.8	7.3
ESF-MD-WATMOVE#10	41+50	TSw	Tptpmn	1	0.1	22.6	NA	28.3	NC	1.3	4.7
ESF-MD-WATMOVE#4	51+50	TSw	Tptpmn	1	0.1	15.4	0.174	8.1	89	0.5	6.8
South Ramp											
ESF-SR-MOISTSTDY#6	63+88	TSw	Tptpul	1	0.2	87.2	0.348	106.2	250	1.2	1.2
ESF-SR-MOISTSTDY#7	64+80	TSw	Tptpul	1	0.2	63.1	0.273	63.6	231	1.0	1.7
ESF-SR-MOISTSTDY#9	66+41	TSw	Tptrn	1	0.03	85.5	0.432	100.1	198	1.2	1.2
ESF-SR-MOISTSTDY#10	66+48	PTn	Tptrv2	2	2.1	17.2	0.136	37.3	126	2.2	6.1

Borehole ID	ESF station[1]	Hydro-geologic unit[2]	Lithologic unit[2]	# samples included in average	Pore-water vol. (mL)	Average concentration (mg/L)			Cl/Br	SO_4 /Cl	Infil. (mm /yr)
						Cl	Br	SO_4			
ESF-SR-MOISTSTDY#11	66+58	PTn	Tptrv3	1	0.9	26.5	0.160	42.0	166	1.6	4.0
ESF-SR-MOISTSTDY#12	66+68	PTn	Tpbt2	1	1.3	29.7	0.178	32.7	167	1.1	3.5
ESF-SR-MOISTSTDY#13	66+79	PTn	Tpbt2	2	26.6	32.2	0.148	27.3	218	0.8	3.3
ESF-SR-MOISTSTDY#14	66+96	PTn	Tpbt4	1	1.5	33.0	0.173	39.6	190	1.2	3.2
ESF-SR-MOISTSTDY#15	67+04	TCw	Tpcpv1	1	1.5	26.8	0.182	33.5	148	1.2	3.9
ESF-SR-MOISTSTDY#16	67+21	TCw	Tpcpv1	2	36.6	39.1	0.150	40.3	262	1.0	2.7
ESF-SR-MOISTSTDY#17	67+29	TCw	Tpcplnc/Tpcpv1	1	0.3	55.3	0.420	69.4	132	1.3	1.9
ESF-SR-MOISTSTDY#18r	67+48	TCw	Tpcplnc	1	0.04	45.3	<0.15	50.0	>300	1.1	2.3
ESF-SR-MOISTSTDY#19	68+26	TSw	Tptpul	1	0.9	17.1	0.109	13.1	158	0.8	6.2
ESF-SR-MOISTSTDY#20	69+36	TSw	Tptrn	1	0.4	150.2	1.202	78.1	125	0.5	0.7
ESF-SR-MOISTSTDY#21	70+54	PTn	Tpbt2	2	20.7	80.9	0.294	94.1	275	1.2	1.3
ESF-SR-MOISTSTDY#22	70+56	PTn	Tpbt2	2	18.7	103.0	0.370	126.9	279	1.2	1.0
ESF-SR-MOISTSTDY#22r	70+56	PTn	Tpbt2	2	36.9	96.1	0.423	124.6	227	1.3	1.1
ESF-SR-MOISTSTDY#25	74+35	TSw	Tptrn	1	0.3	34.5	0.172	27.2	201	0.8	3.1
ESF-SR-MOISTSTDY#27	74+44	TSw	Tptrv1	3	39.5	38.9	0.153	41.1	254	1.1	2.7
ESF-SR-MOISTSTDY#28	74+46	PTn	Tptrv2	1	1.7	43.2	0.209	51.9	207	1.2	2.4
ESF-SR-MOISTSTDY#29	74+53	PTn	Tptrv3	2	36.4	63.2	0.243	50.2	260	0.8	1.7
ESF-SR-MOISTSTDY#30	74+60	PTn	Tpbt2	1	1.3	107.6	0.520	104.5	207	1.0	1.0
ESF-SR-MOISTSTDY#31	74+65	PTn	Tpbt2	2	14.5	97.6	0.462	113.7	211	1.2	1.1
ESF-SR-MOISTSTDY#32	74+72	PTn	Tpbt2	1	2.5	72.4	0.465	74.8	156	1.0	1.5
ESF-SR-MOISTSTDY#33	74+77	PTn	Tpbt2	1	2.2	87.3	0.582	90.7	150	1.0	1.2
ESF-SR-MOISTSTDY#34	74+81	PTn	Tpp	1	1.8	85.1	0.375	88.4	227	1.0	1.2
ESF-SR-MOISTSTDY#35	74+88	PTn	Tpbt3	1	2.0	72.2	0.313	89	231	1.2	1.5
ESF-SR-MOISTSTDY#36	74+90	PTn	Tpbt3	1	1.9	54.0	0.238	64.0	226	1.2	2.0
ESF-SR-MOISTSTDY#37	74+98	PTn	Tpbt4	1	1.1	83.4	0.403	106.8	207	1.3	1.3
ESF-SR-MOISTSTDY#38	75+03	PTn	Tpbt4	1	2.0	74.6	0.296	92.0	253	1.2	1.4
ESF-SR-MOISTSTDY#39	75+04	PTn	Tpcpv1	1	2.0	85.0	0.364	102	234	1.2	1.2

[1] Stationing indicates the distance in meters from the North Portal entrance of the ESF. Boreholes ESF-LPCA-MOISTSTDY#3 and ESF-LPCA-MOISTSTDY#3 were drilled in Alcove #4, which intersects the Main Drift at Station 10+28. Boreholes ESF-MD-

NICHE3566#1, ESF-MD-NICHE3566#2 and ESF-MD-NICHE3566LT#1 were drilled in Niche 3566 (also called Niche #1), which intersects the Main Drift at Station 35+66.

[2] Lithostratigraphic units follow the nomenclature of Buesch et al. (1996).
Data sources: DTN LAJF831222AQ98.010 and DTN LAJF831222AQ98.015

Table 2-2. Variability of chloride, bromide, and sulfate concentrations in selected ESF porewater samples*

(1) Sample aliquot	(2) Cent. (hrs)	(3) Depth (ft)	(4) Pore-water vol. (mL)	(5) % moist. content	(6) % of moist extracted by cent.	(7) Concentration (mg/L)			(8) Weight ratios	
						Cl	Br	SO_4	Cl/Br	SO_4 /Cl
NR#3										
EDC014-1	20	1.7 - 2.1	1.3	9.4	38	42.0	0.200	54.7	210	1.3
EDC015-1	20	2.3 - 3.1	1.3	9.8	36	58.8	0.367	57.8	160	1.0
EDC015-2	20	2.3 - 3.1	0.5	nm	nc	22.3	0.156	25.2	143	1.1
EDC015-2	48	2.3 - 3.1	0.3	7.9	24	38.1	0.246	46.9	155	1.2
EDC016-1	20	3.4 - 3.9	2.1	12.0	48	44.7	0.244	47.0	183	1.1
EDC016-2	Cum	3.4 - 3.9	19.7	nm	nc	40.8	0.222	56.0	184	1.4
EDC017-1	3	5.2 - 5.8	2.0	nm	nc	35.2	0.264	48.0	133	1.4
EDC017-1	27	5.2 - 5.8	0.9	13.5	35	34.9	0.261	45.3	134	1.3
EDC017-2	Cum	5.2 - 5.8	20.4	nm	nc	39.3	0.243	49.1	162	1.3
NR#8										
EDC029a-1	1	4.1 - 4.9	1.2	nm	nc	17.3	0.224	27.4	78	1.6
EDC029a-1	3	4.1 - 4.9	0.3	nm	nc	18.0	0.215	28.6	83	1.6
EDC029a-1	24	4.1 - 4.9	0.7	nm	nc	14.4	0.185	21.6	78	1.5
EDC029c-1	1	4.1 - 4.9	1.2	nm	nc	19.3	0.244	29.9	79	1.5
EDC029c-1	3	4.1 - 4.9	0.3	nm	nc	20.0	0.260	31.3	77	1.6
EDC029c-1	24	4.1 - 4.9	0.7	9.0	33	14.9	0.193	22.0	77	1.5
LPCA#3										
EDC056-2	3	2.1 - 3.1	1.8	nm	nc	26.6	0.340	71.1	78	2.7
EDC056-2	20	2.1 - 3.1	0.8	21.6	36	11.4	0.139	29.2	82	2.6
EDC057-2	3	3.4 - 4.0	0.8	nm	nc	26.3	0.249	43.5	106	1.7
EDC057-2	20	3.4 - 4.0	0.6	17.0	23	21.8	0.268	30.1	81	1.4
EDC058-1	2	5.2 - 5.9	3.3	nm	nc	17.0	0.229	42.1	74	2.5
EDC058-1	19	5.2 - 5.9	1.7	22.9	30	15.0	0.195	36.9	77	2.5
EDC058-2	Cum	5.2 - 5.9	35.5	nm	nc	17.1	0.238	41.0	72	2.4
SR#10										
SR#10-4.0	3	4.0 - 4.5	1.0	nm	nc	20.0	0.154	40.9	130	2.0
SR#10-4.0	21	4.0 - 4.5	0.4	4.4	78	2.1	0.013	4.9	166	2.3
SR#10-4.0a	3	4.0 - 4.5	0.6	nm	nc	22.3	0.170	47.9	132	2.1
SR#10-4.0a	20	4.0 - 4.5	0.2	3.9	57	14.8	0.166	44.5	89	3.0

nm Not measured
nc Not calculated
Cum Porewater sample is a composite of extractions from multiple sample aliquots.
Data source: DTN LAJF831222AQ98.010

Table 2-2 (continued)

*Notes on column headings and entries:

(1) Sample aliquot: upon receipt, each drillcore sample is assigned a unique identifier, then a unique aliquot identifier is assigned to each portion taken from that sample for analysis. For example, the sample collected from the depth interval 2.3 to 3.1 ft in borehole NR#3 was assigned the identifier EDC015, and the two separate portions of this sample that were independently processed were assigned the identifiers EDC015-1 and EDC015-2. The borehole designators have been abbreviated in the table as follows, with their stratigraphy noted in parentheses: NR#3, ESF-NR-MOISTSTDY#3 (Tpcplnc/mv); NR#8, ESF-NR-MOISTSTDY#8 (Tpy); LPCA#3, ESF-LPCA-MOISTSTDY#3 (Tpbt2); SR#10, ESF-SR-MOISTSTDY#10 (Tptrv2).

(2) Cent.: cumulative number of hours for which the drillcore sample had been centrifuged at the time that the porewater sample was extracted for anion analysis. "Cum" indicates that the porewater sample was a composite sample of extractions from multiple sample aliquots such that the centrifuge time was variable.

(3) Depth: distance of drillcore sample from tunnel wall.

(4) Porewater volume: volume of porewater extracted using the ultracentrifuge.

(5) % moist content: initial weight percent moisture content of sample aliquot, determined as the sum of the porewater extracted by the ultracentrifuge and the residual moisture lost during drying in an oven at 105°C.

(6) % of moist extracted by cent: percent of initial moisture content (column 5) extracted using the ultracentrifuge.

(7) Concentration: anion concentrations of extracted pore waters.

(8) Weight ratios: calculated from data in column 7.

Table 3-1. Reproducibility of measured $^{36}Cl/Cl$ ratios in duplicate ESF samples processed between August 1997 and August 1998

Sample location and stratigraphy	Sample aliquot	Date processed	Br/Cl	% CW	$^{36}Cl/Cl \times 10^{-15}$	
					Measured	Corrected*
Station 19+42 Tptpul	E044-2	17-Jan-96	0.28	9	2130 ± 60	2290 ± 74
	E044-4	09-Jul-97	0.31	10	3896 ± 124	4270 ± 159
Station 35+45 Tptpmn	E160-2	26-Jan-96	0.80	27	2726 ± 83	3529 ± 205
	E160-7	09-Jul-97	0.38	13	1553 ± 60	1704 ± 76
Niche 3566 Tptpmn	E330-1	05-Nov-97	0.33	11	547 ± 26	553 ± 29
	E331-1	05-Nov-97	0.039	1	540 ± 31	540 ± 31
	E332-1	05-Nov-97	0.008	0	588 ± 37	588 ± 37
	E332-2	05-Nov-97	0.008	0	618 ± 45	618 ± 45
Alcove 6/1+53 Tptpmn	E333-1	05-Nov-97	0.031	1	521 ± 32	521 ± 32
	E333-2	05-Nov-97	0.083	2	497 ± 22	497 ± 22
Alcove 6/1+68 Tptpmn	E351-1	18-Mar-98	0.14	5	1636 ± 65	1690 ± 69
	E351-2	18-Mar-98	0.14	4	1734 ± 73	1789 ± 77

* Ratios have been corrected for dilution by construction water Cl. The proportion of construction-water chloride (% CW) present in each sample processed for ^{36}Cl is estimated from the measured Br/Cl (halide) ratio (HR_x), using a two-component mixing equation, $\%CW = 100 \times (HR_x - HR_m) / (HR_c - HR_m)$, where HR_m is the Br/Cl ratio of meteoric water (0.009) and HR_c is the Br/Cl ratio of the construction water (3.0) (Fabryka-Martin et al., 1997a).

Data source: DTN LAJF831222AQ98.004

Table 3-2. $^{36}Cl/Cl$ ratios in ESF rock samples analyzed between August 1997 and September 1998

Sample identifier	Station	Stratigraphy	Description	Br/Cl	% CW	$^{36}Cl/Cl \times 10^{-15}$	
						Measured	Corrected*
South Ramp							
E301-1	69+96	TSw Tptrn	Fault with 0.9 m offset	0.164	5	238 ± 10	224 ± 11
E306-3	70+66	TSw Tptpmn	Intersection, 2 small faults	0.145	5	496 ± 19	496 ± 20
E314-1	74+43	TSw Tptrv1	Broken rock, fault zone	0.133	4	348 ± 17	341 ± 18
E352-1	74+55	PTn Tptrv3	Small fault	0.007	0	**487 ± 21**	487 ± 21
E320-1	75+20	PTn Tpcpv	Tpcplnc/Tpcpv contact	0.021	0	457 ± 20	457 ± 20
E322-1	75+47	TCw Tpcplnc	Systematic sample	0.047	1	320 ± 80	318 ± 81
E353-1	76+01	TCw Tpcpln	Intersecting fractures	0.150	5	**492 ± 22**	492 ± 23
E354-1	76+08	TCw Tpcpln	Breccia-filled fracture	0.042	1	**591 ± 27**	592 ± 27
E355-1	76+11	TCw Tpcpln	Fault wallrock	0.033	1	**466 ± 14**	466 ± 14
E356-1	76+11	TCw Tpcpln	Fault gouge(10-20 cm fill)	0.005	0	624 ± 28	624 ± 28
E335-1	77+19	TCw Tpcpmn	Bulk rock	0.121	4	198 ± 8	186 ± 9
E357-1	77+29	TCw Tpcpmn	Pervasively broken rock	0.210	7	615 ± 28	623 ± 30
E358-1	77+31	TCw Tpcpmn	Rubbly material	0.084	3	721 ± 37	727 ± 38
E359-1	77+49	TCw Tpcpmn	Systematic sample	0.039	1	510 ± 20	510 ± 20
E360-1	78+50	TCw Tpcpul	Systematic sample	0.073	2	**973 ± 27**	983 ± 28
Niche 3566							
E332-1	Back	TSw Tptpmn	Breccia fill in cooling joint	0.008	0	588 ± 37	588 ± 37
E332-2	Back	TSw Tptpmn	Breccia fill in cooling joint	0.008	0	618 ± 45	618 ± 45
E330-1	Back	TSw Tptpmn	Breccia fill in cooling joint	0.326	11	547 ± 26	553 ± 29
E331-1	Back	TSw Tptpmn	Breccia fill in cooling joint	0.039	1	540 ± 31	540 ± 31
E336-1	0+07	TSw Tptpmn	Bulk rock	0.472	15	635 ± 150	660 ± 178
Alcove 6							
E337-1	0+30	TSw Tptpmn	Systematic sample	0.181	6	656 ± 23	666 ± 24
E338-1	0+60	TSw Tptpmn	Systematic sample	0.034	1	687 ± 22	689 ± 22
E339-1	0+82	TSw Tptpmn	Intensely fractured rock	0.093	3	697 ± 35	703 ± 36
E340-1	0+93	TSw Tptpmn	Intensely fractured rock	0.022	0	1506 ± 48	1511 ± 48
E296-1	0+95	TSw Tptpmn	Sundance Fault	1.006	33	522 ± 34	533 ± 52
E341-1	0+97	TSw Tptpmn	Sundance Fault	0.010	0	513 ± 23	513 ± 23
E297-1	0+98	TSw Tptpmn	Sundance Fault	0.500	16	499 ± 24	499 ± 29
E342-1	1+00	TSw Tptpmn	Brecciated rock	0.274	9	889 ± 31	926 ± 35
E343-1	1+05	TSw Tptpmn	Fractured rock	0.208	7	1042 ± 30	1080 ± 33
E344-1	1+10	TSw Tptpmn	Faulted joint	0.281	9	850 ± 28	885 ± 32
E345-1	1+17	TSw Tptpmn	Small fault, wall separation	0.048	1	1074± 36	1081 ± 37
E346-1	1+24	TSw Tptpmn	Small breccia-filled fracture	0.195	6	1090± 35	1130 ± 38
E347-1	1+40	TSw Tptpmn	Fault	0.178	6	555 ± 23	558 ± 24
E349-1	1+52	TSw Tptpmn	Ghost Dance fault wallrock	0.134	4	1250± 65	1283 ± 68
E348-1	1+52	TSw Tptpmn	Ghost Dance fault breccia	0.008	0	457 ± 21	457 ± 21
E333-1	1+53	TSw Tptpmn	Ghost Dance fault breccia	0.031	1	521 ± 32	521 ± 32
E333-2	1+53	TSw Tptpmn	Ghost Dance fault wallrock	0.083	2	497 ± 22	497 ± 23
E350-1	1+60	TSw Tptpmn	Large cooling joints	0.166	5	3237± 125	3389 ±135
E351-1	1+68	TSw Tptpmn	Fractured rock betw. joints	0.145	5	1636± 65	1690 ± 69

Sample identifier	Station	Stratigraphy	Description	Br/Cl	% CW	--- $^{36}Cl/Cl \times 10^{-15}$	
						Measured	Corrected*
E351-2	1+68	TSw Tptpmn	Fractured rock betw. joints	0.136	4	1734± 73	1789 ± 77
Alcove 7							
E334-1	1+30	TSw Tptpmn	Intersecting fractures	0.112	3	475 ± 15	474 ± 16
E361-1	1+54	TSw Tptpmn	Breccia zone	0.040	1	539 ± 24	539 ± 24
E362-1	1+67	TSw Tptpmn	Ghost Dance fault breccia	0.007	0	541 ± 25	541 ± 25
E363-1	1+67	TSw Tptpmn	Ghost Dance fault footwall	0.035	1	643 ± 29	644 ± 29
E364-1	1+84	TSw Tptpmn	Fracture with 4 cm offset	0.010	0	569 ± 27	569 ± 27
E365-1	2+00	TSw Tptpmn	Gouge zone	0.042	1	538 ± 26	538 ± 26

* Ratios have been corrected for the presence of construction water (CW). See footnote for Table 3-1.

Data source: DTN LAJF831222AQ98.004

Table 3-3. $^{36}Cl/Cl$ ratios in porewater extracted from ESF drillcore

Drillhole	ESF station	Hydro unit	Stratigraphic unit	Sample identifier	Cl (mg/L)	$^{36}Cl/Cl$ x 10^{-15}
North Ramp						
ESF-NR-MOISTSTDY#1a	7+27	TCw	Tpcplnc	EDC010-3/EDC011-2	19.6	787 ± 63
ESF-NR-MOISTSTDY#2	7+50	TCw	Tpcplnc/mw	EDC012-1/EDC013-2	18.5	1185 ± 60
ESF-NR-MOISTSTDY#3	7+70	TCw	Tpcplnc/mw	EDC016-2	40.8	665 ± 30
ESF-NR-MOISTSTDY#3	7+70	TCw	Tpcplnc/mw	EDC017-2	39.3	719 ± 37
ESF-NR-MOISTSTDY#4	7+72	TCw	Tpcpv2	EDC020-2	47.2	848 ± 41
ESF-NR-MOISTSTDY#13	10+08	PTn	Tpbt2	EDC040-2/EDC041-21	12.1	970 ± 41
South Ramp						
ESF-SR-MOISTSTDY#13	66+79	PTn	Tpbt2	SR#13-5.3-2	31.8	412 ± 37
ESF-SR-MOISTSTDY#16	67+21	PTn	Tpcpv1	SR#16-5.0-2	38.9	719 ± 34
ESF-SR-MOISTSTDY#21	70+54	PTn	Tpbt2	SR#21-5.2-2	80.2	696 ± 32
ESF-SR-MOISTSTDY#22	70+56	PTn	Tpbt2	SR#22-4.7-2	102.3	549 ± 29
ESF-SR-MOISTSTDY#22r	70+56	PTn	Tpbt2	SR#22r-5.1-2	95.6	715 ± 27
ESF-SR-MOISTSTDY#27	74+44	TSw	Tptrv1	SR#27-5.0-3	39.3	623 ± 30
ESF-SR-MOISTSTDY#29	74+53	PTn	Tptrv3	SR#29-5.2-2	63.5	1003 ± 36
ESF-SR-MOISTSTDY#31	74+65	PTn	Tpbt2	SR#31-5.7-2	98.5	551 ± 28

Data source: DTN LAJF831222AQ98.010

Table 3-4. $^{36}Cl/Cl$ ratios in drillcore from Niche 3566

Borehole	Sample identifier	Depth (m)	$^{36}Cl/Cl$ x 10^{-15}
ESF-MD-NICHE3566#1	DCN086-2	6.8 - 7.0	1372 ± 69
ESF-MD-NICHE3566#1	DCN007-2/008-1	9.8 - 10.1	2008 ± 90
ESF-MD-NICHE3566#2	DCN015-2	2.0 - 2.3	1235 ± 62
ESF-MD-NICHE3566#2	DCN024-1/025-2	4.8 - 5.2	2038 ± 99
ESF-MD-NICHE3566LT#1	DCN038-1/039-2	0.5 - 1.5	997 ± 49
ESF-MD-NICHE3566LT#1	DCN048-1/049-2	4.4 - 5.0	1476 ± 75
ESF-MD-NICHE3566LT#1	DCN050-1/051-2	5.1 - 5.9	1252 ± 68
ESF-MD-NICHE3566LT#1	DCN059-2/060-1	8.8 - 9.4	1627 ± 73
ESF-MD-NICHE3566LT#1	DCN062-1	9.6 - 9.7	1705 ± 87
ESF-MD-NICHE3566LT#1	DCN064-2	10.5 - 10.8	1335 ± 67

Data source: DTN LAJF831222AQ98.009

Table 3-5. Cl/Br, SO_4/Cl, and ^{36}Cl/Cl ratios in soils above the ESF South Ramp

Sample	Nearest ESF station	Sample depth (m)	Topographic setting	Cl/Br	SO_4/Cl	^{36}Cl/Cl x 10^{-15}
SRA-16	67+00	0.45	Base of sideslope	103	3.0	2570 ± 95
SRA-15	68+00	0.45	Alluvial terrace	150	3.8	1155 ± 61
SRA-14	68+30	0.75	Channel (Dune Wash)	89	4.3	1010 ± 55
SRA-13	69+10	0.4	Sideslope, near fault	306	3.7	2983 ± 100
SRA-12	70+00	0.45	Sideslope	273	3.1	2970 ± 90
SRA-11	71+10	0.4	Small channel	291	2.2	1730 ± 80
SRA-10	72+20	0.75	Small channel	99	2.3	1889 ± 92
SRA-09	72+60	0.4	Sideslope, near fault	146	1.8	2024 ± 80
SRA-08	73+00	0.3	Sideslope	256	2.8	2327 ± 105
SRA-07	73+65	0.3	Ridgetop (Boundary Ridge)	300	2.8	2332 ± 109
SRA-06	74+00	0.5	Sideslope	253	2.3	nm
SRA-05	75+00	0.5	Sideslope	1108	2.3	3660 ± 170
SRA-04	76+00	0.4	Sideslope	212	2.6	3320 ± 120
SRA-03	77+00	0.5	Ridgetop	144	2.5	nm
SRA-02	77+25	0.3	Fault	210	2.8	nm
SRA-01	78+00	0.5	Ridgetop	272	3.2	nm

nm - not measured
Data source: DTN LAJF831222AQ98.005

Table 3-6. Cl, Br, and SO_4 concentrations and $^{36}Cl/Cl$ ratios in surface runoff

Sample	Collection location	Collection date	Concentration (mg/L)			Cl/Br	SO_4 /Cl	$^{36}Cl/Cl$ x 10^{-15}
			Cl	Br	SO_4			
W055	Snowmelt near Pah Canyon	06-Jan-95	3.4	0.010	8.2	357	2.4	1302 ± 37
W056	Duplicate of W055	06-Jan-95	3.5	0.010	8.5	341	2.4	1363 ± 40
W059	Overland flow in 40-Mile Canyon	24-Jan-95	2.7	0.007	10.4	363	3.9	2510 ± 110
W060	Wren Wash	25-Jan-95	6.8	0.018	19.3	377	2.8	2770 ± 100
W061	Upper Split Wash	25-Jan-95	3.9	0.013	11.1	306	2.9	3240 ± 120
W062	Yucca Wash	26-Jan-95	2.3	0.004	5.5	571	2.4	3350 ± 100
W063	Pah Canyon tributary	26-Jan-95	4.3	0.010	9.8	437	2.3	3290 ± 80
W170	Wren Wash	20-Feb-98	4.2	0.011	13.4	393	3.2	2018 ± 79
W171	Pagany Wash near UZ-4	24-Feb-98	5.6	0.016	32.7	350	5.8	1960 ± 80
W172	Yucca Wash near mouth	24-Feb-98	2.4	0.004	5.8	565	2.4	2062 ± 88

Data source: DTN LAJF831222AQ98.011

Table 6-1. Lithostratigraphic and Structural Settings, $^{36}Cl/Cl$ Values, and Secondary Mineralogy of ESF Sample Sites

Sample[1]	Station	Lithostrati-graphic unit	Sampled feature[2]	Corrected[9] $^{36}Cl/Cl$ $\times 10^{-15}$	Calcite	Opal[3]	Clay/Mord.[4]	Clay/Mord. 2 or more[5]	Feldspar±Cr. Silica±Fe-Ti oxides[6]	Transported Particulates[7]	Mn minerals	Other mineral(s)[8]
E001	1+98	Tpcpll?	fault breccia	518	-[10]	-	●	-	●	●	●	-
E008	1+99.8	Tpcp	fault breccia	2138[11]	●	-	●	-	●	●	●	-
E009	1+99.8	Tpcp	fault breccia	2444	-	-	●	-	-	●	●	-
E010	1+99.8	Tpcp	fault breccia	720	-	-	●	-	?	●	●	-
E011	1+99.8	Tpcp	fault breccia	2378	●	●	?	?	?	●	●	-
E012	1+99.8	Tpcp	fault breccia	2398	-	-	●	-	●	●	●	●
E007	2+03	Tmbt1	bedrock	519	-	-	-	-	-	-	-	-
E163	4+94	Tpcpul	syst./bedrock	485	-	-	-	-	-	-	●	-
E073	5+04	Tpcpul	fracture	468	-	-	●	-	-	-	●	-
E164	7+00	Tpcpul	syst./bedrock	571	-	-	-	-	-	-	-	-
E165	7+70	Tpcpln/Tpcpv	subunit contact	496	-	●	●	-	-	-	●	?
E166	7+70	Tpcpln/Tpcpv	subunit contact	484	-	-	●	-	-	-	●	-
E167	7+70	Tpcpv2	subunit contact	427	-	-	●	-	-	-	●	-
E188	8+26.5	Tpcpv1	bedrock	766	-	-	-	-	-	-	-	-
E189	8+26.5	Tpcpv1/Tpbt4	contact	625	-	-	●	-	-	-	-	●
E190	8+26.5	Tpbt4	bedrock	647	-	-	●	-	-	-	?	●
E244	8+38	Tpbt3	fault	488	-	-	-	-	-	-	●	-
E168	8+59	Tpcpv1	above contact	1096	●	-	●	-	-	-	●	-
E169	8+59	Tpcpv1/Tpbt4	contact/fault	1096	-	-	●	-	-	-	-	-
E170	8+59	Tpbt4	bedrock/fault	635	-	-	●	-	-	-	●	-
E191	8+75	Tpbt3	subunit	904	-	●	●	-	-	-	-	●
E192	8+75	Tpbt3	subunit contact	698	-	●	-	-	-	-	●	●
E171	8+90	Tpp	below contact	1335	-	-	●	-	-	-	-	●
E172	8+90	Tpbt3/Tpp	contact	637	-	-	●	-	-	-	-	●
E173	8+90	Tpbt3	above contact	806	-	-	?	-	-	-	●	●
E174	9+00	Tpp	syst./bedrock	660	-	-	-	-	-	-	-	-
E126	10+34	Tpbt2	fault	633	●	●	●	-	-	-	-	●
E130	10+41	Tpbt2	fault	773	-	-	●	-	-	-	-	●
E197	10+62.5	Tptrv1	subunit contact	1452	-	-	●	-	-	-	-	-
E027	11+00	Tptrv1	syst./bedrock	1076	-	-	●	-	●	-	●	-
E213	12+36.5	Tptrn	broken rock	719	-	-	-	-	●	-	●	-
E028	12+44	Tptrn	cooling jts.	2637	-	-	●	-	●	●	-	●
E214	12+44	Tptrn	cooling jts.	750	-	-	●	●	●	-	●	-
E215	12+49	Tptrn	cooling jts.	668	-	-	●	-	●	-	●	-
E029	13+00	Tptrn	syst./bedrock	640	-	-	-	-	●	-	-	-
E030	13+67	Tptrn	cooling jts.	1621	-	-	●	-	●	-	-	-
E031	14+00	Tptrn	shear zone	2398	-	-	-	-	●	-	-	-

Table 6-1. Lithostratigraphic and Structural Settings, $^{36}Cl/Cl$ Values, and Secondary Mineralogy of ESF Sample Sites (cont.)

Sample[1]	Station	Lithostrati-graphic unit	Sampled feature[2]	Corrected $^{36}Cl/Cl$ $\times 10^{-15}$	Calcite	Opal[3]	Clay/Mord.[4]	Clay/Mord. 2 or more[5]	Feldspar±Cr. Silica±Fe-Ti oxides[6]	Transported particulates[7]	Mn minerals	Other mineral(s)[8]
E033	14+41	Tptrn	fault breccia	876	●	●	-	-	●	-	-	-
E035	15+05	Tptrn	fracture	628	●	●	●	-	●	-	●	-
E036	16+12	Tptrn	cooling jt.	382	●	●	-	-	●	-	-	●
E037	16+19	Tptrn	fracture	982	-	-	●	-	-	●	-	-
E038	17+00	Tptrn	syst./bedrock	714	-	-	-	-	●	-	●	-
E040	18+96	Tptpul	broken rock	1642	(●)[12]	-	●	-	●	-	-	-
E041	19+00	Tptpul	syst./bedrock	746	-	-	-	-	●	-	●	-
E042	19+31	Tptpul	breccia	3019	●	-	-	-	-	-	-	-
E044	19+42	Tptpul	breccia	2290	●	-	-	-	●	-	-	-
E216	20+71	Tptpul	fractures	842	-	-	●	-	●	-	●	●
E045	21+00	Tptpul	syst./bedrock	799	-	-	-	-	●	-	-	-
E046	22+71	Tptpul	fractures	862	●	-	-	-	●	-	-	-
E047	23+00	Tptpul	syst./bedrock	663	-	-	-	-	-	-	-	-
E050	24+40	Tptpul	fault breccia	2579	●	-	-	-	●	-	-	-
E020	24+68	Tptpul	fracture	814	●	●	-	-	●	-	-	-
E217	26+19	Tptpul	cooling joints	522	-	-	●	-	●	-	●	-
E218	26+36	Tptpul	fractured rock	603	-	-	●	-	●	-	●	-
E219	26+46	Tptpul	fractured rock	578	-	-	●	-	●	-	●	-
E052	26+79	Tptpul/tpmn	shear zone	2036	●	-	-	-	●	-	-	-
E220	26+79	Tptpul/tpmn	fract. bedrock	565	-	-	●	-	●	-	●	-
E058	27+66	Tptpmn	fault breccia	458	-	-	-	●	●	●	●	-
E141	29+00	Tptpmn	syst./bedrock	922	-	-	-	-	●	-	-	-
E142	29+21	Tptpmn	fracture	583	●	-	-	-	-	-	-	-
E143	29+65	Tptpmn	fault breccia	1077	-	-	-	●	●	-	●	-
E144	29+73	Tptpmn	cooling jt.	815	●	-	-	●	●	-	-	-
E149	31+64	Tptpmn	cooling jt.	631	●	-	●	-	-	-	●	-
E150	33+00	Tptpmn	syst./fr. bedrock	1341	-	-	-	-	-	-	●	-
E151	33+16	Tptpmn	lith. cavity	529	●	●	-	-	●	-	-	-
E152	34+28	Tptpmn	fract. bedrock	4105	●	-	-	●	●	-	●	-
E153	34+32	Tptpmn	cooling jts.	3291	●	-	●	-	-	●	●	-
E154	34+71	Tptpmn	cooling jts.	3767	(●)[12]	-	-	●	-	-	●	-
E154	34+71	Tptpmn	breccia	803	(●)[12]	-	-	●	-	●	●	-
E155	35+00	Tptpmn	syst./bedrock	1013	-	-	●	-	●	●	●	-
E156	35+00	Tptpmn	broken rock	626	-	-	-	-	●	-	-	-
E157	35+03	Tptpmn	cooling jts.	(1339)	●	-	-	-	-	-	●	-

Table 6-1. Lithostratigraphic and Structural Settings, $^{36}Cl/Cl$ Values, and Secondary Mineralogy of ESF Sample Sites (cont.)

Sample[1]	Station	Lithostrati-graphic unit	Sampled feature[2]	Corrected $^{36}Cl/Cl$ $\times 10^{-15}$	Calcite	Opal[3]	Clay/Mord.[4]	Clay/Mord. 2 or more[5]	Feldspar±Cr. Silica±Fe-Ti oxides[6]	Transported particulates[7]	Mn minerals	Other mineral(s)[8]
E158	35+08	Tptpmn	cooling jts.	(2605)	●	-	-	●	-	-	●	-
E160	35+45	Tptpmn	cooling jts.	3329	(●)[12]	-	-	●	●	●	●	-
E161	35+58	Tptpmn	cooling jt.	(2141)	●	-	-	●	●	-	●	-
E175	35+93	Tptpmn	fault breccia	(2840)	(●)[12]	-	-	●	●	●	●	-
E177	37+00	Tptpmn	syst./bedrock	484	-	-	-	-	-	-	●	-
E178	37+60	Tptpmn	cool. jt./breccia	471	-	-	-	●	●	-	●	-
E179	37+68	Tptpmn	cool. jt./breccia	363	●	-	-	●	●	-	●	-
E179	37+68	Tptpmn	broken wallrock	397	-	-	-	-	●	●	●	-
E182	38+79	Tptpmn	cool. jt./breccia	379	-	-	●	-	●	-	●	-
E183	38+95	Tptpmn	cool. jt./breccia	745	-	-	-	●	●	-	●	-
E184	39+00	Tptpmn	syst./fractures	536	-	-	-	-	●	-	●	-
E185	39+39	Tptpmn	frct./lith. cavity	897	●	-	●	-	●	-	●	-
E186	39+47	Tptpmn	cool. jt./breccia	561	(●)[12]	-	●	-	●	-	●	-
E187	39+61	Tptpmn	cool. jt./breccia	540	●	-	●	-	●	-	●	-
E221	41+00	Tptpmn	syst./cool. jts.	773	-	-	-	-	●	-	●	-
E198	41+65	Tptpmn	cool. jts./br. rock	*291*[13]	-	-	-	●	●	-	●	-
E222	42+55	Tptpmn	cool. jts./shear	531	(●)[12]	-	-	●	●	-	●	-
E199	43+00	Tptpmn	syst./bedrock	1042	-	-	-	●	●	-	●	-
E201	43+63	Tptpmn	cooling jts.	1974	-	-	-	-	●	-	●	-
E202	44+20	Tptpmn	cooling jts.	3463	-	-	●	-	●	-	●	-
E203	44+21	Tptpmn	cooling joints	849	-	-	●	-	●	-	●	-
E204	44+22	Tptpmn	cooling joints	772	-	-	-	●	●	●	●	-
E205	45+00	Tptpmn	syst./cool. jts.	1514	-	-	-	-	●	-	●	-
E207	45+79	Tptpmn	fractured rock	593	(●)[12]	-	●	-	-	-	●	-
E223	47+00	Tptpmn	syst./ frct. rock	734	-	-	-	-	-	-	●	-
E224	49+00	Tptpmn	syst./cool. jts.	499	-	-	-	●	●	-	●	-
E226	49+56	Tptpmn	cool. jts./breccia	456	●	-	-	●	●	-	●	-
E227	49+89	Tptpmn	cool. jts./breccia	497	●	-	-	-	●	-	●	-
E230	51+00	Tptpmn	syst./fract. rock	555	-	-	-	-	●	-	●	-
E231	51+07	Tptpmn	cooling joints	709	(●)[12]	-	●	-	●	-	●	-
E233	51+73	Tptpmn	fractures	647	(●)[12]	-	●	-	●	-	●	-
E234	52+43	Tptpmn	cooling joints	367	(●)[12]	-	●	-	-	-	●	●
E236	53+00	Tptpmn	syst./fract. rock	417	-	-	-	-	●	-	●	-
E237	53+61	Tptpmn	broken rock	539	-	-	-	-	●	-	●	-
E238	54+20	Tptpmn	cool. jts./breccia	727	-	-	-	●	●	-	●	-

Table 6-1. Lithostratigraphic and Structural Settings, $^{36}Cl/Cl$ Values, and Secondary Mineralogy of ESF Sample Sites (cont.)

Sample[1]	Station	Lithostrati-graphic unit	Sampled feature[2]	Corrected $^{36}Cl/Cl$ $\times 10^{-15}$	Calcite	Opal[3]	Clay/Mord.[4]	Clay/Mord. 2 or more[5]	Feldspar±Cr. Silica±Fe-Ti oxides[6]	Transported particulates[7]	Mn minerals	Other mineral(s)[8]
E239	55+00	Tptpmn	syst./fract. rock	464	-	-	-	-	●	-	●	-
E241	56+85	Tptpmn	cool. jts./breccia	778	(●)[12]	-	-	-	●	-	●	-
E242	56+93	Tptpmn	cool. jt./breccia	1117	(●)[12]	-	-	-	●	-	●	-
E252	57+00	Tptpmn	syst./fractures	388	●	-	-	-	●	-	●	-
E255	58+77	Tptpmn	below frcts.	*140*	-	-	-	-	●	-	●	-
E256	59+00	Tptpll	syst./fract. rock	361	-	-	●	-	●	-	●	-
E290	59+98	Tptpmn	syst./fract. rock	*205*	-	?	●	-	●	-	●	-
E258	61+92	Tptpmn	fractures	*276*	-	-	-	●	●	-	●	-
E260	62+05	Tptpmn	fault	*261*	-	?	-	-	●	-	●	-
E266	63+26	Tptpmn	fractures	486	-	-	-	-	●	-	●	-
E267	63+30	Tptpmn	fault	427	(●)[12]	-	-	-	●	-	●	-
E270	63+81	Tptpul	fractured rock	439	-	-	-	-	●	-	●	-
E271	64+00	Tptpul	fractured rock	467	●	-	-	●	●	-	●	-
E272	64+34	Tptpul	broken rock	467	-	-	●	-	●	-	●	-
E274	64+93	Tptpul	fracture/breccia	491	●	●	-	-	●	-	-	-
E275	65+00	Tptrl	syst./fractures	443	●	●	-	-	-	-	●	-
E268	65+20	Tptrl	fractures/breccia	468	(●)[12]	-	-	-	-	-	●	-
E277	65+80	Tptrn	fracture zone	424	(●)[12]	(●)[12]	-	-	●	-	●	-
E279	66+15	Tptrn	fault breccia	402	●	●	-	-	●	●	●	●
E280	66+40	Tptrn	fault breccia	*238*	●	●	-	-	●	-	●	-
E281	67+00	Tpbt3	systematic	453	-	-	-	-	-	-	-	-
E283	67+27	Tpcpv2/1	thin bed	470	-	-	●	-	-	-	-	-
E284	67+35	Tpcplnc/pv2	subunit contact	502	-	-	●	-	●	-	●	●
E284	67+35	Tpcpv2	subunit contact	509	-	-	●	-	●	-	●	-
E289	67+61	Tpcpv1	fault margin	589	-	-	●	-	-	-	●	●
E285	67+73	Tpcpv2/1	thin bed	468	-	-	●	-	-	-	●	-
E286	67+87	Tpcpv	fault/graben	475	●	-	-	●	●	-	●	●
E287	67+87	Tptr	fault/graben	517	-	-	-	●	●	-	●	-
E288	67+90	Tptpul	broken rock/fault	557	-	-	●	-	●	-	●	-
E298	68+00	Tptpul	syst./bedrock	606	-	-	-	-	●	-	●	-
E292	69+00	Tptrn	syst./cool. jt.	414	-	-	-	-	●	-	●	-
E293	69+14.5	Tptrn	cool. jt./breccia	454	-	-	-	-	●	-	●	-
E294	69+32.5	Tptrn	cool. jt./breccia	473	-	-	-	-	●	-	●	-
E295	69+41.7	Tptrn	cool. jt./breccia	476	●	●	-	-	●	-	●	-
E299	69+47	Tptrn	syst./shear zone	441	-	-	●	-	●	-	●	-
E300	69+68	Tptrn	fracts./fault(?)	354	(●)[12]	-	-	-	●	-	●	-

Table 6-1. Lithostratigraphic and Structural Settings, $^{36}Cl/Cl$ Values, and Secondary Mineralogy of ESF Sample Sites (cont.)

Sample[1]	Station	Lithostrati-graphic unit	Sampled feature[2]	Corrected $^{36}Cl/Cl$ $\times 10^{-15}$	Calcite	Opal[3]	Clay/Mord.[4]	Clay/Mord. 2 or more[5]	Feldspar±Cr. Silica±Fe-Ti oxides[6]	Transported particulates[7]	Mn minerals	Other mineral(s)[8]
E301	69+95.8	Tptrn	fault breccia	*224*	●	●	●	-	●	-	●	-
E302	70+19	Tpbt2	fault breccia	*327*	-	-	●	-	●	-	-	●
E303	70+36	Tpbt2	fault	439	-	-	-	-	-	-	-	-
E304	70+50	Tpbt2	syst./bedrock	491	-	-	-	-	-	-	-	●
E306	70+66	Tptpmn	fault breccia	499	-	-	●	-	-	-	●	-
E309	71+41	Tptpmn	fault	445	-	-	●	-	●	-	●	-
E310	71+50	Tptpmn	syst./frct. rock	441	-	-	-	●	●	-	●	-
E312	72+69	Tptpul	fault breccia	463	-	-	-	-	●	-	●	-
E313	73+48	Tptrl	syst./shear	367	-	-	-	-	●	-	●	-
E314	74+43	Tptrn	fault	*341*	(●)[12]	(●)[12]	(●)[12]	-	-	-	●	-
E315	74+49	Tptrv3	syst./bedrock	435	-	-	●	-	●	-	-	-
E317	75+09	Tpcpv1	subunit contact	402	-	-	-	-	-	-	-	-
E320	75+20	Tpcpv2	fract./breccia	457	●	●	●	-	●	-	●	●
E322	75+47.5	Tpcplnc	syst./frct. rock	*318*	(●)[12]	-	●	-	●	●	●	-
E325	76+30	Tpcpln	fault wall rock	380	-	-	-	-	-	-	●	-
E327	76+50	Tpcpln	syst./frct. rock	*281*	●	●	-	-	-	-	●	-
E329	77+10	Tpcpln	cool. jts./fault	394	●	-	●	-	●	-	●	-
E335	77+19	Tpcpmn	fract. rock	*186*	●	●	●	-	●	-	●	-
				Alcove 2 (ESF Station 1+68)								
E228	0+25.5	Tpcpul	bedrock	359	-	-	●	-	●	-	●	-
				Alcove 3 (ESF Station 7+54)								
E229	0+14	Tpcpln	bedrock	558	-	-	●	-	-	-	●	-
				Alcove 6 (Northern Ghost Dance Fault Alcove, ESF Station 37+37))								
E296	0+95	Tptpmn	broken rock	533	-	-	●	-	●	●	●	-
E297	0+98	Tptpmn	fault breccia	499	-	-	●	-	●	●	●	●
				Alcove 7 (Southern Ghost Dance Fault Alcove, ESF Station 50+64)								
E334	1+37.9	Tptpmn	fractures	474	●	-	-	-	●	-	●	-

Table 6-1. Lithostratigraphic and Structural Settings, $^{36}Cl/Cl$ Values, and Secondary Mineralogy of ESF Sample Sites (cont.)

Sample[1]	Station	Lithostrati-graphic unit	Sampled feature[2]	Corrected $^{36}Cl/Cl$ $\times 10^{-15}$	Calcite	Opal[3]	Clay/Mord.[4]	Clay/Mord. 2 or more[5]	Feldspar±Cr. Silica±Fe-Ti oxides[6]	Transported particulates[7]	Mn minerals	Other mineral(s)[8]
				Niche 1 (ESF Station 35+60)								
E330	0+13.5	Tptpmn	breccia/wet zone	553	-	-	-	-	-	-	●	-
E331	0+13.5	Tptpmn	breccia/wet zone	540	-	-	●	-	●	-	●	-
E332	0+13.5	Tptpmn	breccia/wet zone	588	-	-	●	-	●	-	●	-
E332	0+13.5	Tptpmn	breccia/wet zone	618	-	-	-	-	●	-	●	-

Notes

[1]Samples were divided into separate splits for isotopic and mineralogic analysis. Mineralogic data were also recorded for the sample sites In cases where more than one split of a sample was measured for chlorine isotopic ratios, there are separate entries for each analyzed split or the value reported in this table is the highest value obtained.
[2]Abbreviations: br. rock = broken rock, cooling jt., cool. jt. = cooling joint; fr. (or fract.) bedrock = fractured bedrock; frct(s). = fracture(s) or fractured; syst. = systematic sample collected at fixed intervals.
[3]As used here, opal is transparent, colorless to light-colored, and typically fluoresces yellow-green in short-wave UV light. X-ray diffraction analysis of selected samples indicates opal-A. The silica in sample E126 has no discernible morphology. The opal in sample E192 (and some of the opal in E191 and E295) has a morphology suggestive of opal-CT. A translucent character is suggestive of opal-CT (E274, E295, E327). Queried entries "?" (E260, E290) refer to glassy, silica-rich coatings usually associated with microbreccia.
[4]This category includes clay and/or mordenite. The clay is predominantly smectite, but may include palygorskite.
[5]An entry in this column indicates the presence of two or more distinct deposits of different colors, as identified by binocular microscopy.
[6]This category includes minerals inferred to be of early to late syngenetic origin. Reported occurrences in this category are limited to minerals in growth position on the rock surfaces. Cr. Silica = crystalline silica, including quartz, chalcedony, cristobalite, tridymite, opal-CT.
[7]This category includes physically transported particulates, mostly silt- and sand-size material. Deposits of clay-size material are not included here even though some clays are transported.
[8]This category includes fluorite (E012, E036, E126?, E234), zeolite (E130, E165?, E189?, E191, E192, E216, E284, E297), hematite (other than specular hematite of vapor-phase origin; E126, E189, E190, E304), chabazite, kenyaite, and moganite (E320), and unidentified minerals.
[9]Chlorine-36 data are from DTN LAJF831222AQ98.004. Measured values have been adjusted for any presence of construction water.
[10]"-" = mineral not observed; "●" = mineral present; "?" = presence of mineral uncertain.
[11]Values in boldface denote samples containing a component of bomb-pulse chlorine ($^{36}Cl/Cl$ values > 1250×10^{-15}) inferred to be less than 50 years old.
[12]Calcite (or opal or clay) was not present in the aliquot for mineralogic characterization but was observed at the collection site in fractures or voids (E040, E154, E160, E186, E207, E242, E277) or in fractures adjacent to the fault (E175, E267) or in the same fault (E314).
[13]Italicized values are below 350 and may denote samples with longer water residence times than elsewhere.

Data Source: LASL831222AQ98.002

Table 7-1. Characterization of Cl, Br, and SO_4 concentrations in construction water

	ESF construction water	Cross drift construction water*	All samples
Sampling dates	27-Apr-95 to 30-Apr-97	09-Mar-98 to 05-Jun-98	27-Apr-95 to 05-Jun-98
No. of samples collected for analysis	25	11	36
Average mg/L Cl	7.04 ± 0.50	7.03 ± 0.31	7.03 ± 0.45
Average mg/L Br	19.9 ± 2.1	18.0 ± 0.9	19.3 ± 2.0
Average mg/L SO_4	18.6 ± 1.8	18.2 ± 0.6	18.5 ± 1.5
Average Br/Cl	2.85 ± 0.32	2.57 ± 0.16	2.76 ± 0.30
Average SO_4/Cl	2.66 ± 0.17	2.60 ± 0.11	2.64 ± 0.16

* Includes three samples of applied surface infiltration water for the Alcove 1 seepage study

Data source: LAJF831222AQ98.003

Table 7-2. Summary of construction water detected in drillcore samples from Test Zones 1 and 2

	Test Zone #1	Test Zone #2
Borehole	ECRB-TZ1#1	ECRB-TZ2#1
Angle of hole	90° (horizontal, left rib)	90° (horizontal, left rib)
Total depth	2 m	2 m
# samples analyzed	7	5
# samples with construction water	5	2
	Depth Br/Cl	Depth Br/Cl
Depth intervals with construction water	0.0 - 0.1 m 0.094 0.1 - 0.2 m 0.036 0.3 - 0.4 m 0.036 1.2 - 1.5 m 0.021 1.8 - 2.0 m 0.032	0.4 - 0.5 m 0.019 1.0 - 1.2 m 0.033
Borehole	ECRB-TZ1#2	ECRB-TZ2#2
Angle of hole	45°	45°
Total depth	5 m	5 m
# samples analyzed	9	12
# samples with construction water	1	2
	Depth Br/Cl	Depth Br/Cl
Depth intervals with construction water	0.7 - 0.8 m 0.022	0.0 - 0.1 m 0.868 0.3 - 0.5 m 0.042
Borehole	ECRB-TZ1#3	ECRB-TZ2#3
Angle of hole	0° (vertical, invert)	0° (vertical, invert)
Total depth	10 m	10 m
# samples analyzed	16	14
# samples with construction water	2	7
	Depth Br/Cl	Depth Br/Cl
Depth intervals with Construction water	0.0 - 0.1 m 0.022 5.2 - 5.4 m 0.033	0.1 - 0.3 m 0.209 1.8 - 2.1 m 0.053 2.7 - 3.0 m 0.047 4.8 - 5.0 m 0.031 6.6 - 6.7 m 0.036 7.2 - 7.4 m 0.033 9.8 - 10.0 m 0.035
Borehole	ECRB-TZ1#4	ECRB-TZ2#4
Angle of hole	0° (vertical, invert)	0° (vertical, invert)
Total depth	15 m	15 m
# samples analyzed	21	10
# samples with construction water	1	2
	Depth Br/Cl	Depth Br/Cl
Depth intervals with construction water	0.0 m 0.037	0.0 m 0.920 0.0 - 0.3 m 0.056

Data source: DTN LAJF831222AQ98.008

Table 8-1. Cl, Br, and SO_4 concentrations and $^{36}Cl/Cl$ ratios in selected Alcove 1 seeps

Sample identifier	Collection date	Grid location (see Fig. 8-1)	Concentration (mg/L)			Cl/Br	SO_4/Cl	$^{36}Cl/Cl \times 10^{-15}$
			Cl	Br	SO_4			
W173	11-Mar-98	R 21	0.90	0.09	5.6	10	6.2	nm
W180	07-Apr-98	R 21	20.4	0.22	7.9	94	0.4	nm
WA-015	05-May-98	J 7	514	15.2	641	34	1.2	563 ± 23
WA-045	06-May-98	J 1	382	13.4	402	28	1.1	483 ± 57
WA-397	15-May-98	J 1	283	14.9	323	19	1.1	610 ± 25
WA-777	02-Jun-98	J 7	285	77.9	449	3.7	1.6	595 ± 29
WA-782	02-Jun-98	J 1	207	71.1	272	2.9	1.3	568 ± 24

Data source: DTN LAJF831222AQ98.012

Borehole	Collection date	Sample identifier	Concentrations (mg/L)			Weight ratios			$^{36}Cl/Cl \times 10^{-15}$
			Cl	Br	SO_4	Cl/Br	Br/Cl x 10^{-3}	SO_4/Cl	
UE-29 a#1	06-Nov-97	W161	8.15	0.070	16.5	116	8.6	2.0	1312 ± 52
UE-29 a#2	06-Nov-97	W162	8.30	0.070	15.6	119	8.4	1.9	1289 ± 48
USW SD-9	12-Sep-94	W045	7.05	0.059	NM	120	8.3	NC	497 ± 19
USW UZ-14 (1900')	25-Feb-98	W167	6.39	0.052	13.1	123	8.1	2.0	NM
USW UZ-14 (1900')	25-Feb-98	W166	6.59	0.052	13.2	126	7.9	2.0	NM
USW UZ-14 (1900')	25-Feb-98	W165	6.46	0.048	13.0	134	7.5	2.0	563 ± 27
USW UZ-14 (2150')	26-Feb-98	W168	7.46	0.047	13.5	158	6.3	1.8	NM
USW UZ-14 (2150')	26-Feb-98	W169	7.40	0.049	13.6	150	6.7	1.8	495 ± 24
UE-25 UZ#16	25-Feb-93	W024	170	0.437	NM	390	2.6	NC	NM
UE-25 UZ#16	25-Feb-93	W025	457	0.475	NM	963	1.0	NC	42 ± 3
UE-25 WT#3	23-Jun-98	W220	6.41	0.031	20.0	207	4.8	3.1	NM
UE-25 WT#3	22-Jun-98	W217	6.46	0.037	20.2	176	5.7	3.1	NM
UE-25 WT#3	22-Jun-98	W218	6.36	0.030	20.1	211	4.7	3.2	NM
UE-25 WT#3	22-Jun-98	W219	6.52	0.036	20.2	179	5.6	3.1	NM
USW WT-10	18-Jan-96	W132	7.17	0.050	31.9	142	7.0	4.5	526 ± 39
UE-25 WT#12	19-Aug-95	W133	6.62	0.054	24.2	122	8.2	3.7	563 ± 13
UE-25 WT#12	21-Aug-95	W134	6.52	0.052	23.8	126	7.9	3.6	568 ± 14
UE-25 WT#12	22-Aug-95	W108	6.92	0.049	24.8	141	7.1	3.6	583 ± 21
UE-25 WT#17	04-Jun-98	W194	15.6	2.833	13.9	6	181	0.9	NM
UE-25 WT#17	04-Jun-98	W193	15.4	2.956	15.9	5	192	1.0	NM

Borehole	Collection date	Sample identifier	Concentrations (mg/L)			Weight ratios			$^{36}Cl/Cl \times 10^{-15}$
			Cl	Br	SO_4	Cl/Br	Br/Cl x 10^{-3}	SO_4/Cl	
UE-25 WT#17	01-Jul-98	W214	14.7	2.694	1.69	5	184	0.1	NM
UE-25 WT#17	01-Jul-98	W215	6.70	0.179	22.1	37	26.7	3.3	NM
UE-25 WT#17	01-Jul-98	W216	7.01	0.322	20.4	22	45.9	2.9	NM
USW WT-24	22-Oct-97	W157	NM	NM	NM	NC	NC	NC	596 ± 13
USW WT-24	10-Dec-97	W163	8.59	1.122	16.6	8	131	1.9	569 ± 14
*USW UZ-1	21-Jul-83	W001	10.35	NM	20.6	NC	NC	2.0	999 ± 80
*USW VH-1	30-Jul-92	W006	8.83	0.080	NM	NC	NC	NC	540 ± 11
*UE#25 p1	06-Jun-90	W002	25.3	0.089	73.1	284	3.5	2.9	132 ± 10

NM Not measured
NC Not calculated
* Non-Q data (see Appendix B footnote)

Data sources: DTN LAJF831222AQ98.011 and LAJF831222AN98.013

Table 9-2. Br/Cl ratios in WT-24 drillcore

Sample	Depth range (m)	Stratigraphic unit	Br/Cl
WTB001	515.1 - 515.2	Tptpv3 (Basal vitrophyre of Topopah Spring Tuff)	0.37
WTB003	522.8 - 523.0	Tptpv3 (Basal vitrophyre of Topopah Spring Tuff)	0.025
WTB004	524.9 - 525.2	Tptpv2 (Moderately welded base of Topopah Spring Tuff)	0.37
WTB005	528.3 - 528.6	Tptpv2 (Moderately welded base of Topopah Spring Tuff)	0.17

Data source: DTN LAJF831222AQ98.006

Table 9-3. Cl, Br, and SO_4 concentrations and $^{36}Cl/Cl$ ratios in regional wells and springs (data from DTN LAJF831222AQ98.011)

Well or Spring	Collection date	Sample identifier	Concentrations (mg/L)			Weight ratios			$^{36}Cl/Cl \times 10^{-15}$
			Cl	Br	SO_4	Cl/Br	Br/Cl x 10^{-3}	SO_4/Cl	
NTS Well #8	04-Nov-97	W159	7.47	0.065	15.0	115	8.7	2.0	606 ±27
NTS Well #20	05-Nov-97	W160	11.3	0.061	29.8	185	5.4	2.6	551 ±18
ER30-1-L (well)	31-Jan-95	W074	6.58	0.090	13.2	73	13.6	2.0	453 ±17
ER30-1-U (well)	07-Feb-95	W070	6.42	0.169	14.2	38	26.3	2.2	460 ±15
U-20 WW (well)	31-May-95	W102	11.6	0.065	30.0	178	5.6	2.6	523 ±15
Amargosa River Canyon Spring Area 1,vent 4	10-Jun-98	W196	55.8	0.109	225	510	2.0	4.0	NM
Amargosa River Canyon Spring Area 2, CA	10-Jun-98	W195	64.4	0.118	282	546	1.8	4.4	NM
Anvil Spring	16-Jul-98	W212	44.7	0.181	133	247	4.0	3.0	NM
Barrachman Spring	15-Jul-98	W207	65.8	0.158	192	416	2.4	2.9	NM

Well or Spring	Collection date	Sample identifier	Concentrations (mg/L)			Weight ratios			$^{36}Cl/Cl \times 10^{-15}$
			Cl	Br	SO_4	Cl/Br	Br/Cl x 10^{-3}	SO_4/Cl	
Bray Spring	16-Jul-98	W211	8.63	0.042	28.6	206	4.9	3.3	NM
Captain Jack Spring NTS	25-Jun-98	W200	3.81	NM	8.28	NC	NC	2.2	NM
Chappo Spring CA	11-Jun-98	W197	48.8	0.040	109	1207	0.8	2.2	NM
Chappo Spring, CA	11-Mar-98	W178	49.7	0.058	112	852	1.2	2.3	130 ±6
Comb Pk Spring NTS	16-Jun-98	W199	3.41	NM	5.43	NC	NC	1.6	NM
DeLee Spring	14-Jul-98	W203	6.66	0.030	28.3	223	4.5	4.3	NM
DeLee Spring	14-Jul-98	W204	6.51	0.031	27.8	213	4.7	4.3	NM
Funeral Spring	16-Jul-98	W213	14.1	0.069	49.5	205	4.9	3.5	NM
Lowe Spring	14-Jul-98	W205	34.3	0.100	159	343	2.9	4.6	NM
McCracken Spring	14-Jul-98	W202	129	0.365	278	354	2.8	2.2	NM
Nelson Spring	15-Jul-98	W208	28.6	0.081	167	355	2.8	5.8	NM
Nelson Spring	15-Jul-98	W209	28.6	0.080	167	355	2.8	5.8	NM
Oneill Spring	15-Jul-98	W206	7.94	NM	47.5	NC	NC	6.0	NM
Payton Spring	15-Jul-98	W210	47.3	0.188	168	252	4.0	3.6	NM
Tecopa Hot Springs, CA	11-Mar-98	W177	365	0.332	502	1101	0.9	1.4	63 ±4
Water Pipe Butte Spring	06-Nov-97	W158	8.55	0.068	19.2	125	8.0	2.2	1666 ±59
Whiterock Spg NTS	25-Jun-98	W201	9.62	0.038	22.7	251	4.0	2.4	NM
Willow Spring, China Ranch CA	10-Mar-98	W176	83.9	0.152	405	550	1.8	4.8	227 ±11

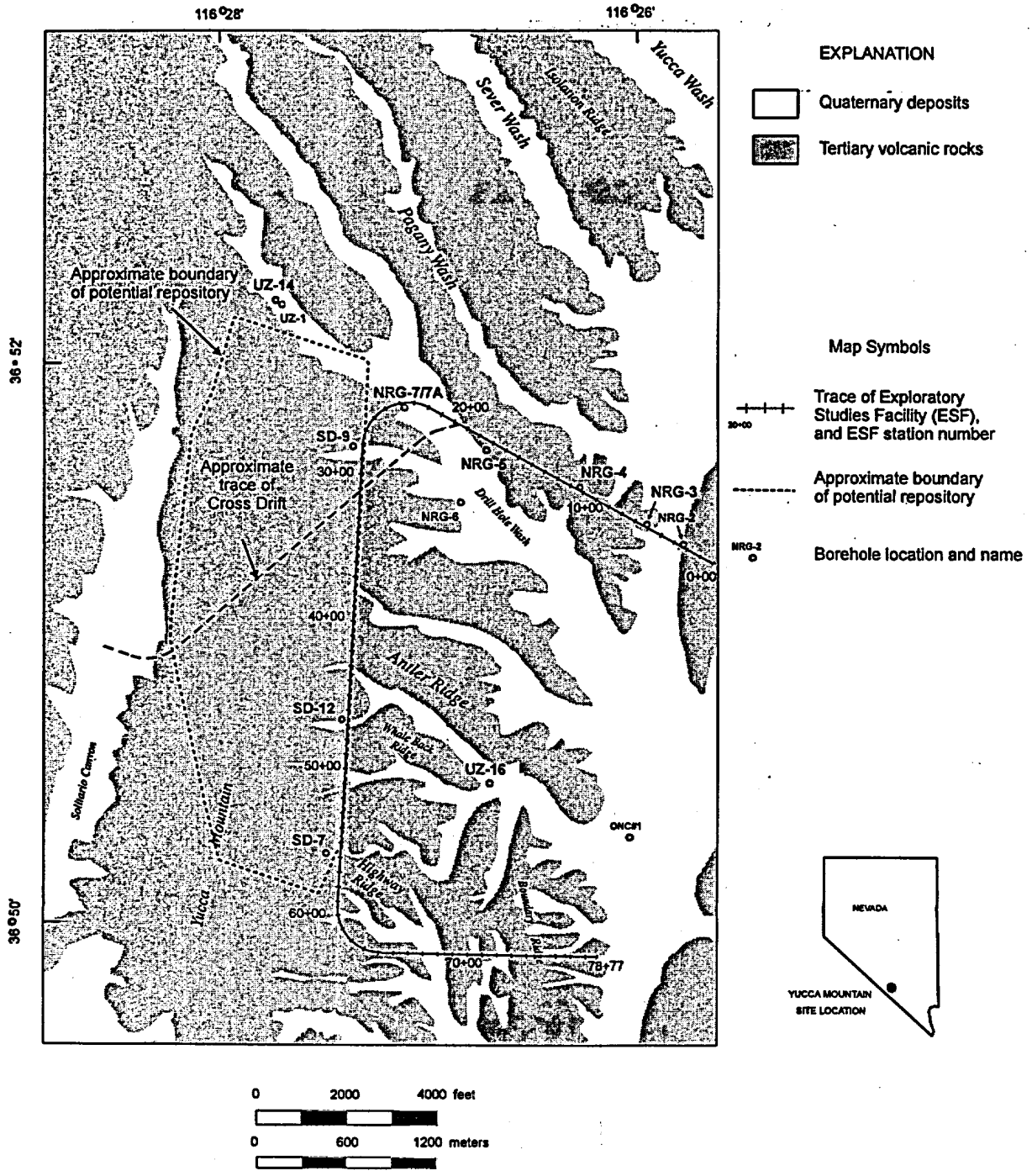

Figure 1-1. Index map of Yucca Mountain, Nevada, showing the trace of the ESF and Cross Drift and locations of selected boreholes.

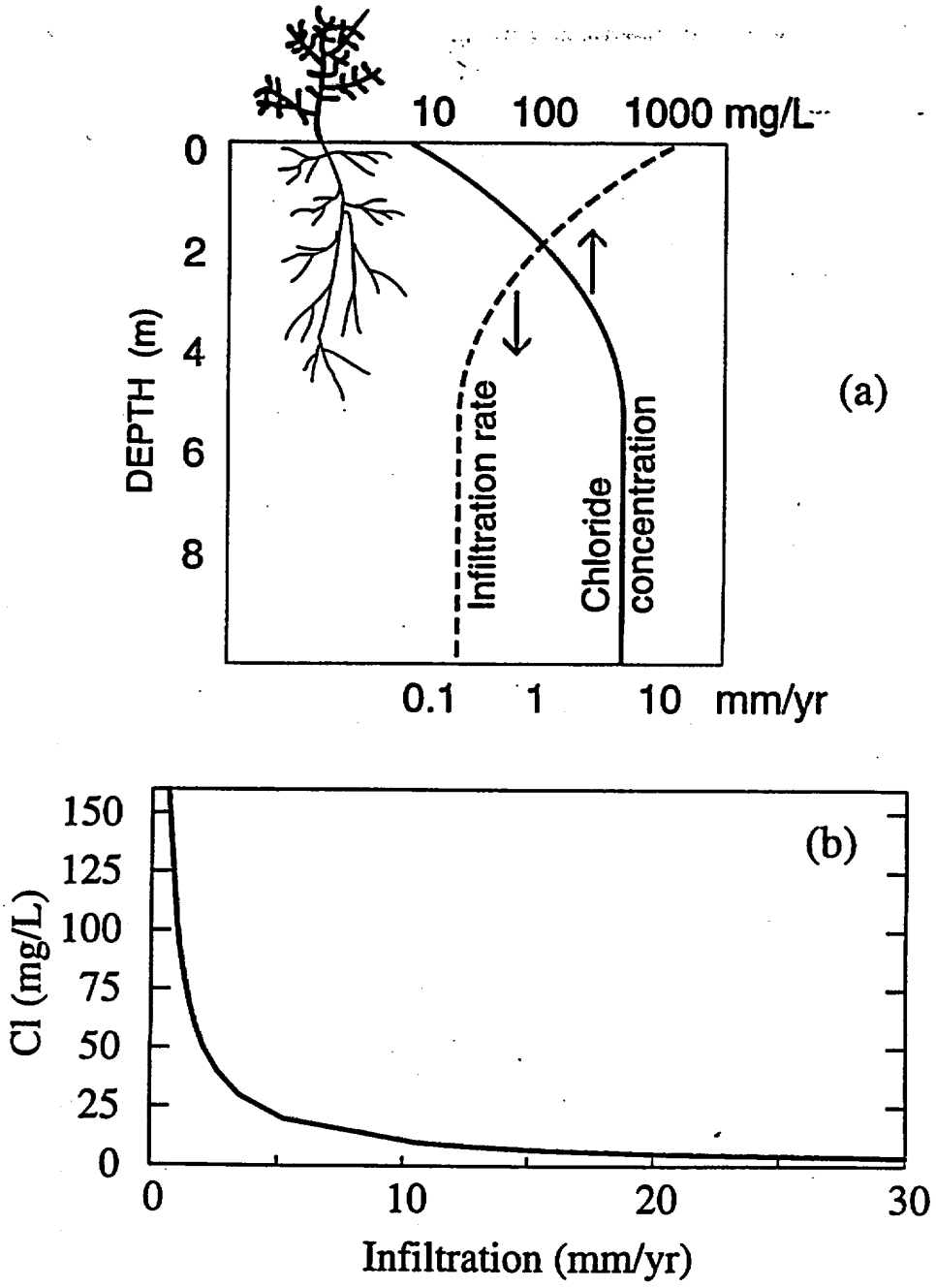

Figure 2-1. Chloride mass balance (CMB) method. (a) Schematic diagram illustrating the underlying basis of the CMB method. (b) Plot showing Cl concentrations as a function of infiltration, assuming 170 mm/yr precipitation with a Cl concentration of 0.62 mg/L (Fabryka-Martin et al., 1997a, section 5).

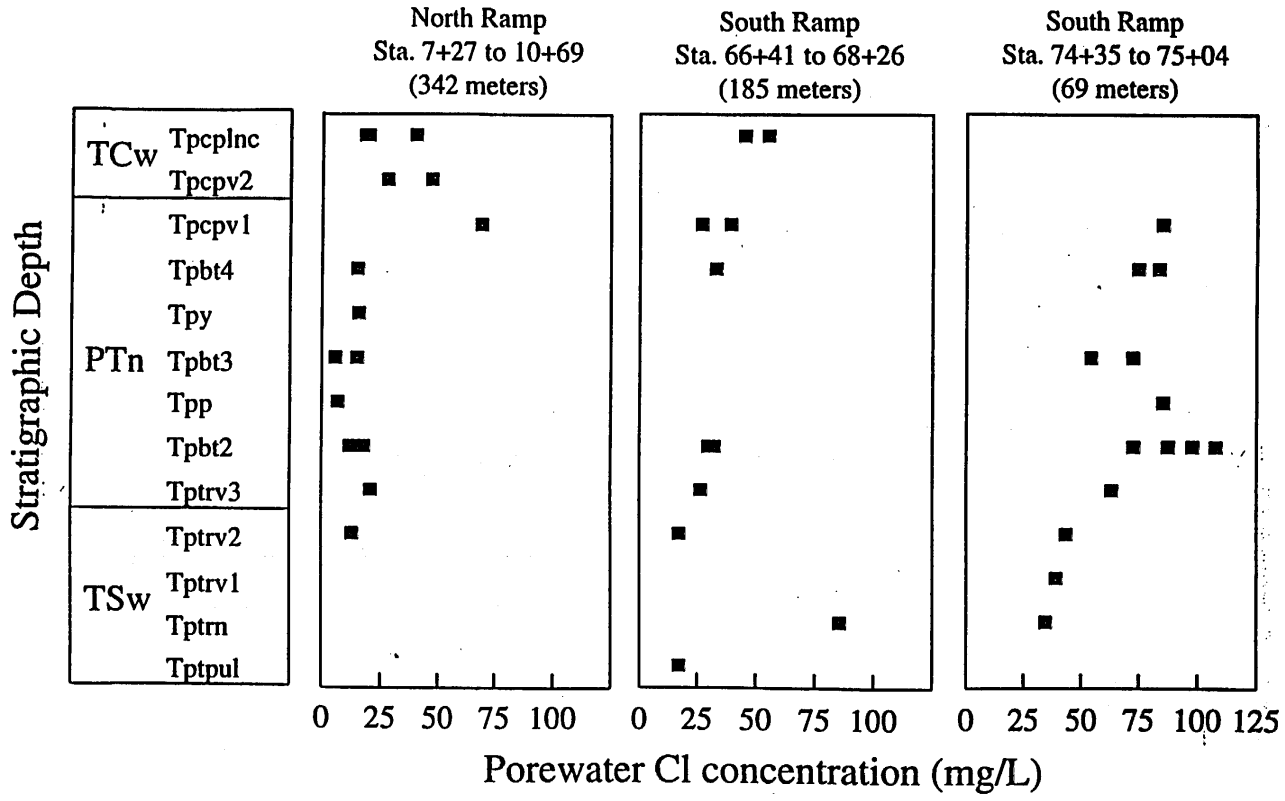

Figure 2-2. Cl porewater concentrations as a function of stratigraphic depth (data from Table 2-1). Six data points from the South Ramp that fall outside the range of stations indicated are not shown.

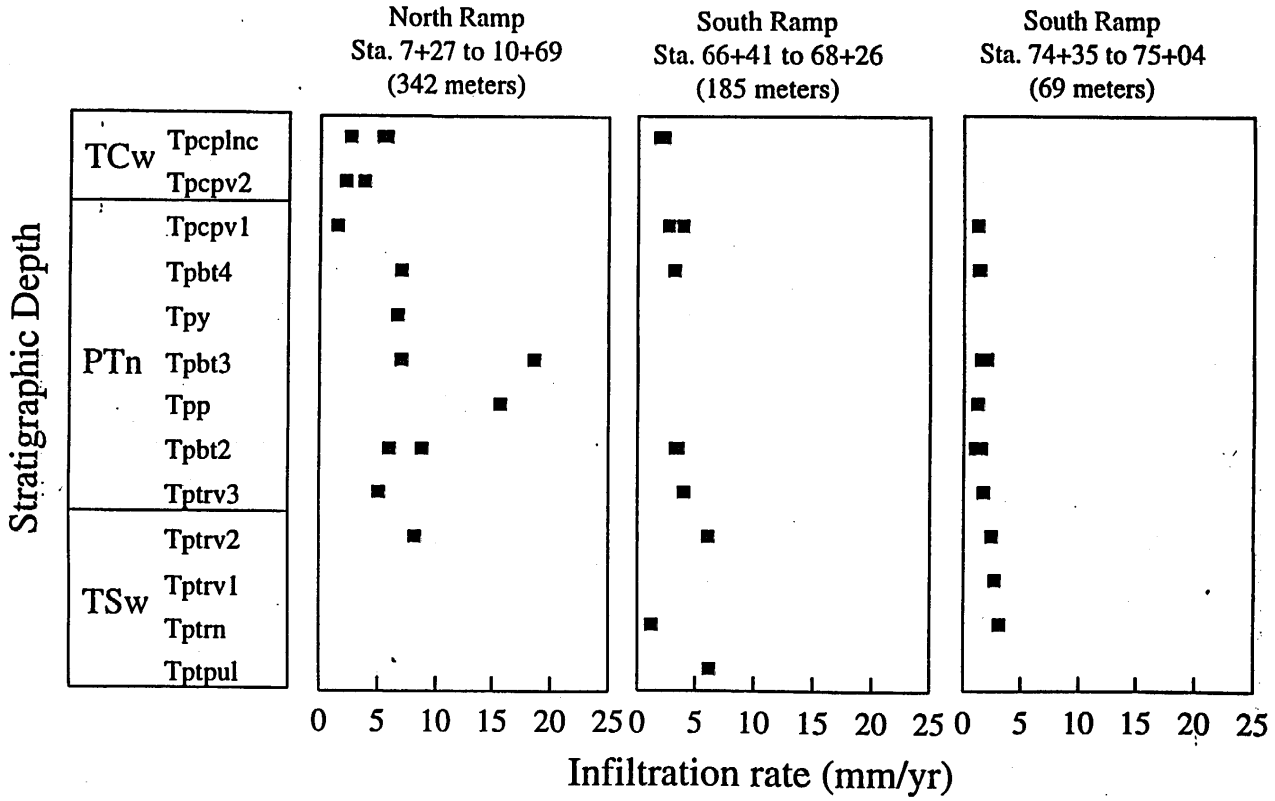

Figure 2-3. Infiltration rates calculated from Cl porewater concentrations as a function of stratigraphic depth (data from Table 2-1). Six data points from the South Ramp that fall outside the range of stations indicated are not shown.

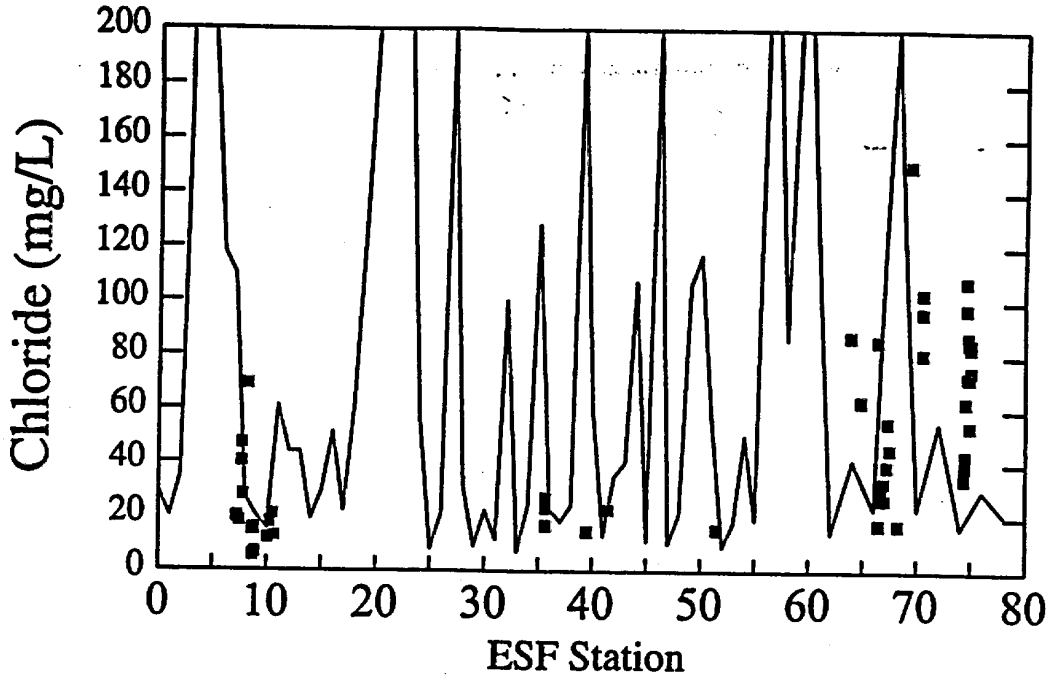

Figure 2-4. Measured Cl porewater concentrations (points) compared against Cl concentrations (curve) calculated from the surface infiltration model of Flint et al. (1996).

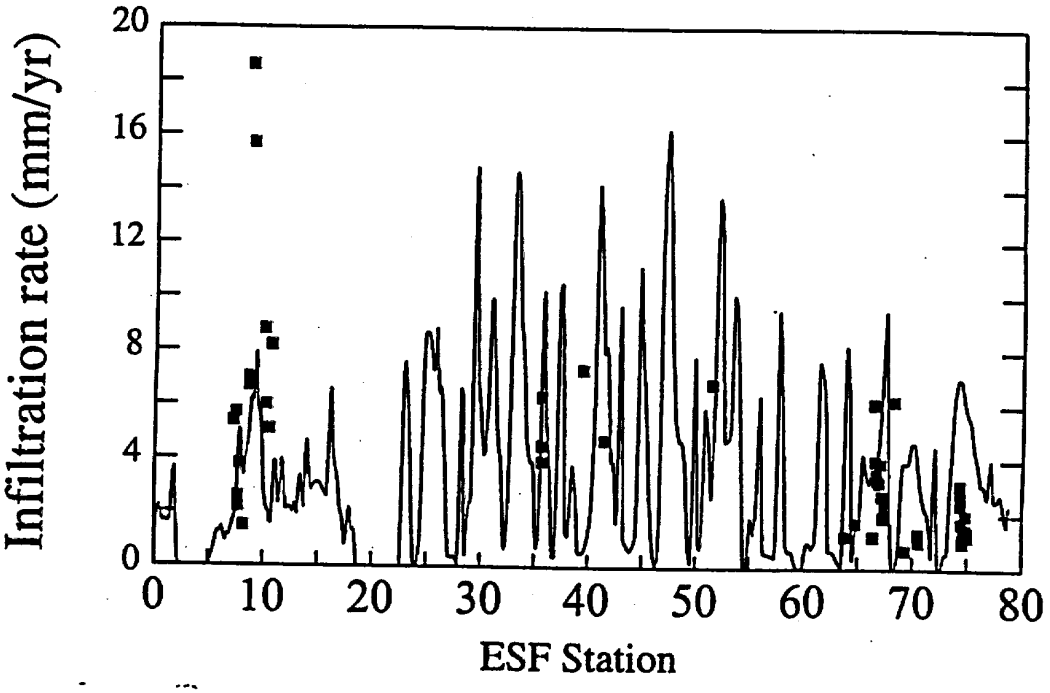

Figure 2-5. Infiltration rates calculated from measured Cl concentrations (points) compared against those (curve) of the surface infiltration model of Flint et al. (1996).

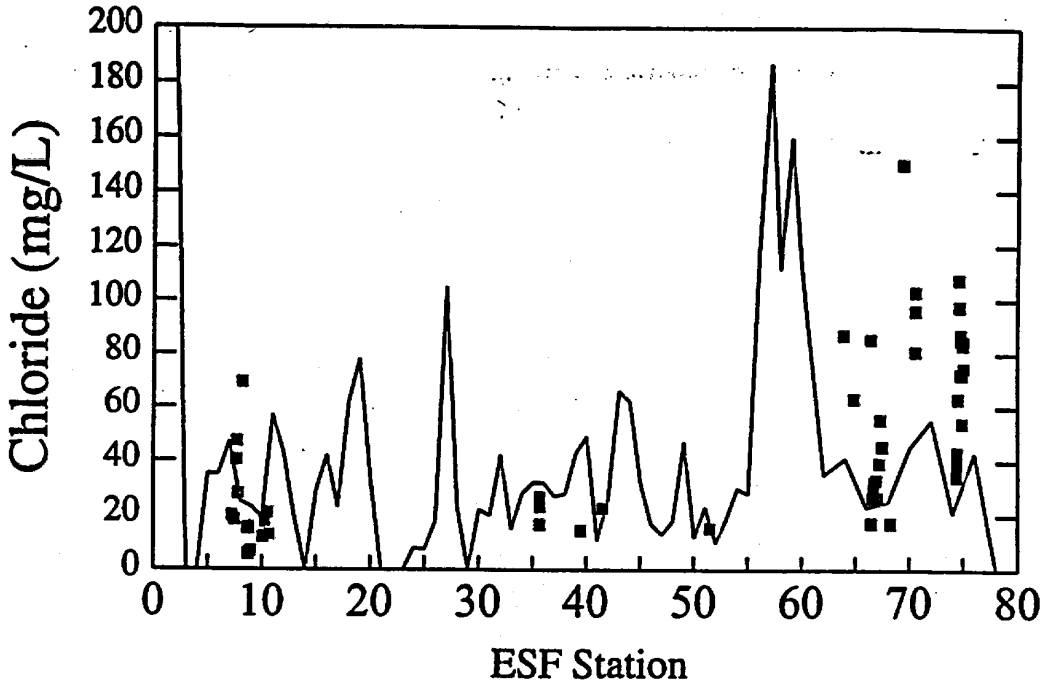

Figure 2-6. Measured Cl porewater concentrations (points) compared against Cl concentrations (curve) predicted for ESF porewaters by the site-scale solute transport model (see section 5).

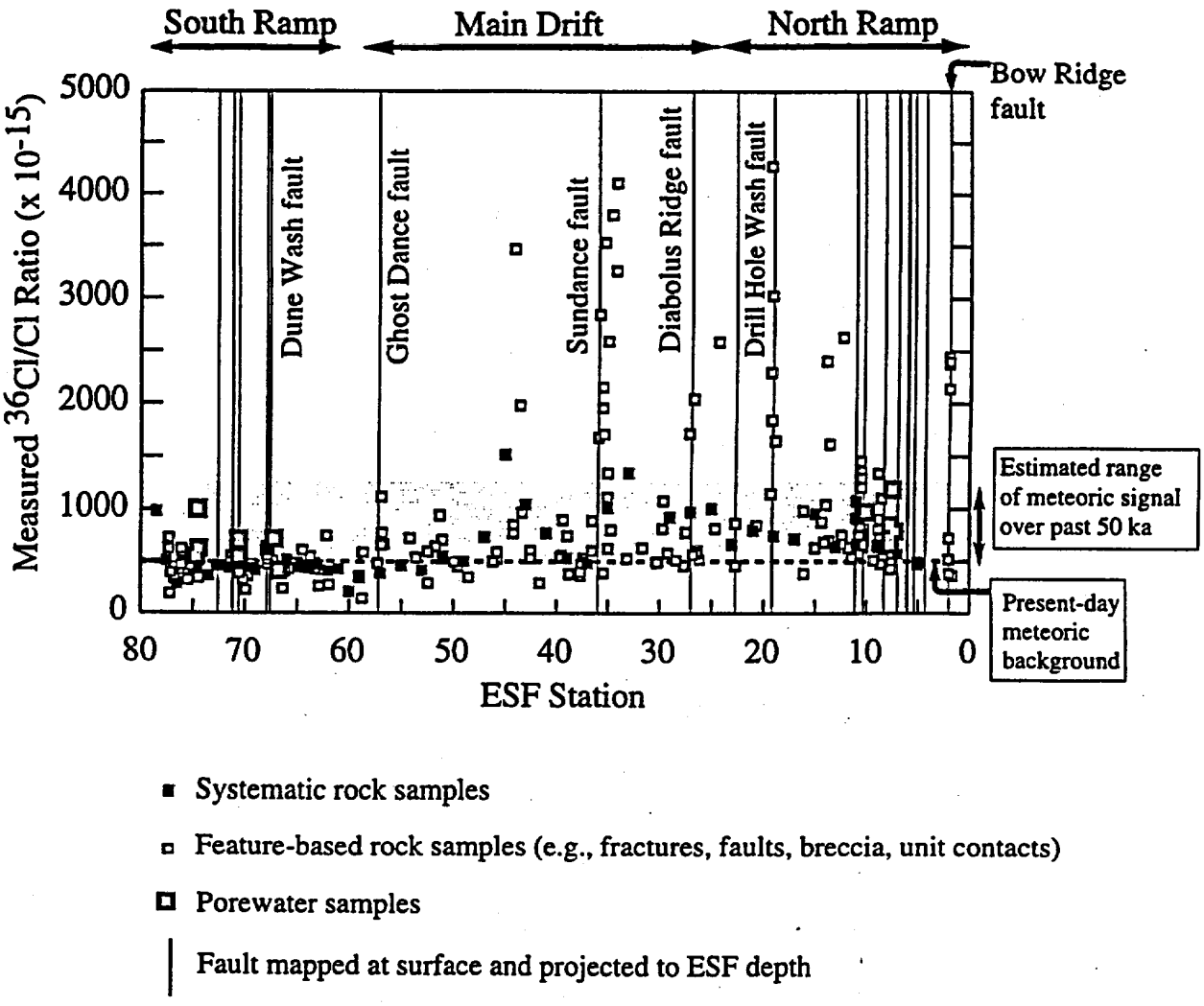

Figure 3-1. Distribution of $^{36}Cl/Cl$ measured for ESF samples. Analytical uncertainties are less than 10%. Data source: DTN LAJF831222AQ98.004 and LAJF831222AQ98.010.

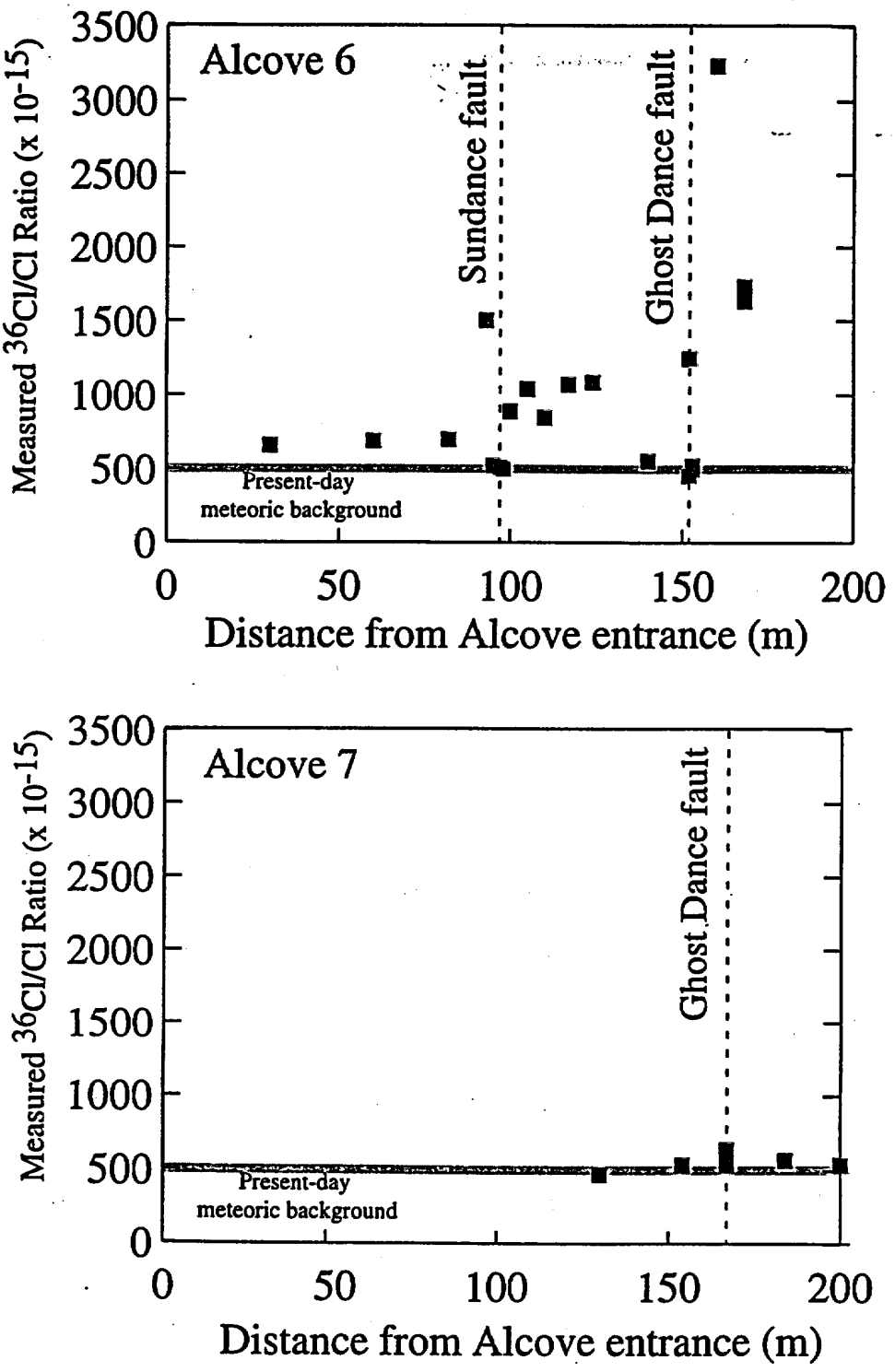

Figure 3-2. Distribution of $^{36}Cl/Cl$ ratios measured for samples from ESF Alcoves 6 and 7. Analytical uncertainties are less than 10%. Data source: DTN LAJF831222AQ98.004.

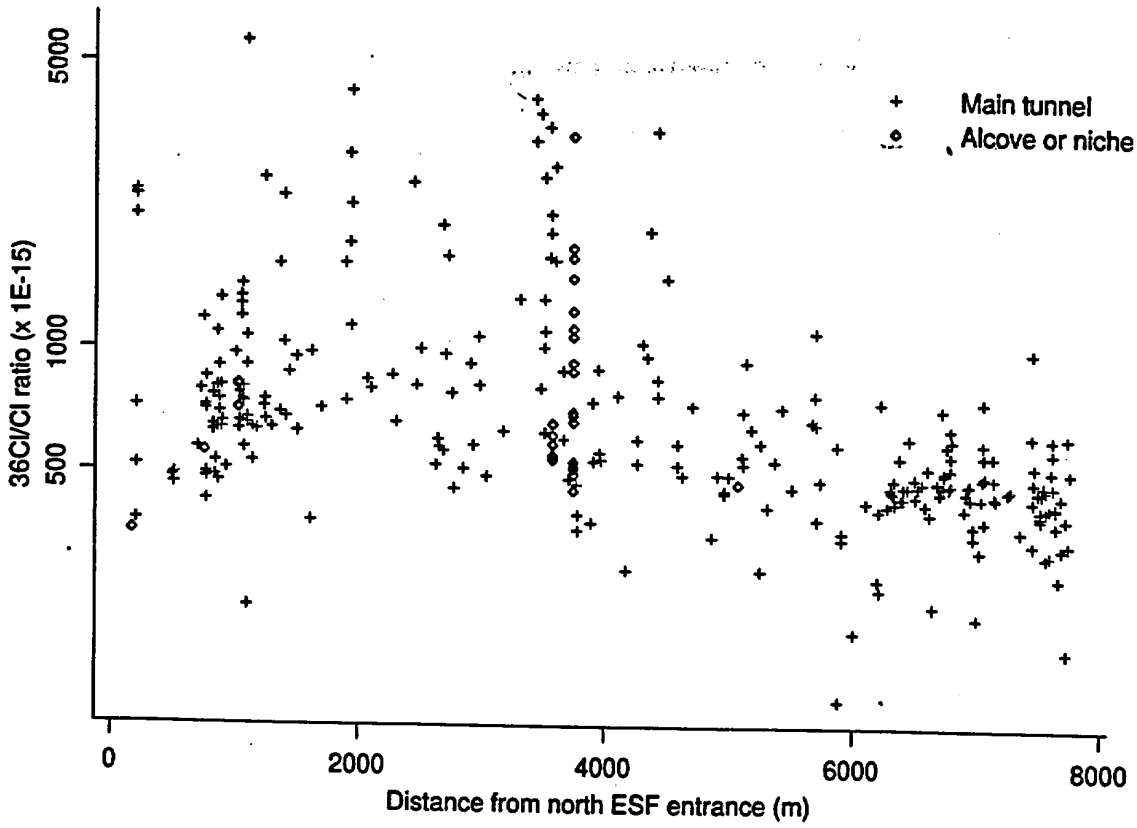

Figure 4-1. $^{36}Cl/Cl$ ratio data

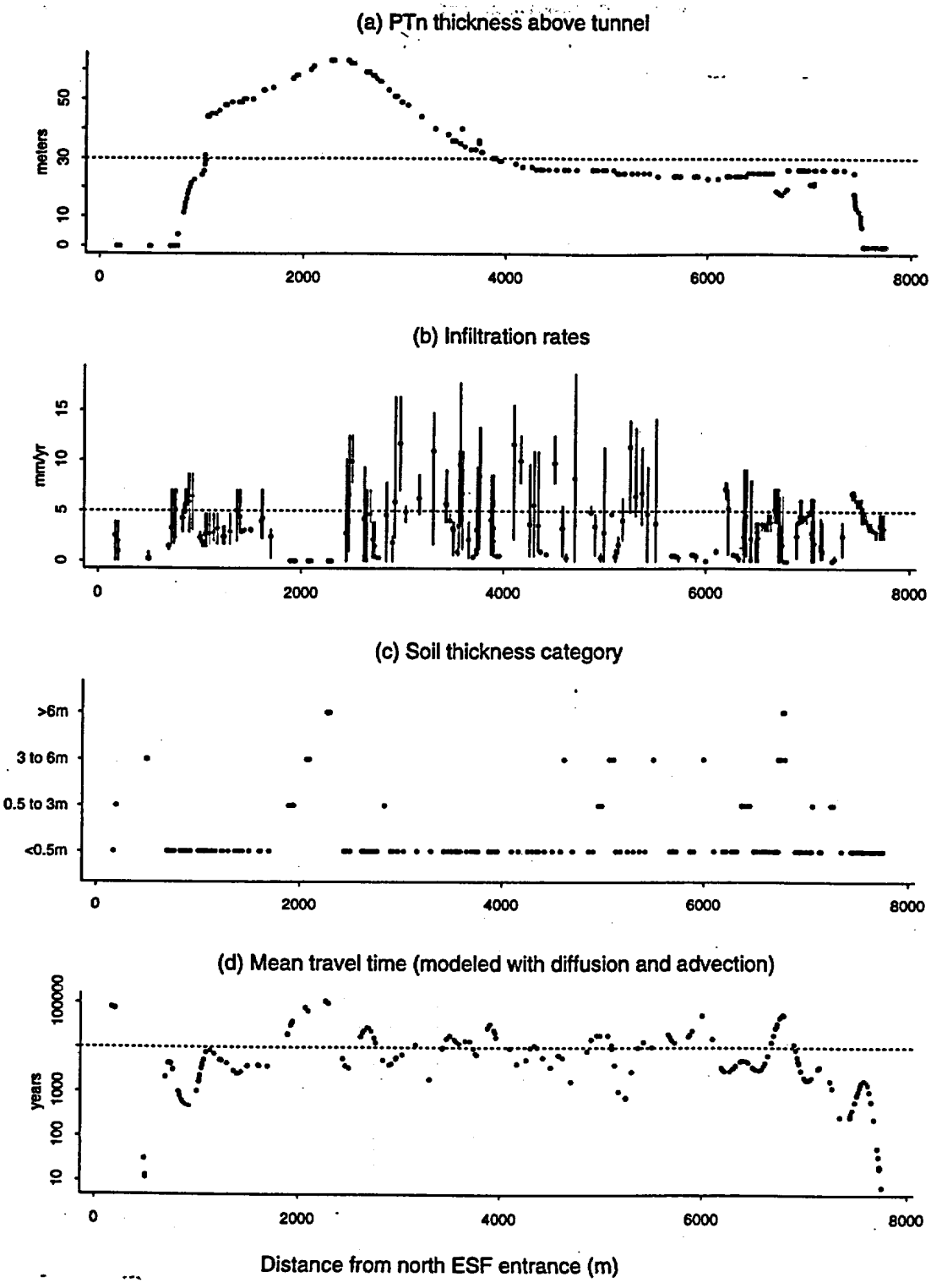

Figure 4-2. Covariates measured or modeled for ESF sample locations

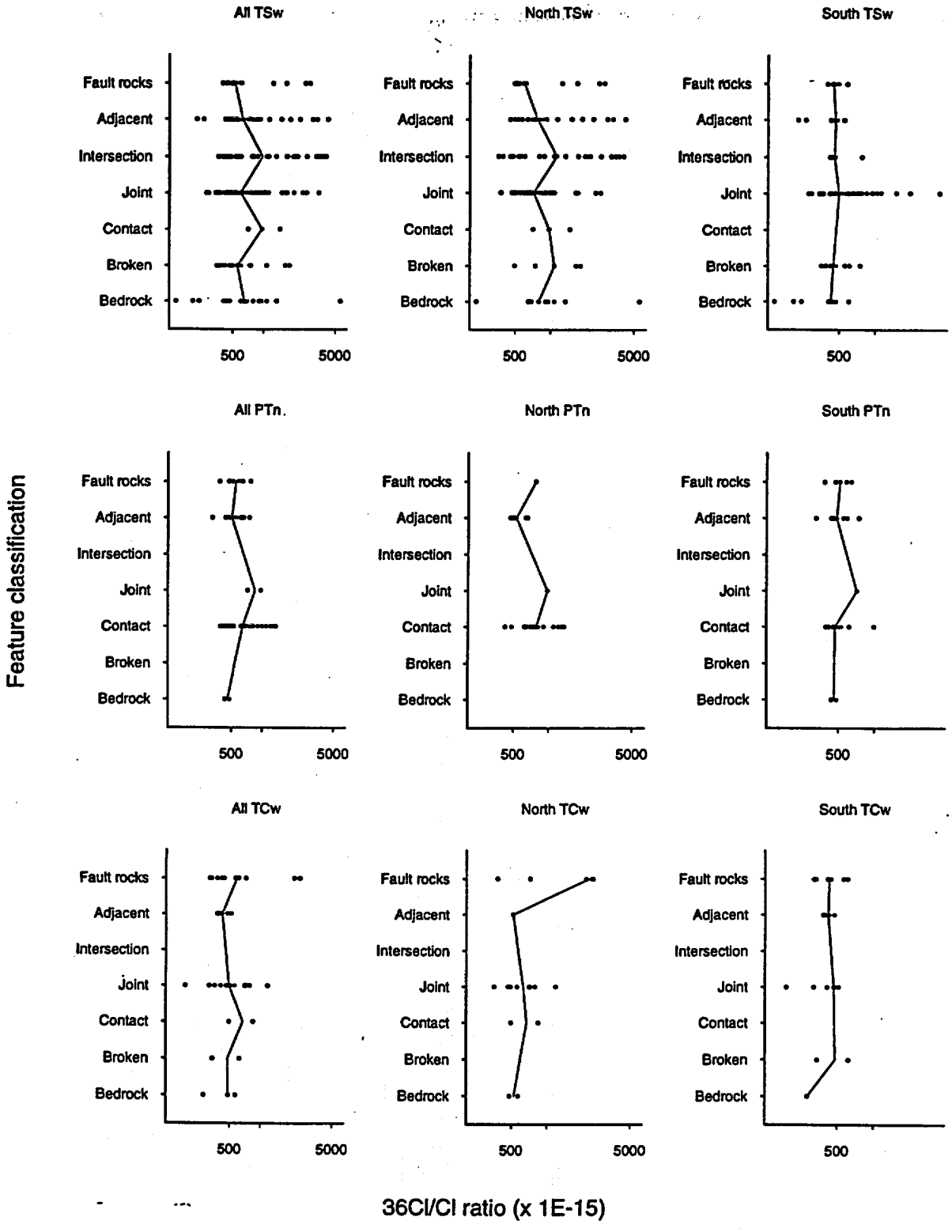

Figure 4-3(a). $^{36}Cl/Cl$ ratio as a function of feature classification (defined in Table 4-2)

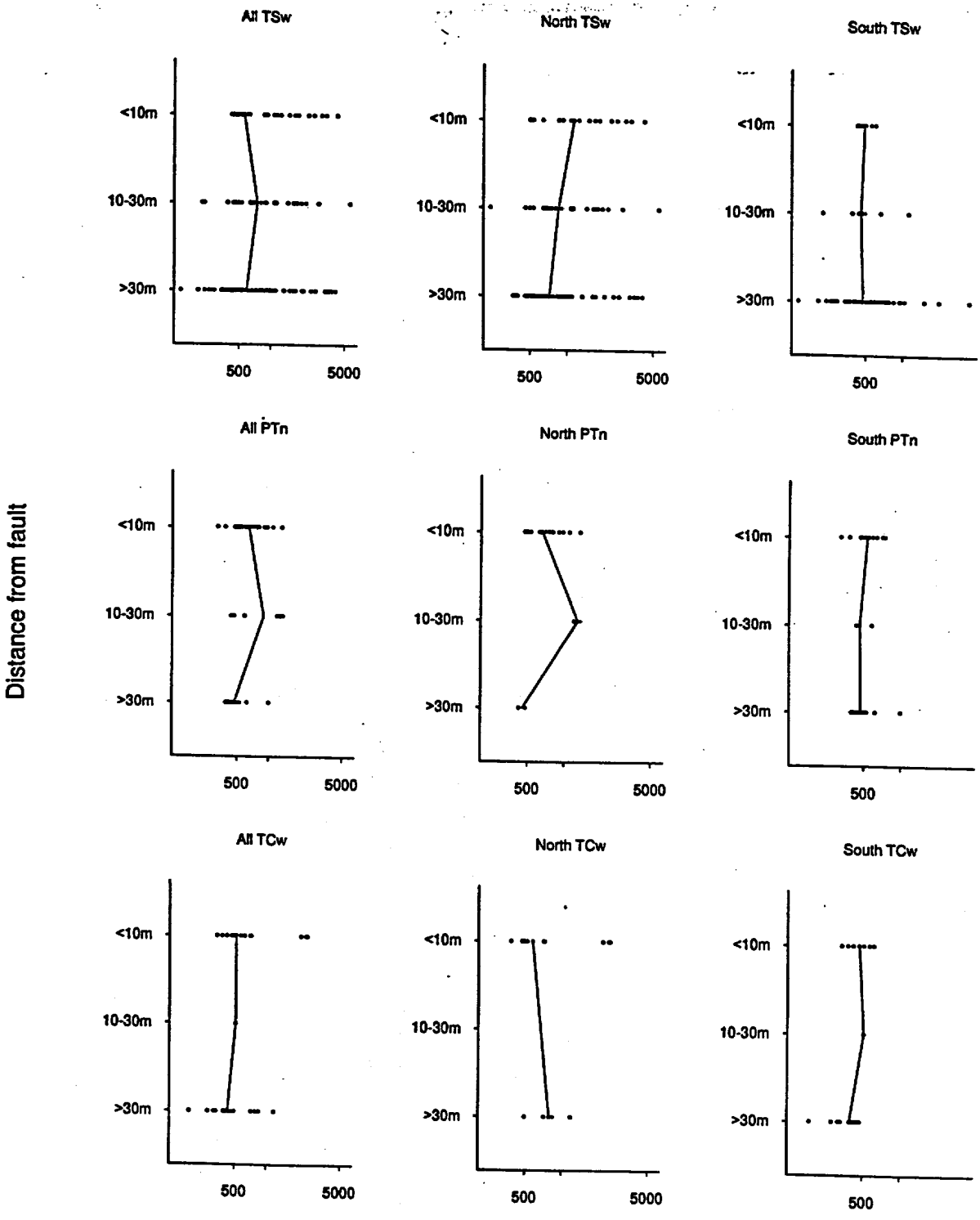

Figure 4-3(b). $^{36}Cl/Cl$ ratio as a function of distance from fault

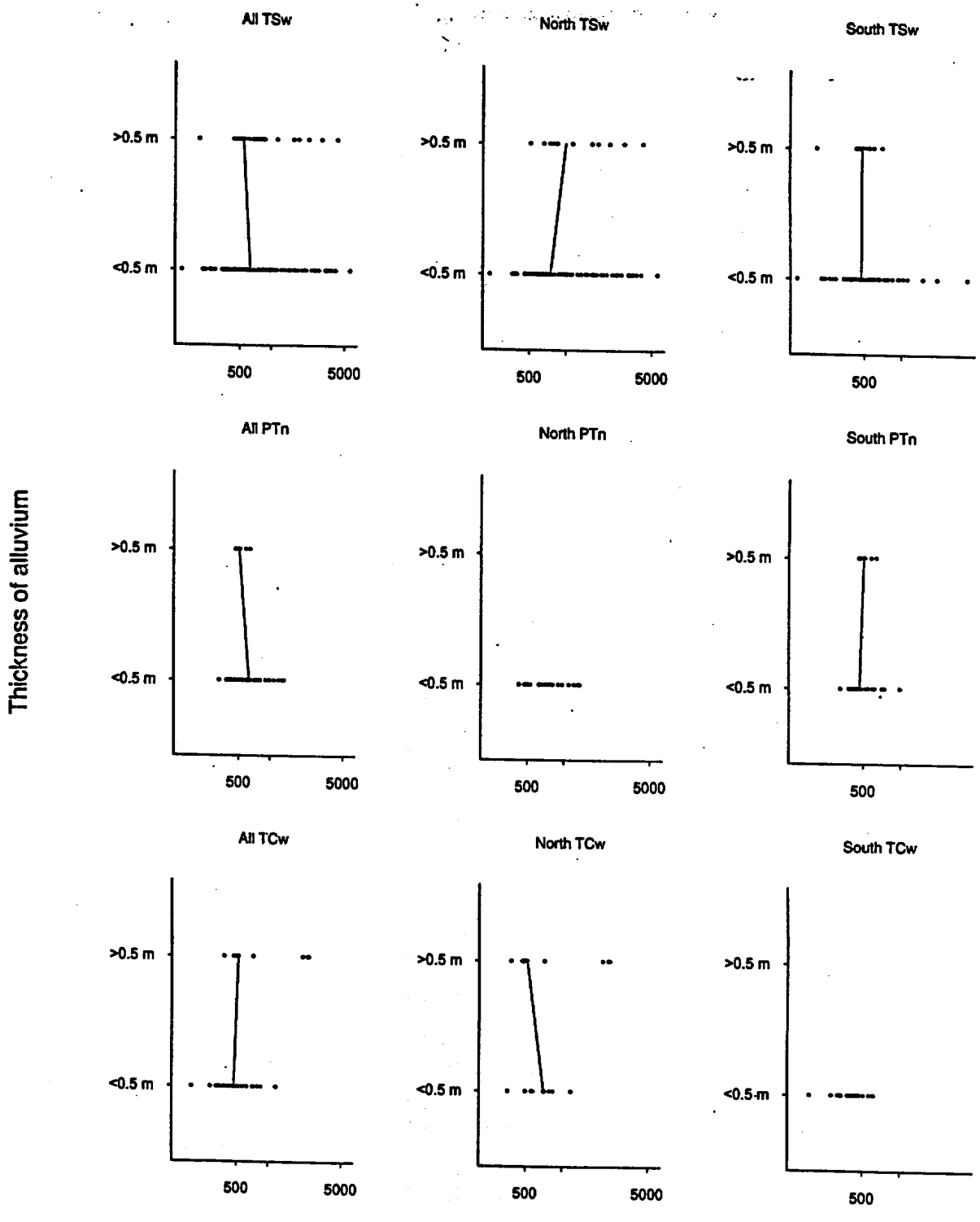

Figure 4-3(c). $^{36}Cl/Cl$ ratio as a function of thickness of alluvial overburden

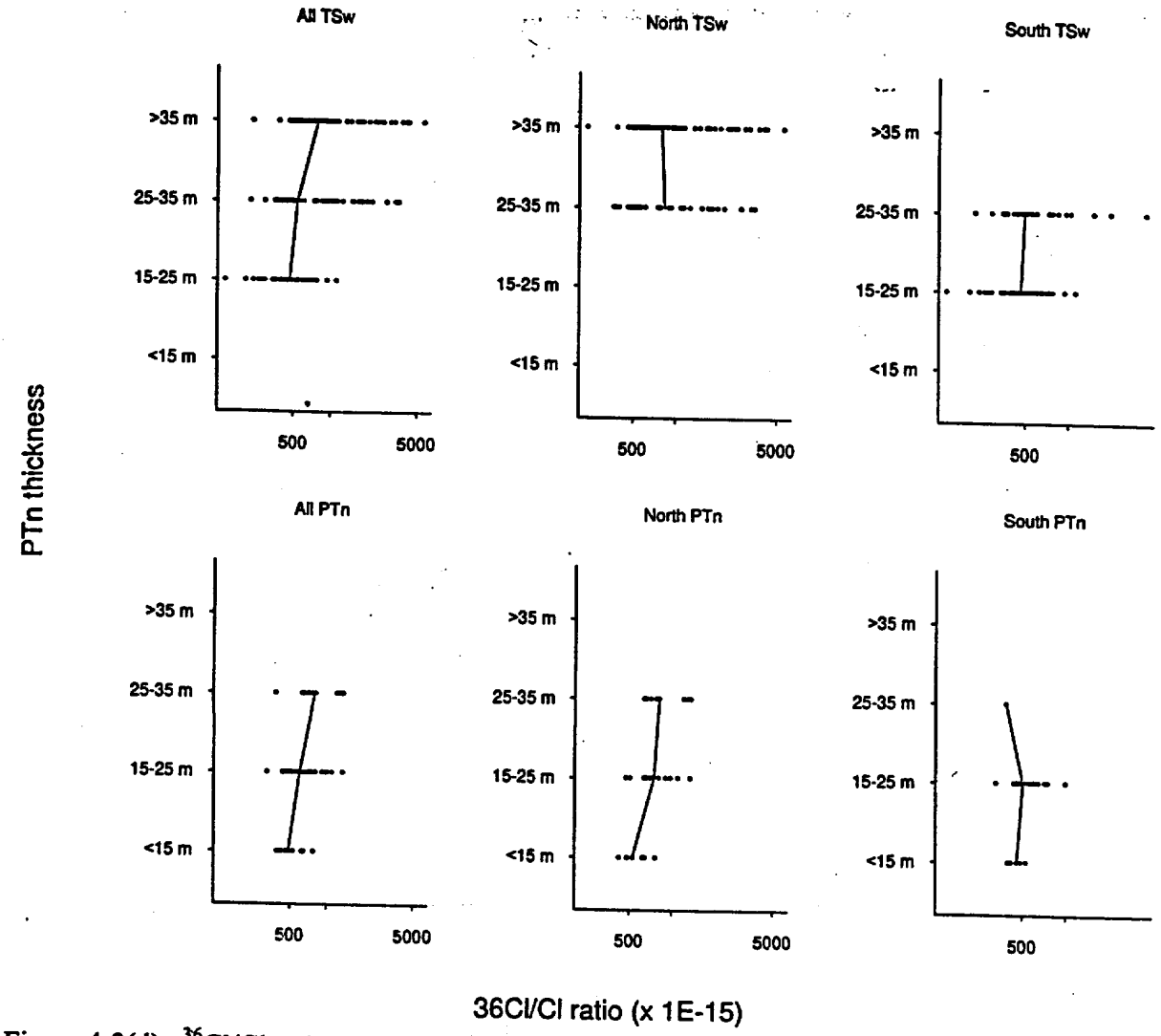

Figure 4-3(d). $^{36}Cl/Cl$ ratio as a function of thickness of overlying PTn

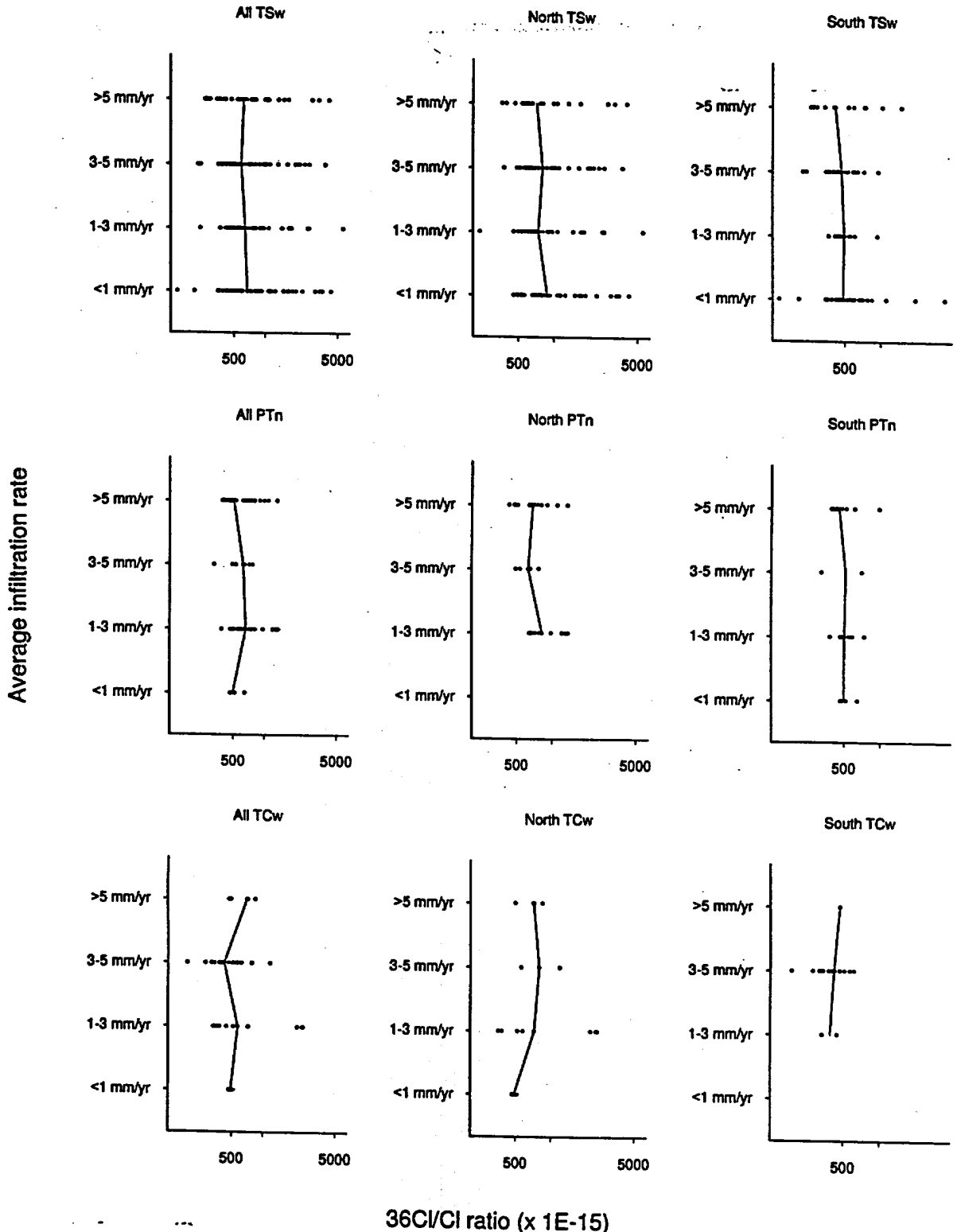

Figure 4-3(e). $^{36}Cl/Cl$ ratio as a function of average infiltration rate

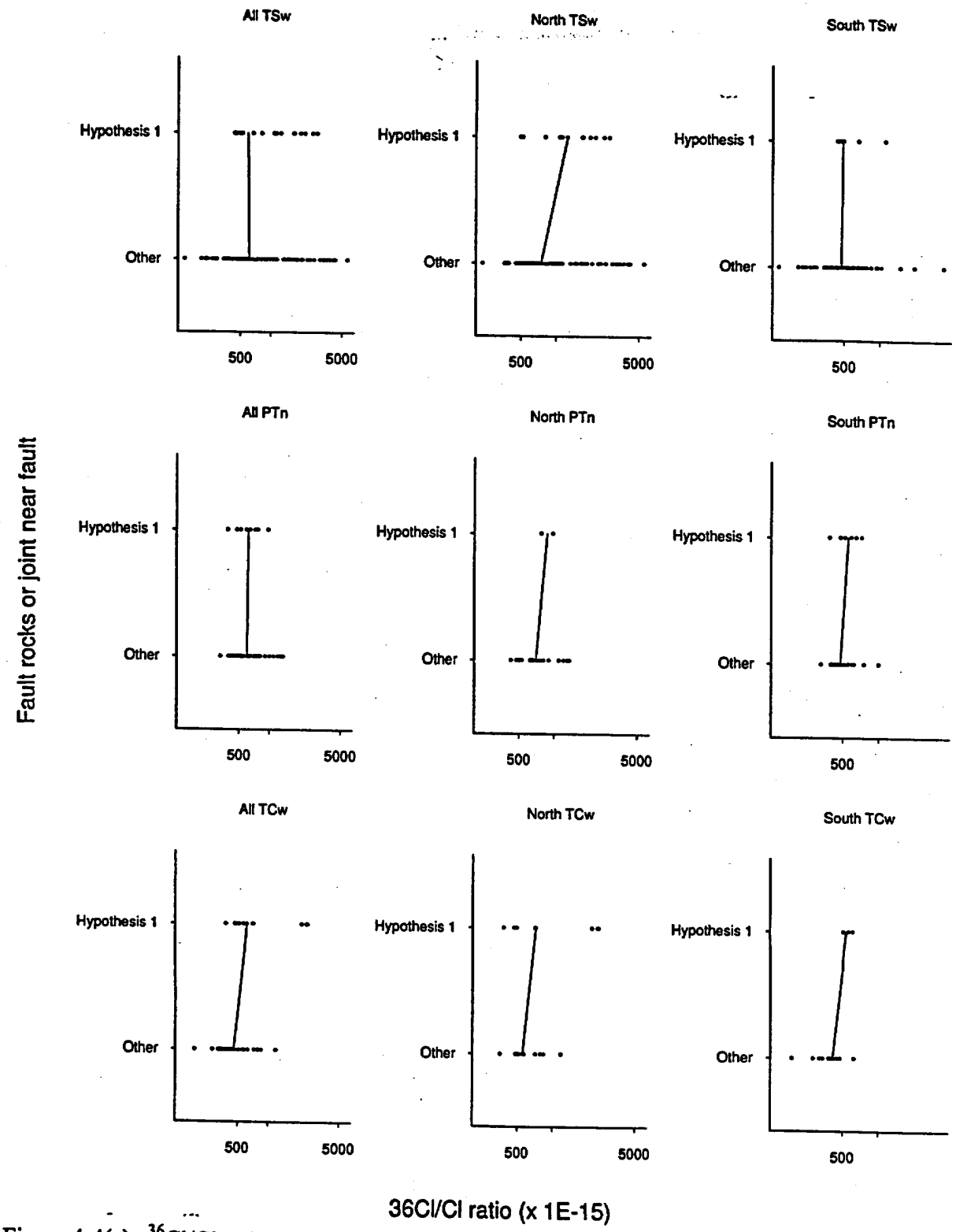

Figure 4-4(a). $^{36}Cl/Cl$ ratio to test hypothesis that bomb pulse is associated with structural features in fault zones

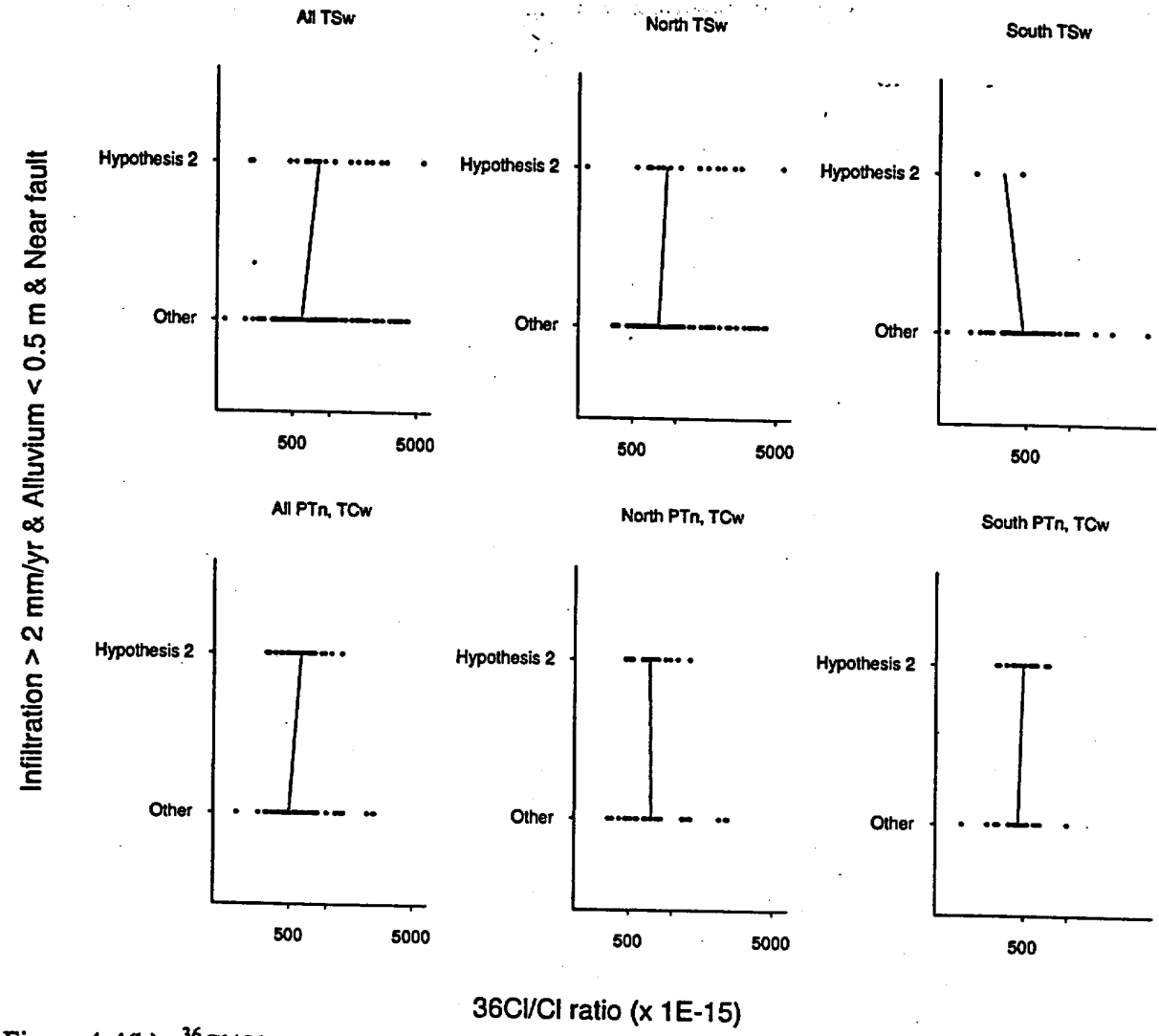

Figure 4-4(b). $^{36}Cl/Cl$ ratio to test hypothesis that bomb pulse is associated with infiltration > 2 mm/yr and alluvial overburden < 0.5m in fault zones (within 30m of faults)

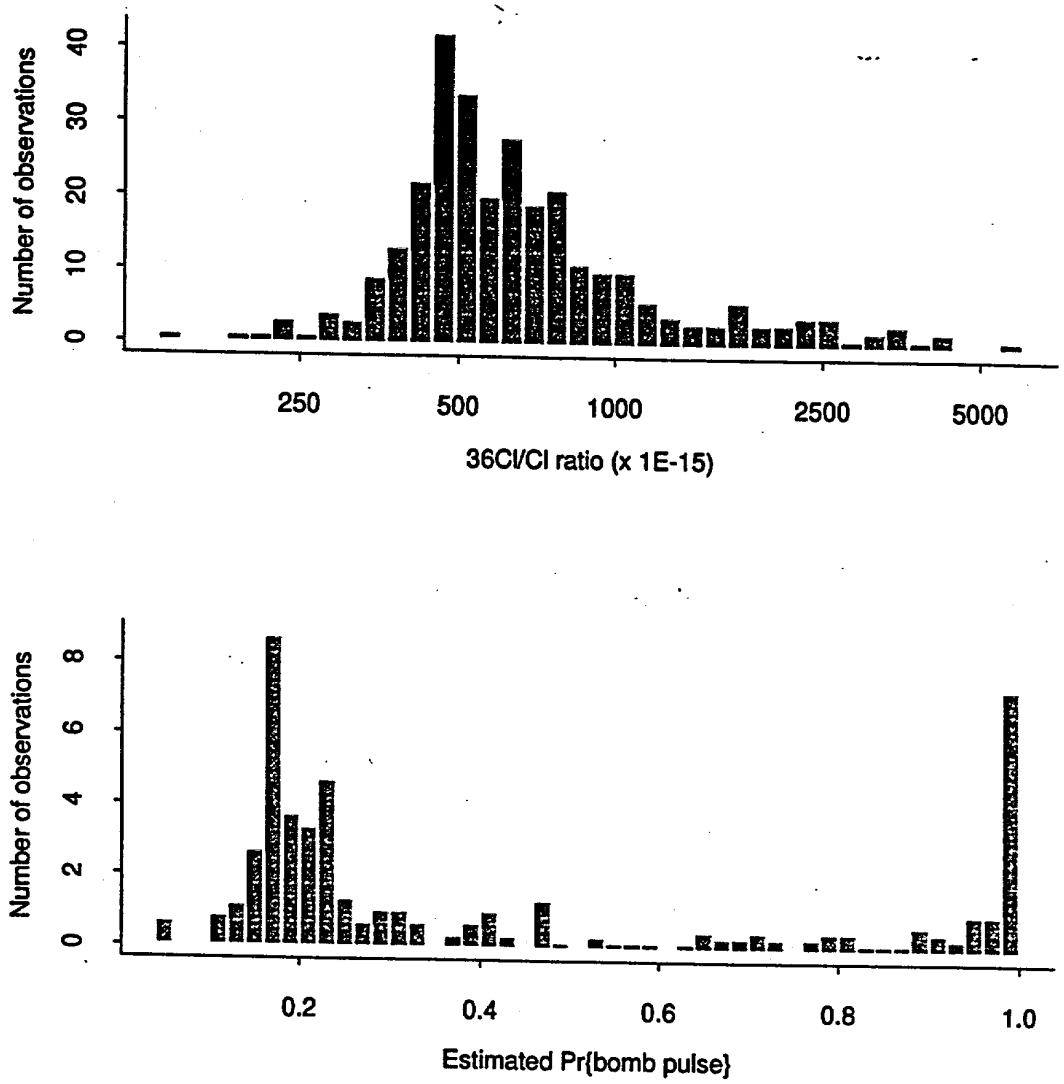

Figure 4-5. Histograms of $^{36}Cl/Cl$ ratio data and of estimated probabilities of bomb pulse

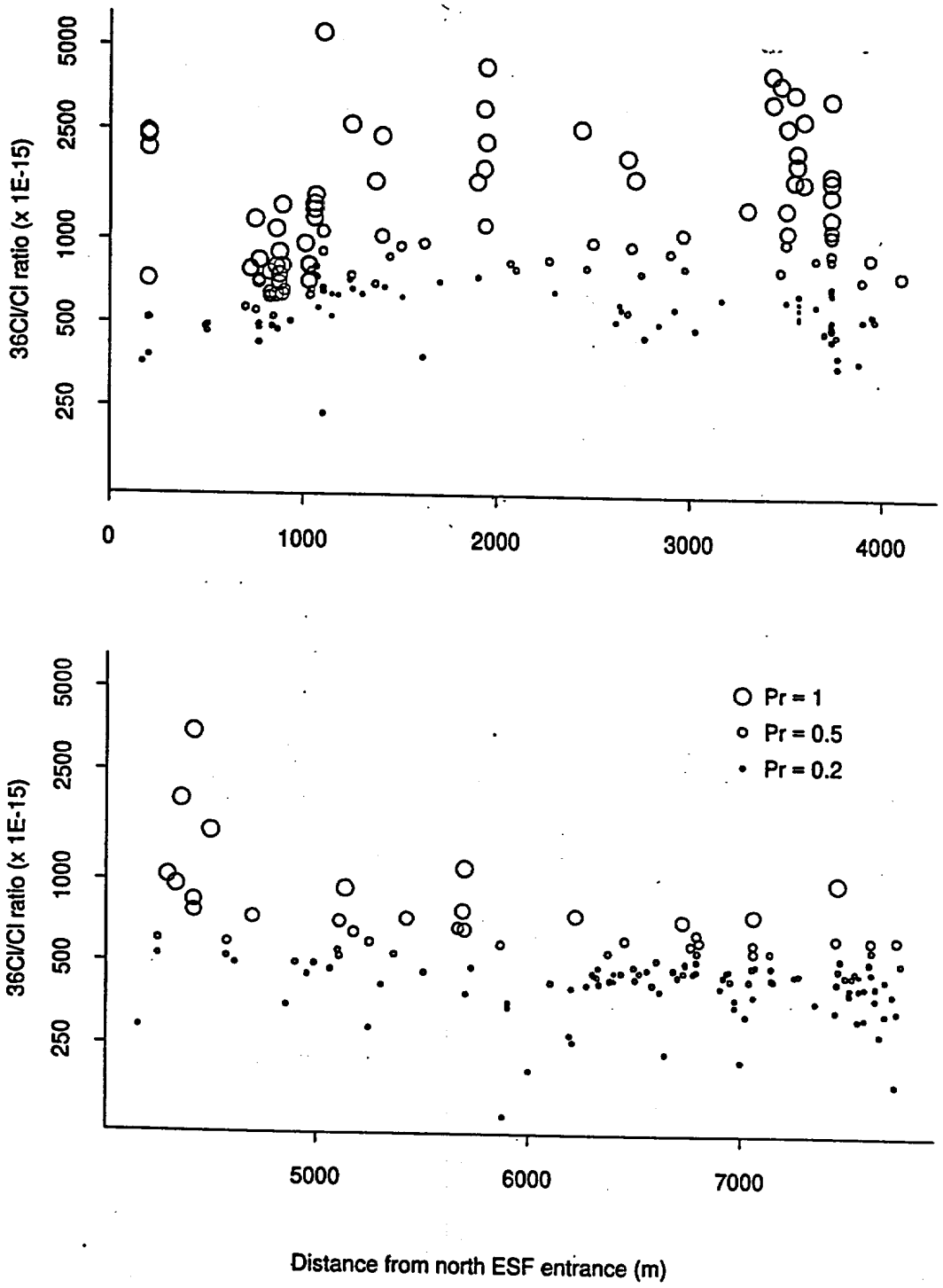

Figure 4-6. Probability classification of $^{36}Cl/Cl$ ratio data

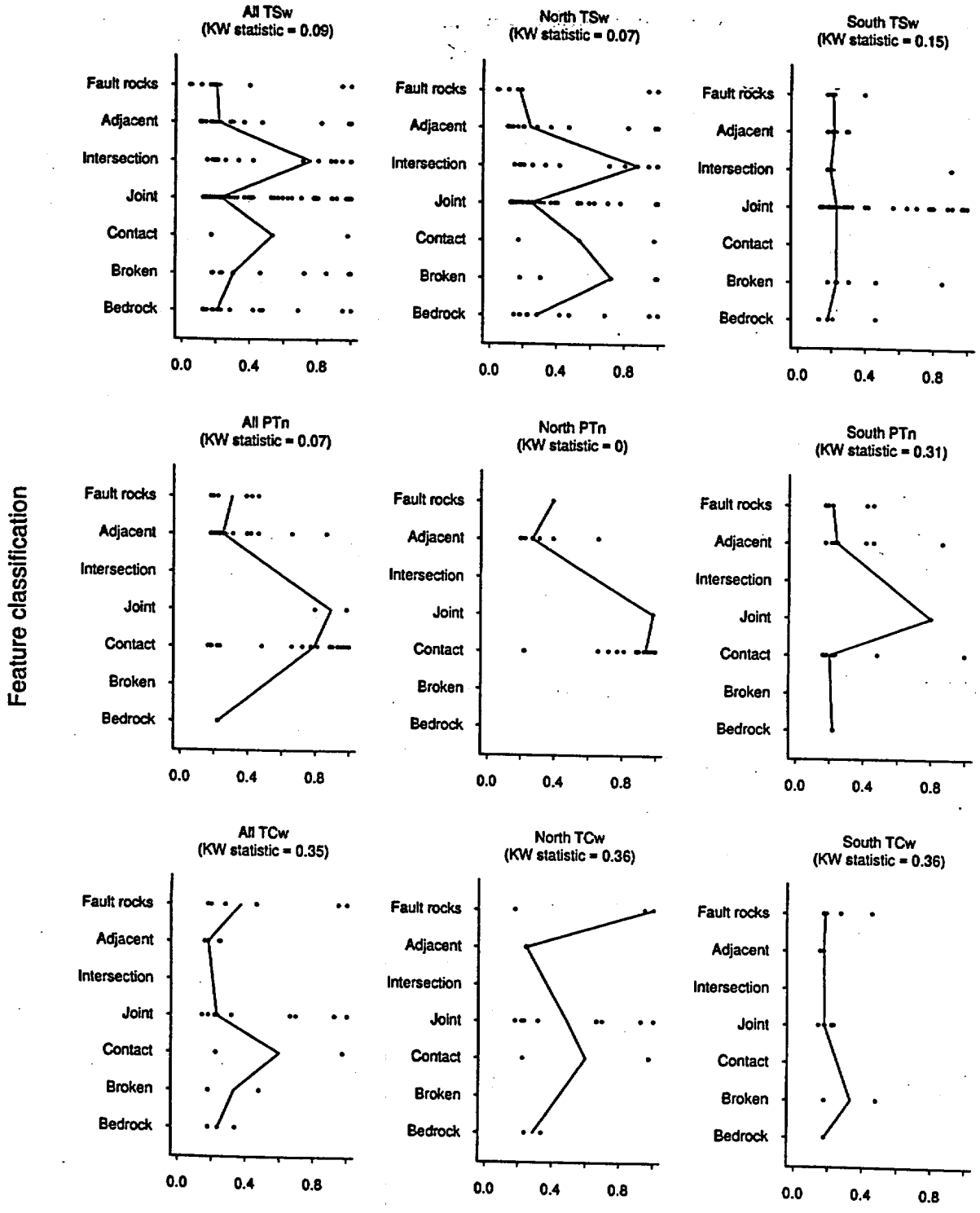

Figure 4-7(a). Estimated probability of bomb pulse as a function of feature classification

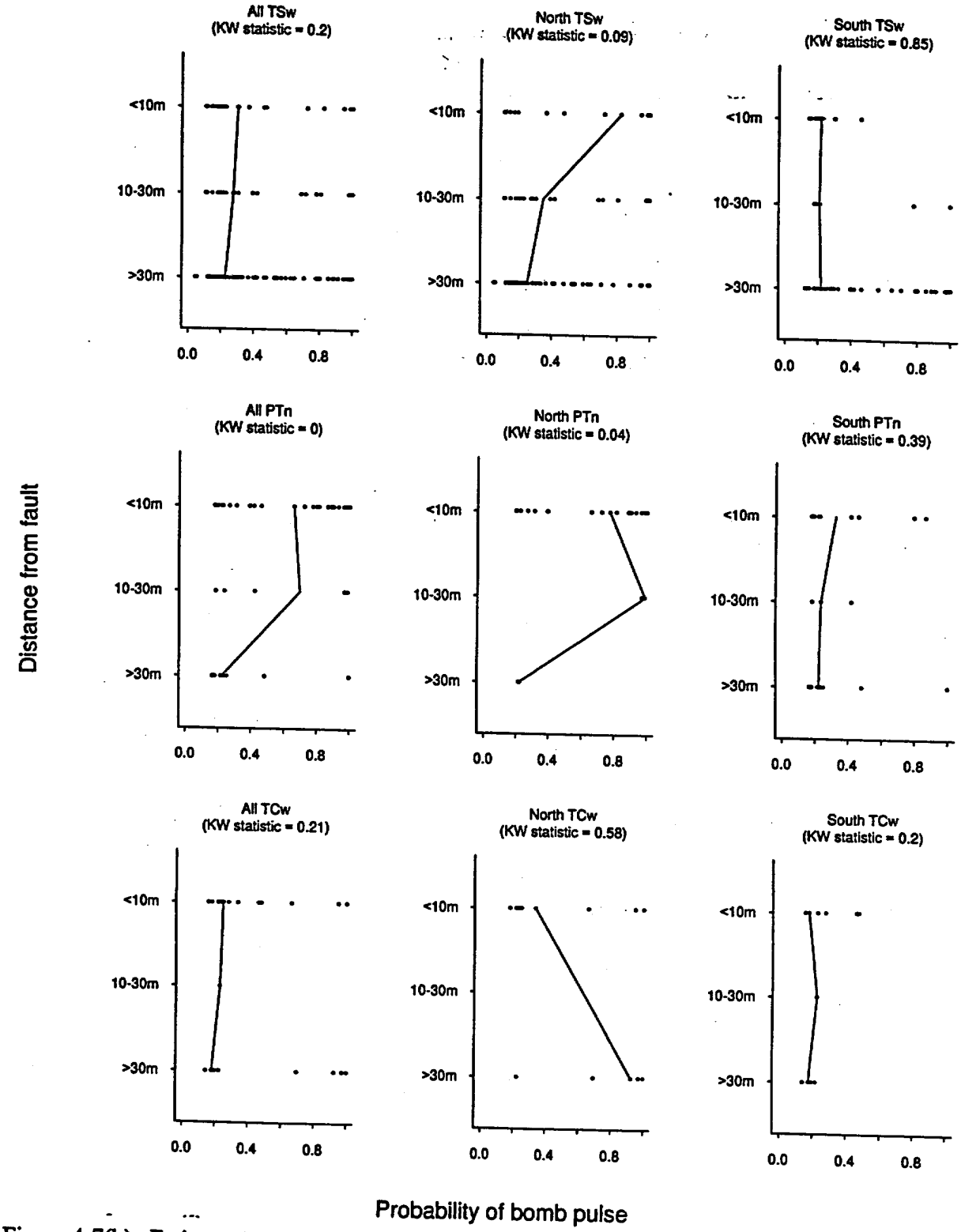

Figure 4-7(b). Estimated probability of bomb pulse as a function of distance from fault

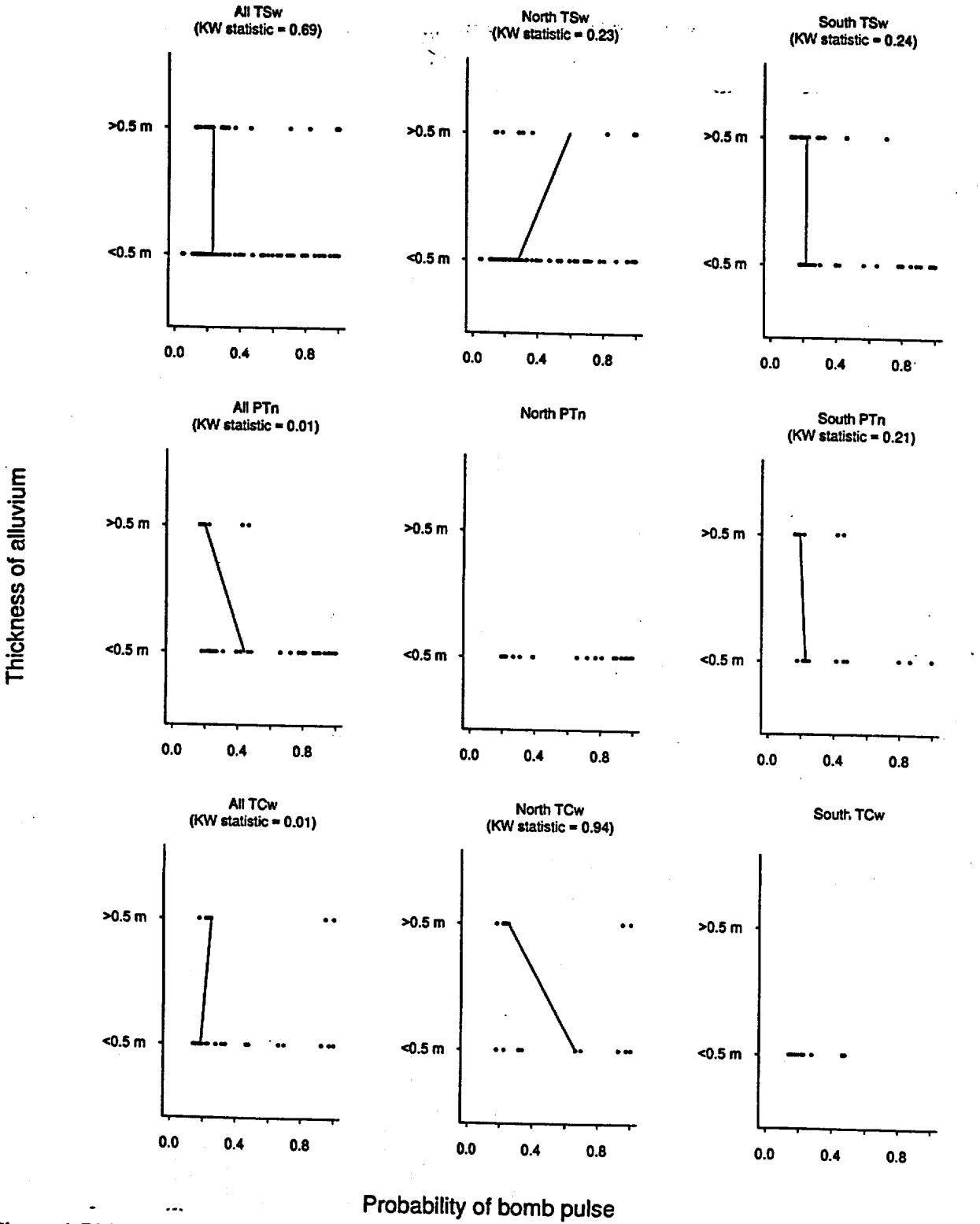

Figure 4-7(c). Estimated probability of bomb pulse as a function of thickness of alluvial overburden

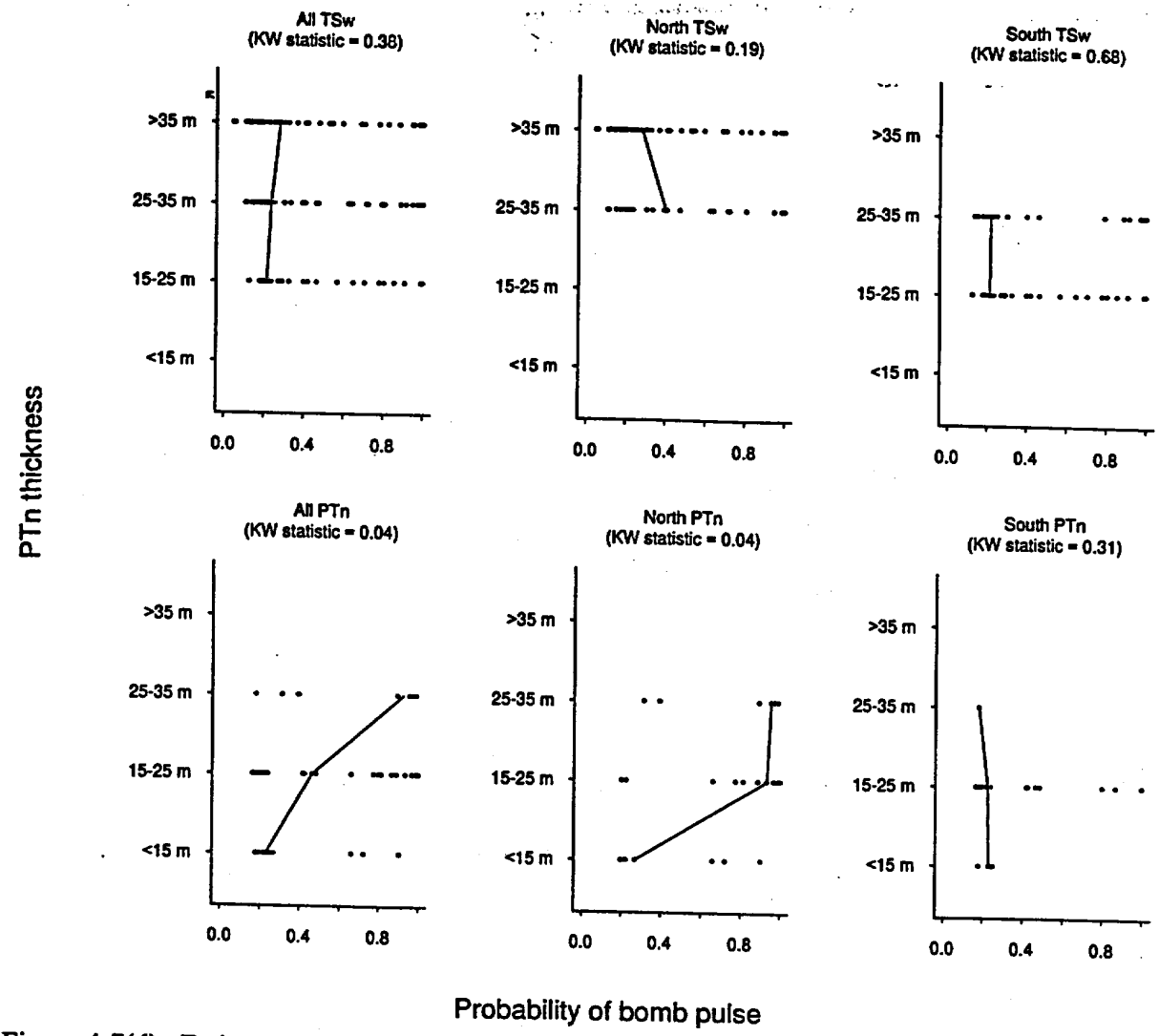

Figure 4-7(d). Estimated probability of bomb pulse as a function of thickness of overlying PTn

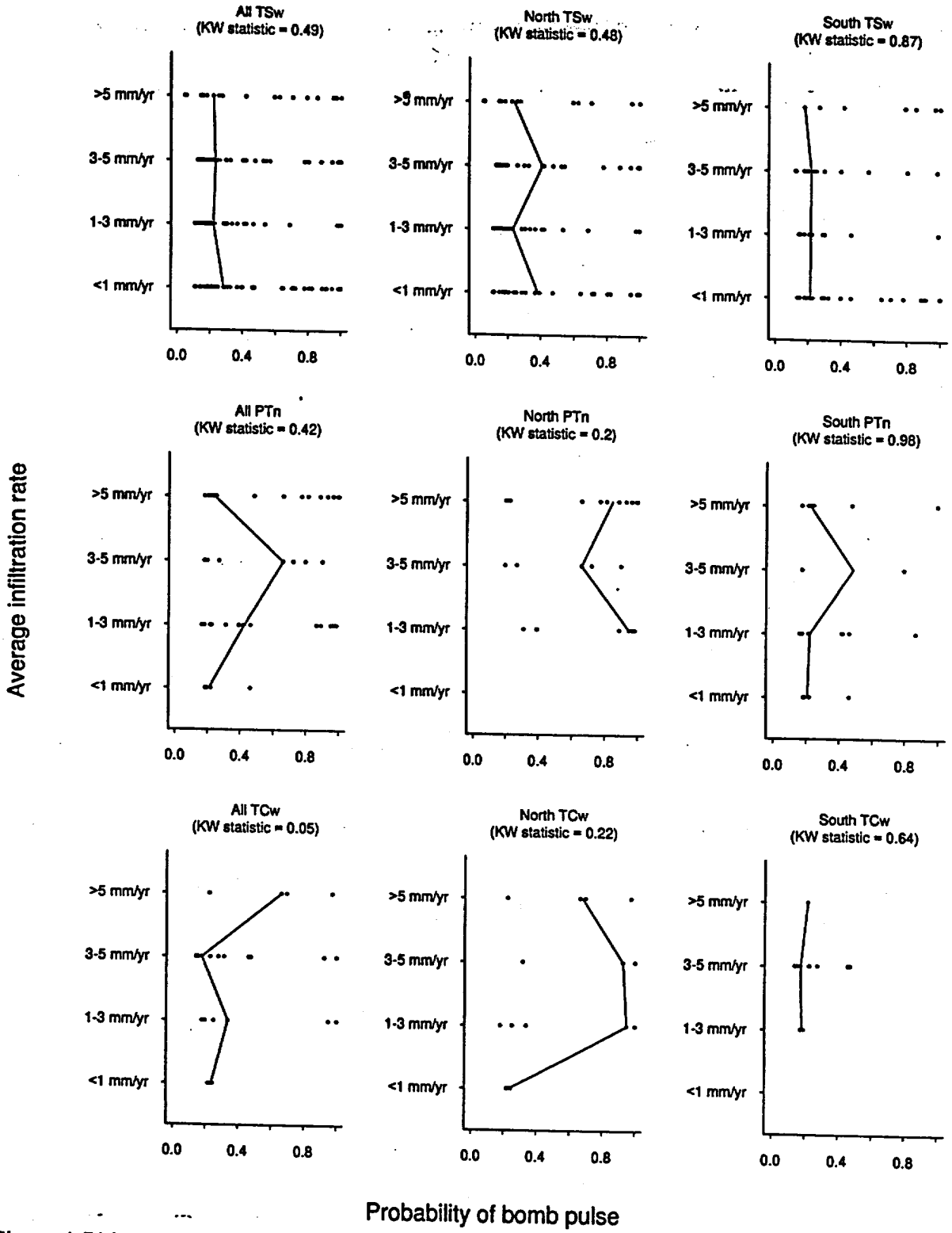

Figure 4-7(e). Estimated probability of bomb pulse as a function of average infiltration rate

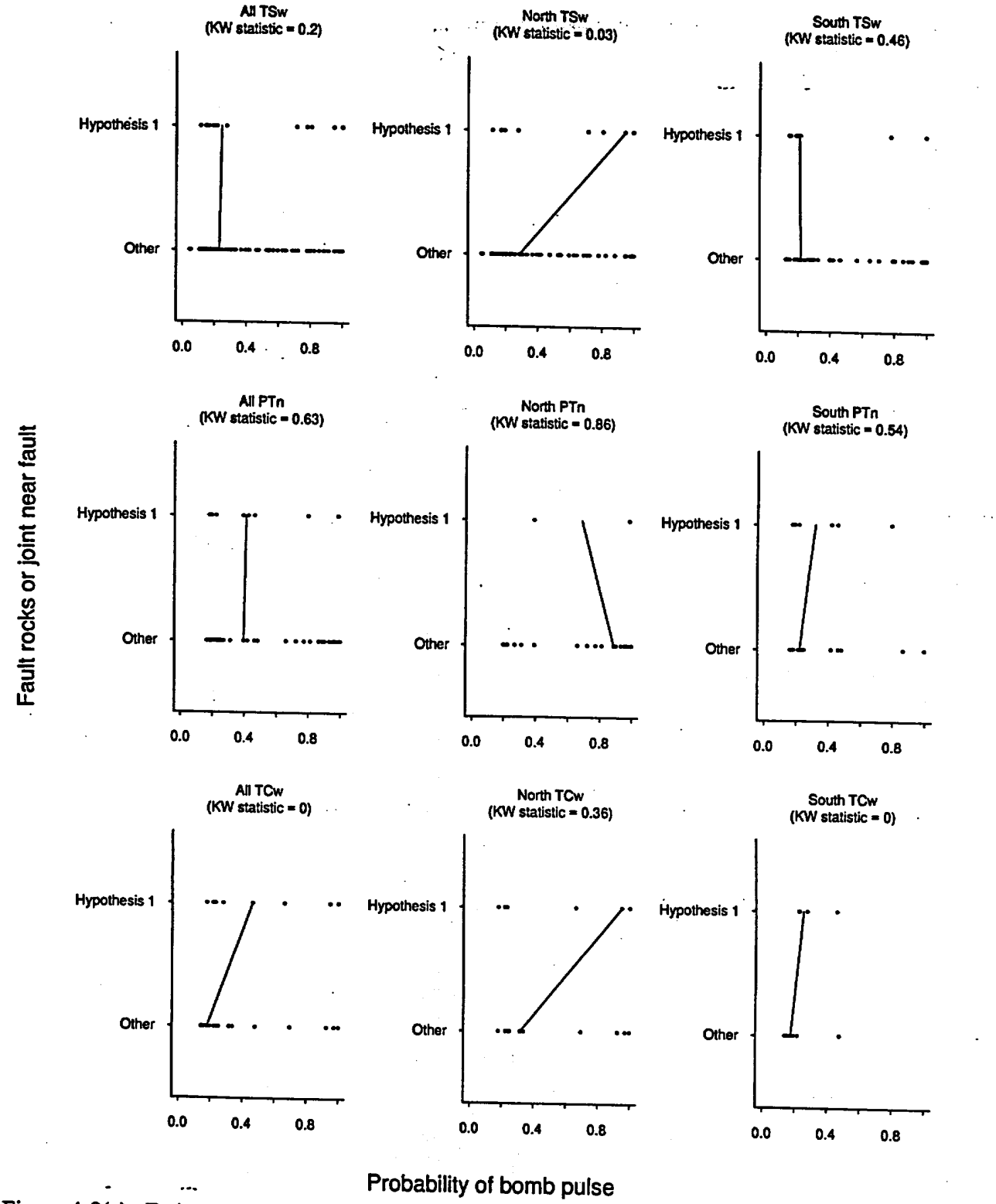

Figure 4-8(a). Estimated probability of bomb pulse to test hypothesis that bomb pulse is associated with structural features in fault zones

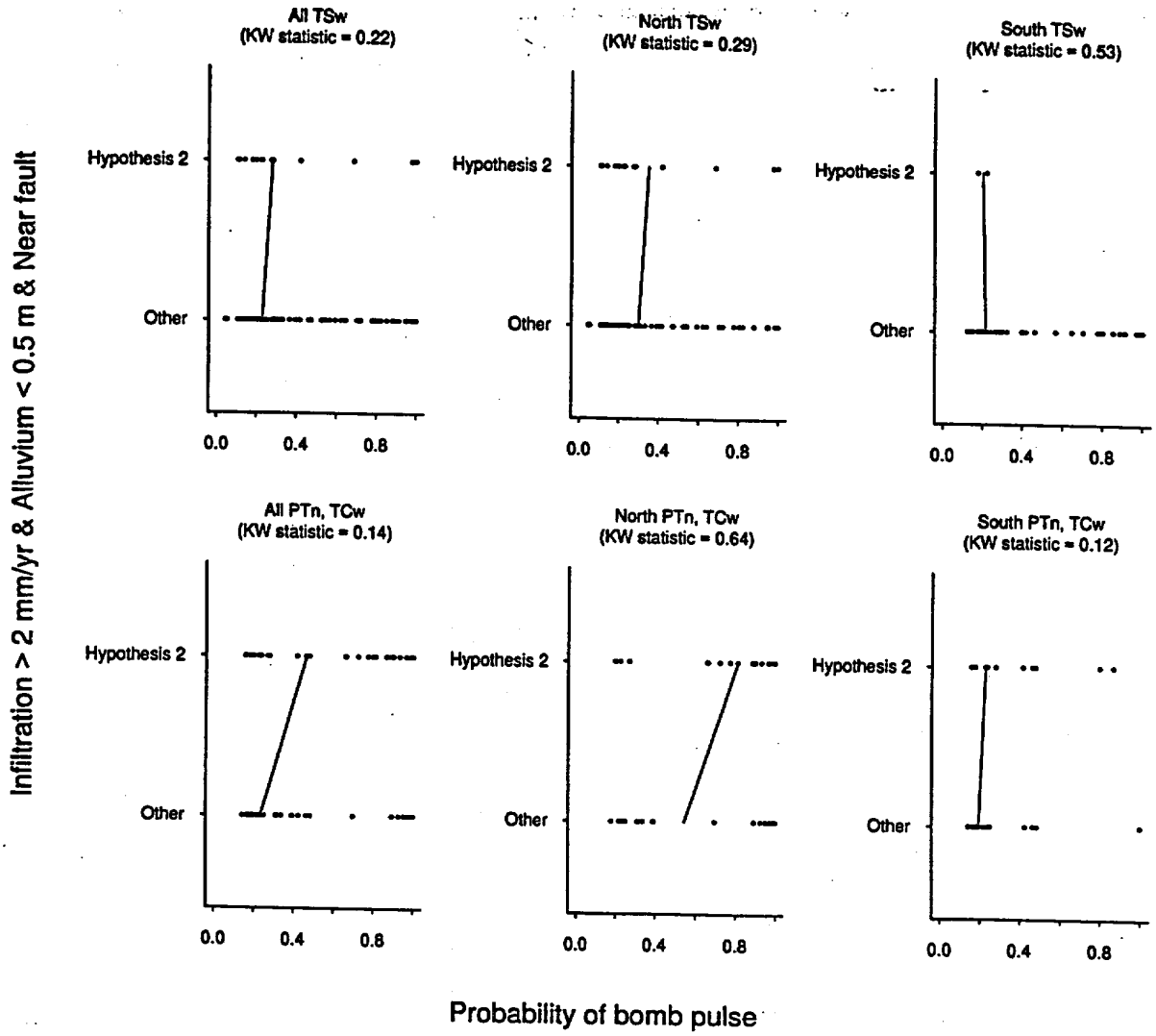

Figure 4-8(b). Estimated probability of bomb pulse to test hypothesis that bomb pulse is associated with infiltration > 2 mm/yr and alluvial overburden < 0.5m in fault zones (within 30m of faults)

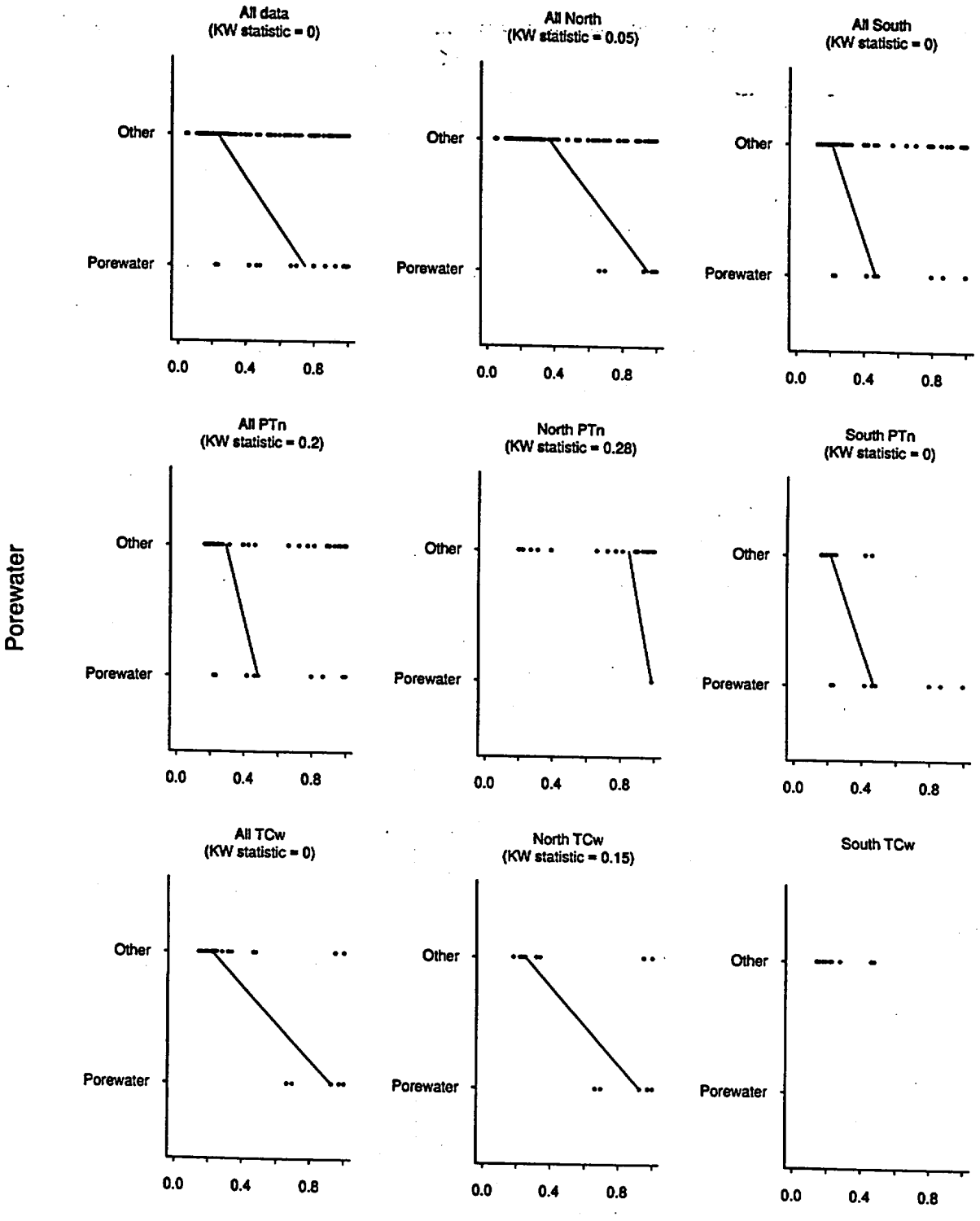

Figure 4-9. Estimated probability of bomb pulse in porewater samples

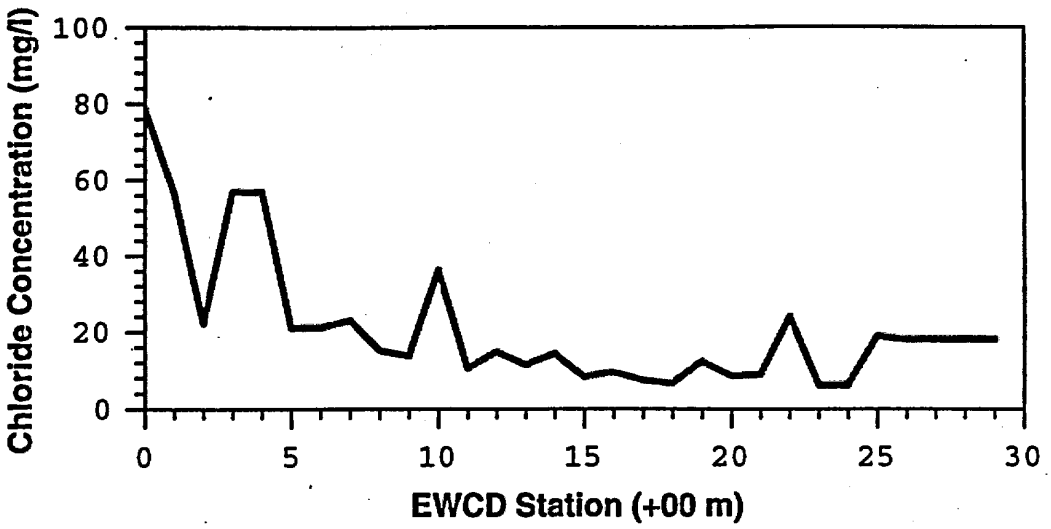

Figure 5-1. Simulated chloride concentrations in the EWCD.

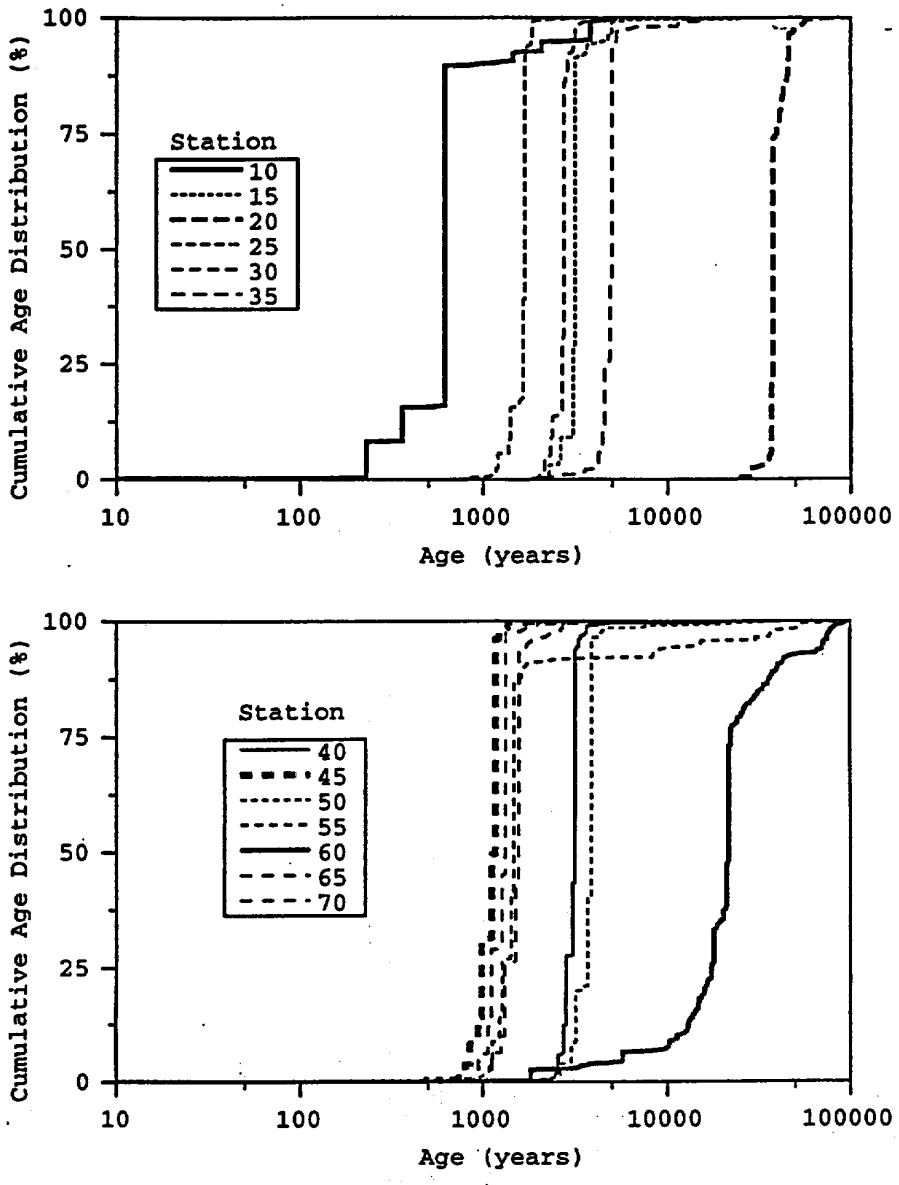

Figure 5-2. Individual cumulative age distribution curves for ESF stations every 100m. Stations before 10+00 and after 70+00 are not included as they are not overlain by PTn.

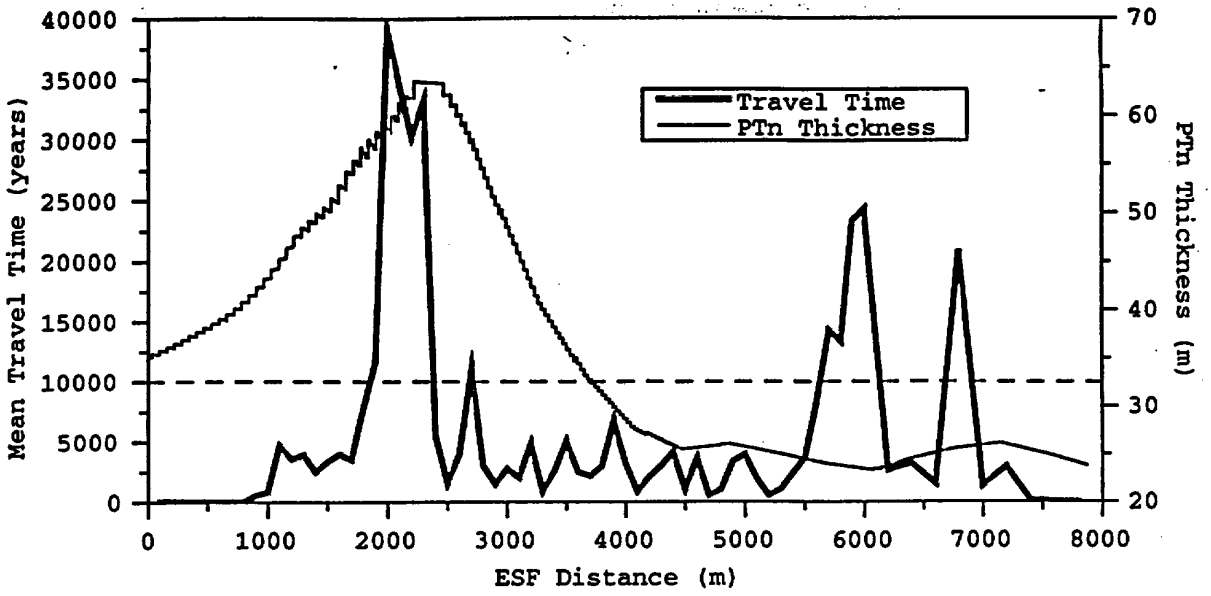

Figure 5-3. Mean simulated travel time to the ESF compared with the PTn thickness above stations along the ESF.

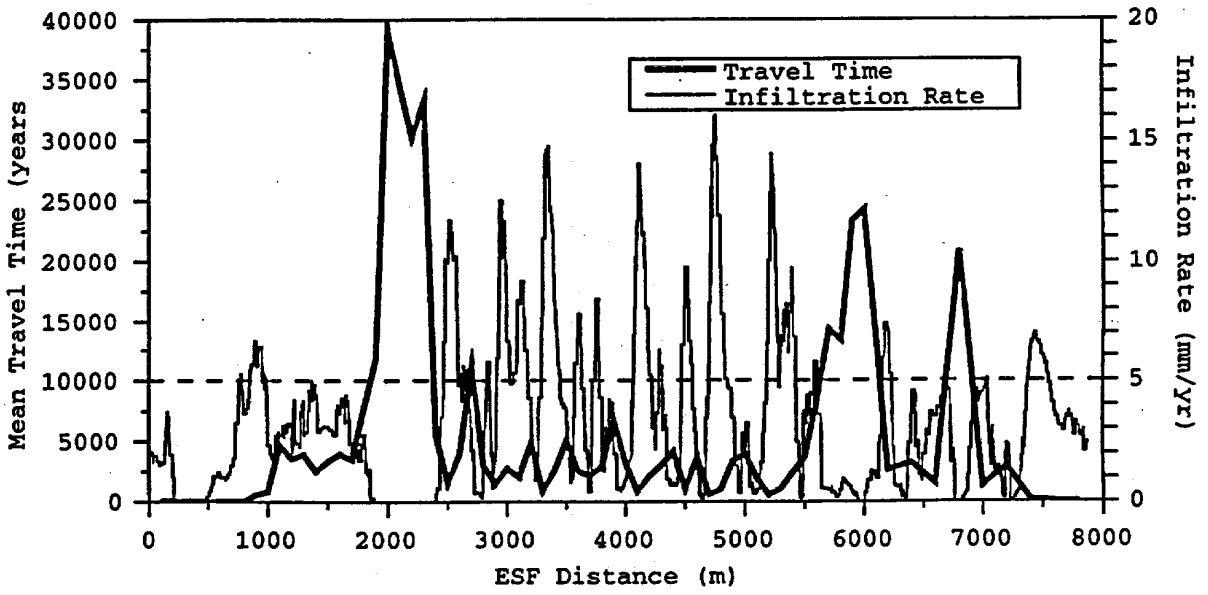

Figure 5-4. Mean simulated travel time to the ESF compared with the average infiltration rate over a 50 m radius area above stations along the ESF

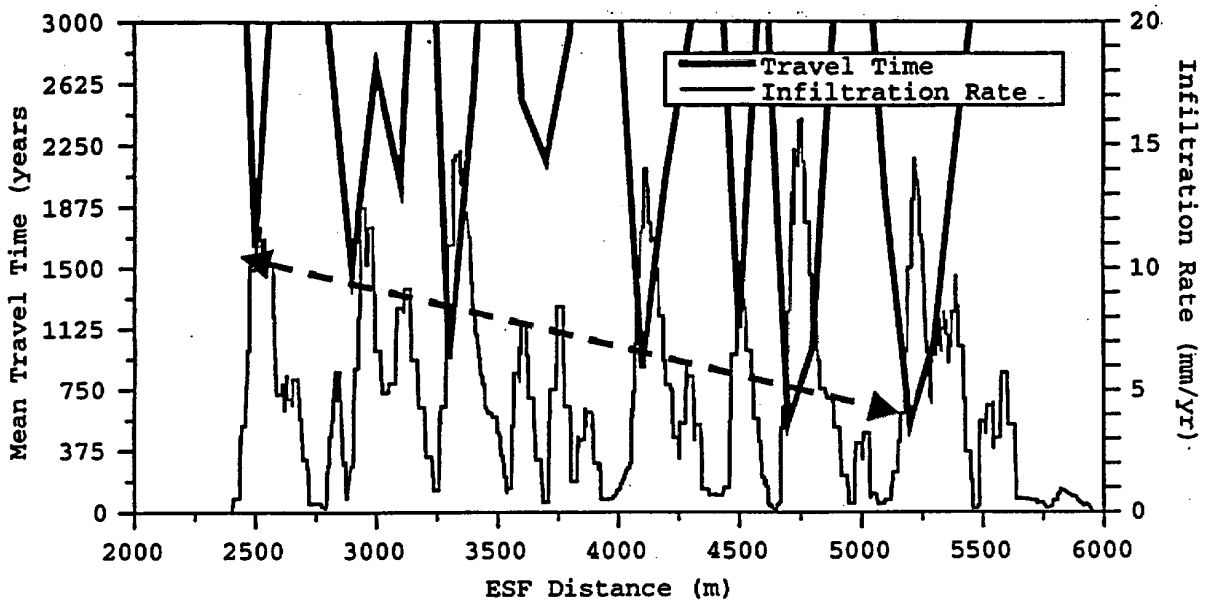

Figure 5-5. Comparison of minimum mean travel times correlated with maximum estimated infiltration rates. For high infiltration rates, mean travel times decrease with decreasing PTn thickness to the south.

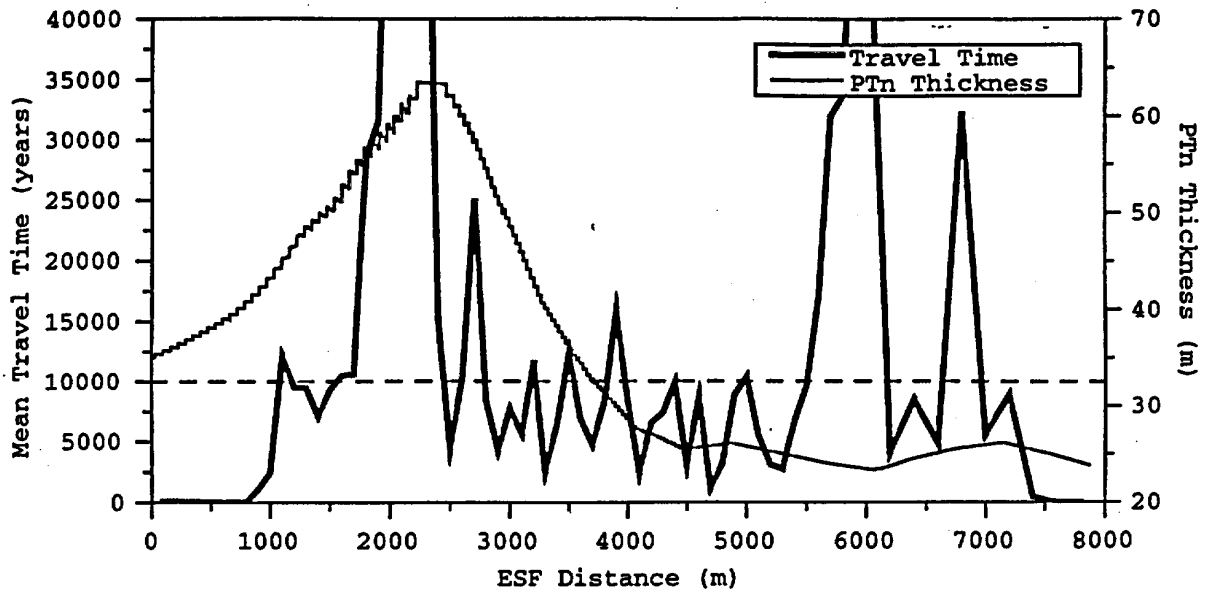

Figure 5-6. I/3 Infiltration Model: Mean simulated travel time to the ESF compared with the PTn thickness above stations along the ESF.

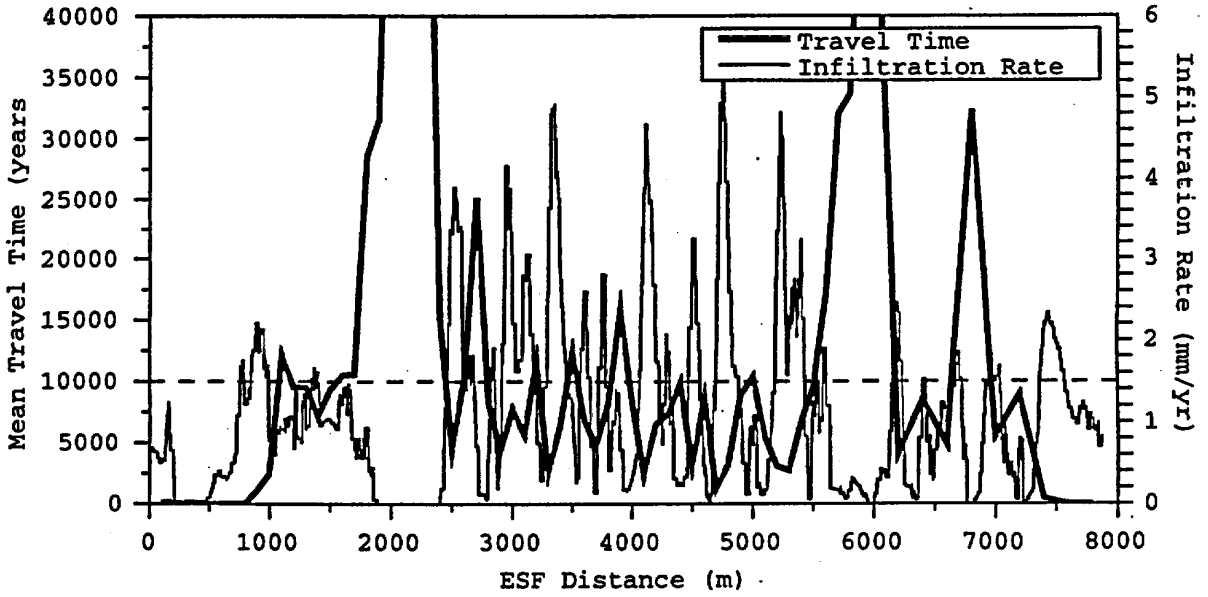

Figure 5-7. I/3 Infiltration Model: Mean simulated travel time to the ESF compared with the average infiltration rate over a 50 m radius area above stations along the ESF.

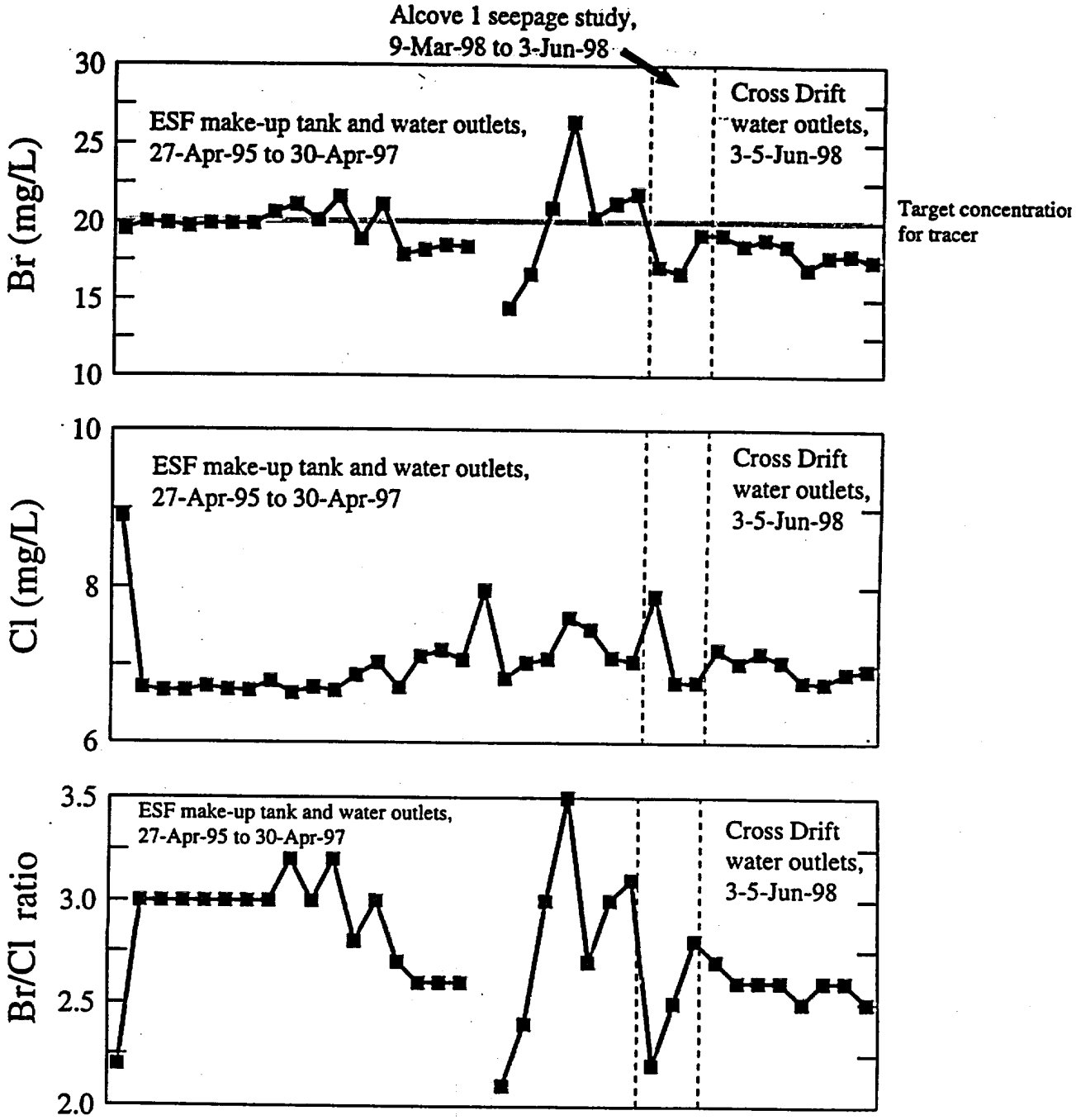

Figure 7-1. Temporal variations in Br and Cl concentrations and Br/Cl ratios in construction water

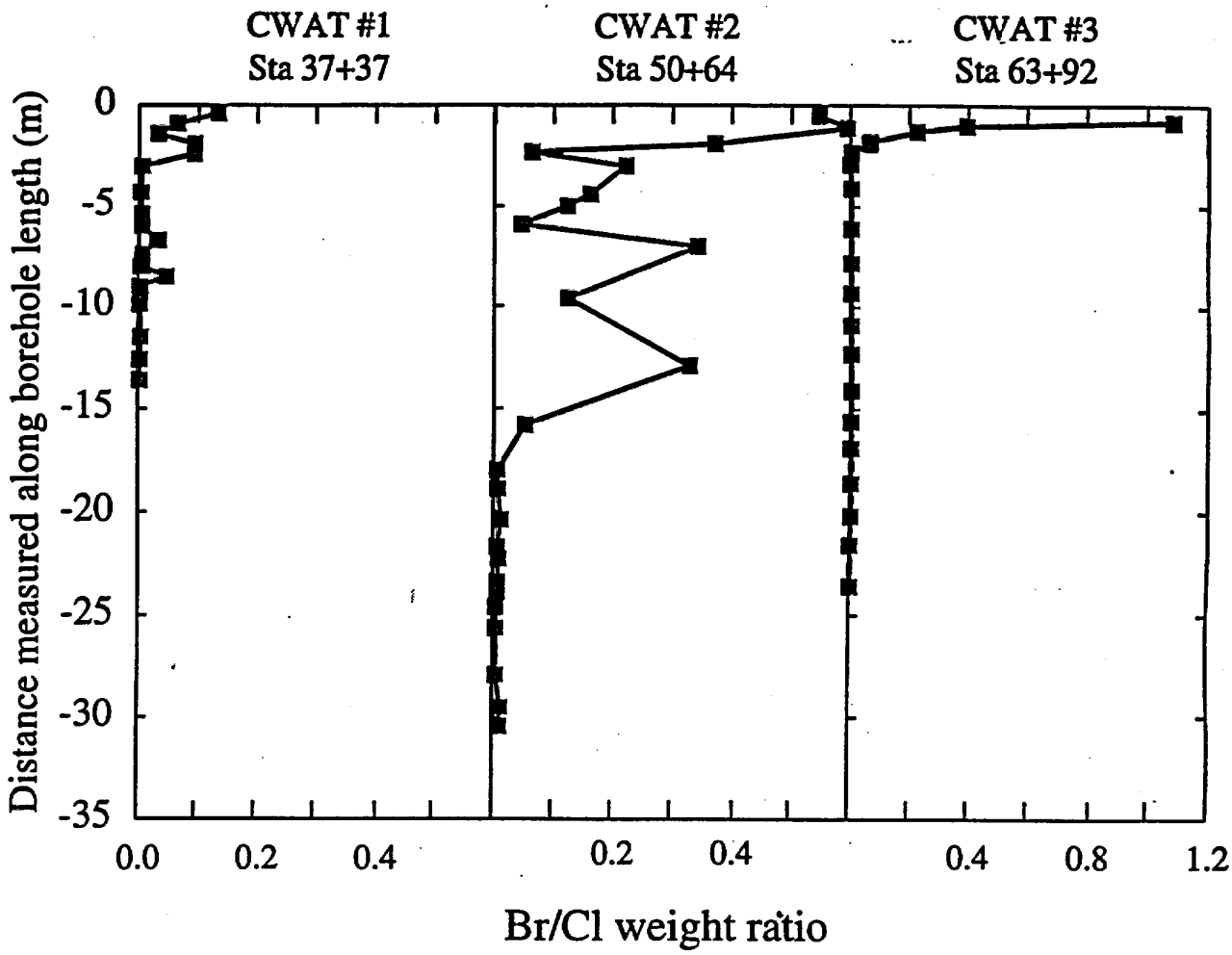

Figure 7-2. Construction water penetration in slanted CWAT drillholes (data from DTN LAJF831222AQ98.007).

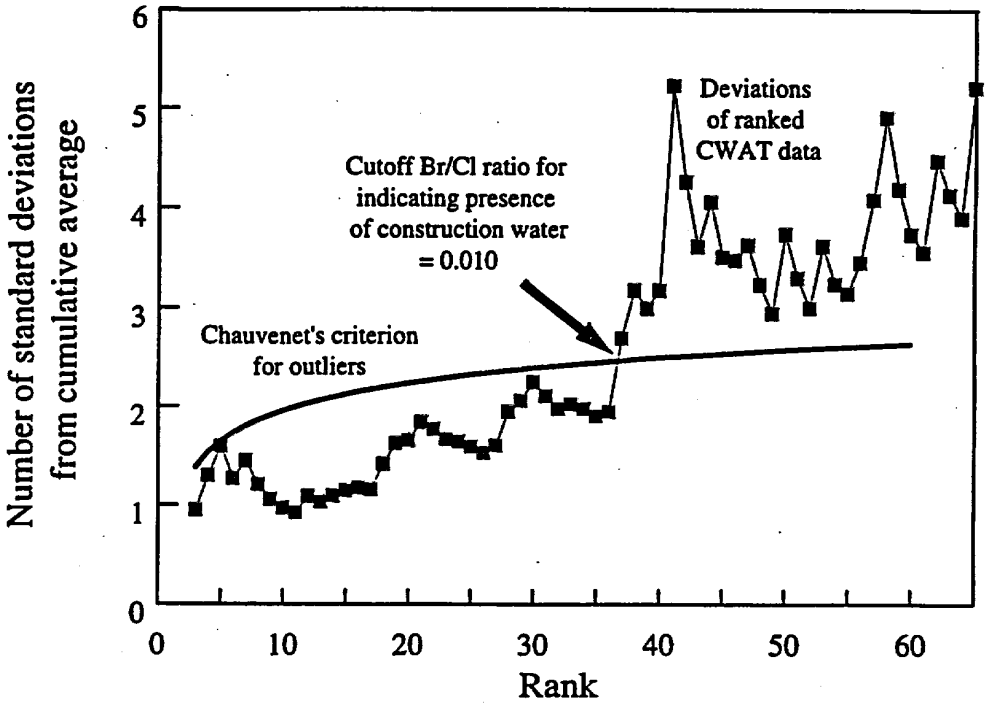

Figure 7-3. Cutoff Br/Cl ratio for the presence of traced construction water in CWAT drillcore samples (data from DTN LAJF831222AQ98.007).

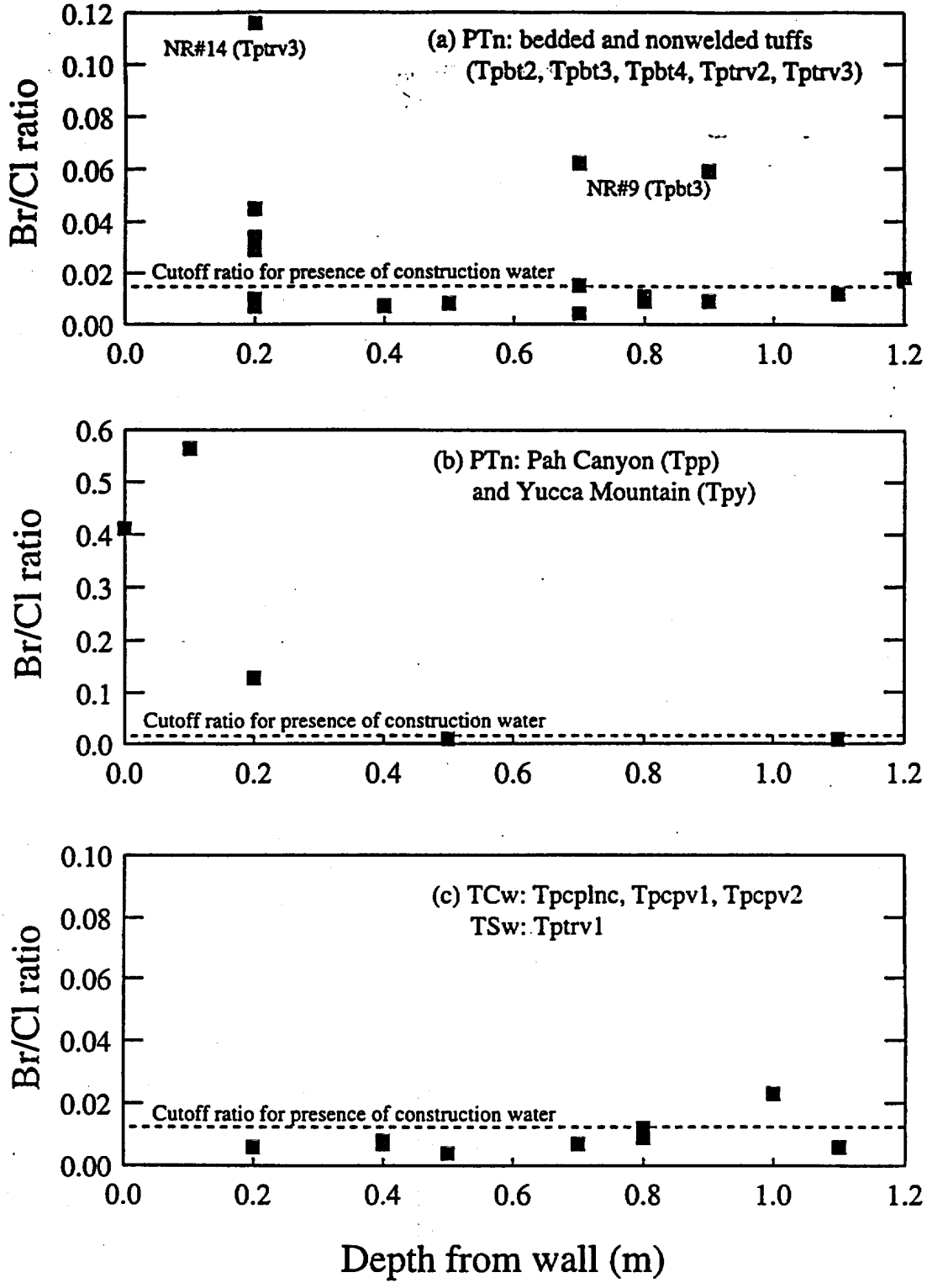

Figure 7-4. Penetration of construction water in horizontal North Ramp drillholes. Data source: DTN LAJF831222AQ98.014

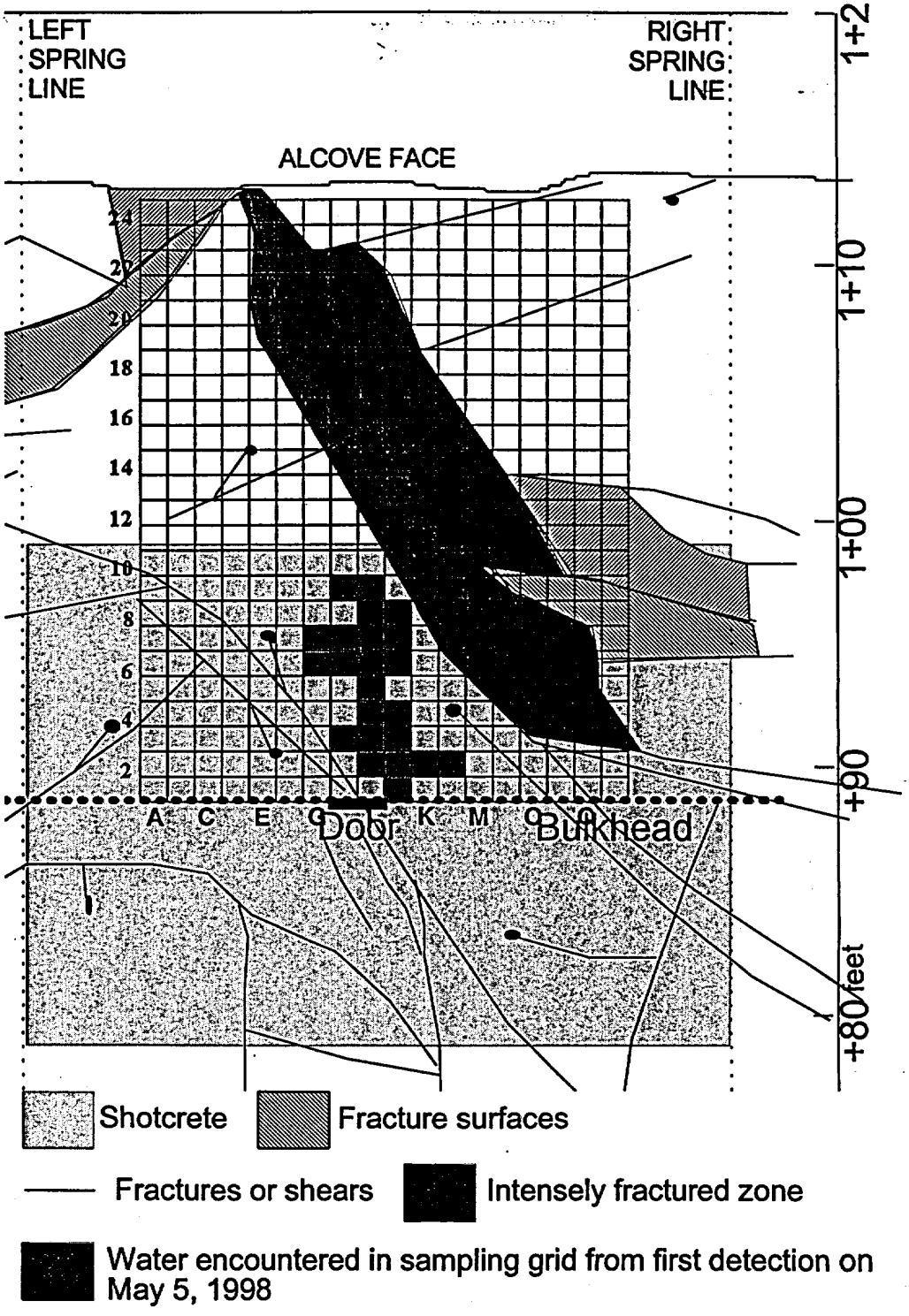

Figure 8-1. Grid pattern used for seepage collectors in Alcove 1.

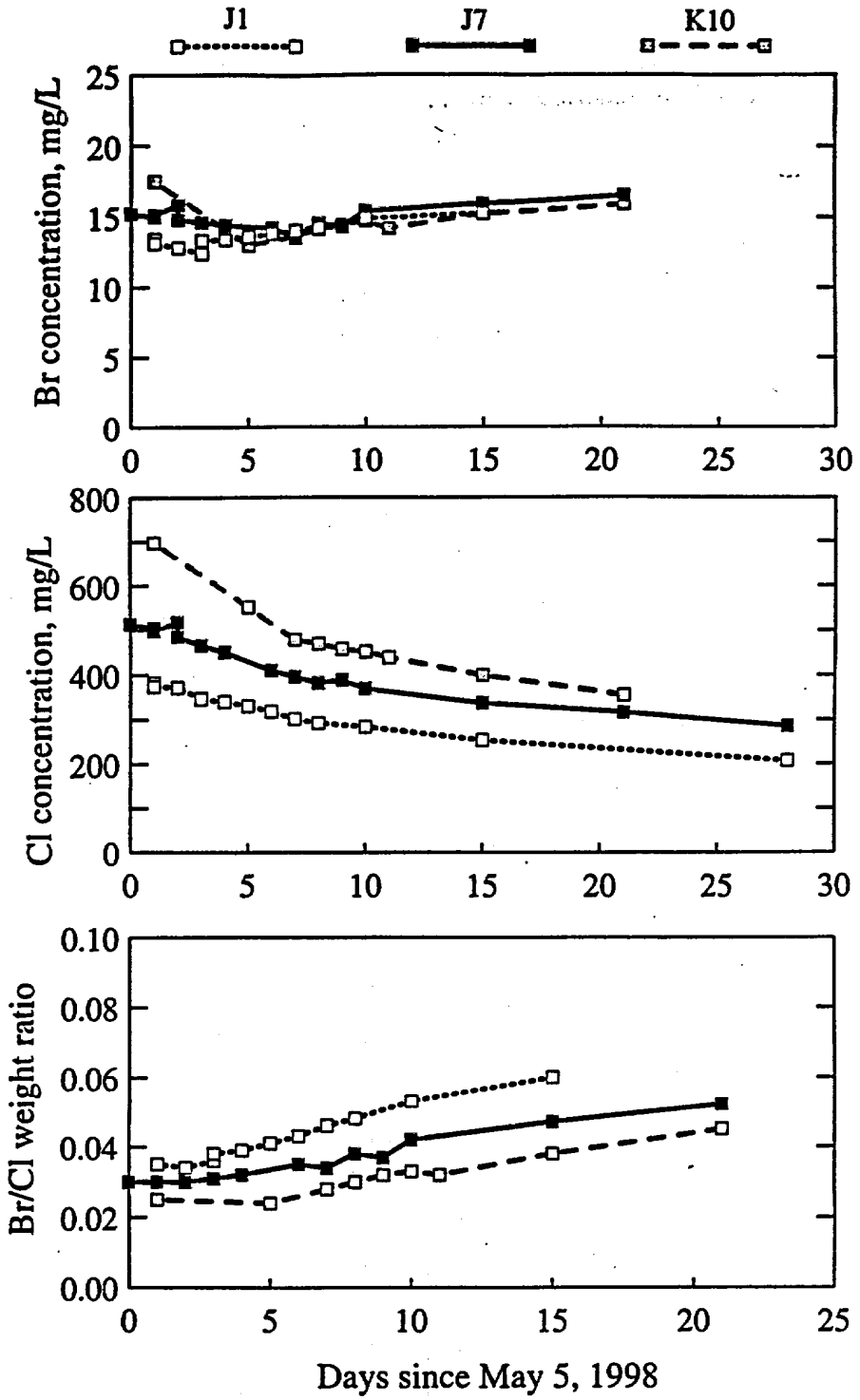

Figure 8-2. Variations in Cl and Br seepage concentrations at specific grid locations in Alcove 1 as a function of time. The collection grid in Alcove 1 is shown in Figure 8-1.

APPENDIX A. MIXTURE MODELS FOR ^{36}Cl/Cl DATA FROM THE ESF

A plot of the ^{36}Cl/Cl ratio data versus distance along the tunnel suggests a varying background level underlying the obvious spikes that are associated with the "bomb pulse" (see Figure 4-1). This appendix describes a method for modeling this variable background signal. Once an estimate is available, the probability that a given observation contains bomb-pulse ^{36}Cl can be estimated independently of the background.

Descriptive mixture modeling using the EM algorithm

The structure of the ^{36}Cl/Cl ratio data was initially explored by fitting a mixture distribution to the data. A mixture distribution with $k > 1$ components is one that can be represented by a probability density function (PDF) of the form

$$f(x) = \pi_1 f_1(x; \theta_1) + \ldots + \pi_k f_k(x; \theta_k), \qquad \text{(A-1)}$$

where

$$\pi_j > 0 \text{ for } j = 1, \ldots, k \text{ and } \pi_1 + \ldots + \pi_k = 1 \qquad \text{(A-2a)}$$

$$f_j(x; \theta_j) \bullet\ 0 \text{ for all } x \text{ and } \bullet\ f_j(x; \theta_j)\, dx = 1,\ j = 1, \ldots, k, \qquad \text{(A-2b)}$$

(that is, each $f_j(.,\theta_j)$ is a probability density function in its own right, with some parameters θ_j). The cumulative probability distribution function (CDF) of the mixture distribution is similarly equal to a weighted sum of the CDFs of its components:

$$F(x) = \int_{-\infty}^{x} f(t)dt = \int_{-\infty}^{x} \sum_{j=1}^{k} \pi_j f_j(t;\theta_j)dt = \sum_{j=1}^{k} \pi_j F_j(x,\theta_j). \qquad \text{(A-3)}$$

The parameters θ_j of each component (e.g., a mean and standard deviation) as well as the coefficients π_j can be estimated using an iterative algorithm known as the EM (Expectation-Maximization) algorithm (see for example Titterington et al., 1985). To use this algorithm, an initial guess must be supplied for each of the parameters, but the algorithm is extremely robust to these initial guesses, that is, it converges to a final estimate that appears to be independent of the starting point.

Various combinations of $k = 2$, 3, and 4 components were tried, always including at least one component intended to represent background and one component to represent the bomb pulse A similar mixture hypothesis with two components, one representing background and one representing the bomb pulse, is implicit in William Murphy's work (Murphy 1997). The third component, when present, represents a second background distribution, that is, background is itself being modeled as a mixture in this case. The fourth component was an attempt to represent the contribution from porewater with little or no ^{36}Cl, but when a fourth component was included, the iterative EM algorithm shifted its parameters, initialized at the low end of the data range, into the main background range, effectively using these additional degrees of freedom to

refine its estimate of one of the background components. Ultimately, therefore, fits were obtained by excluding data less than 250 x 10^{-15}; otherwise the upper background distribution, centered about 700 x 10^{-15}, widens to capture these values. (The lower background distribution, centered about 450 x 10^{-15}, "wants" to be even narrower than it is, and will not widen to capture the lower tail.) This indicates that another component to the mixture distribution is needed to capture the low signals. Such a component is fully warranted as those signals represent decayed ^{36}Cl due to very long travel times. In the next iteration of this analysis, a "decayed signal" component will be included. However, here it is captured as a fourth component in the Bayesian analysis described later in this appendix.

Adequate fits to all the data (excluding values less than 250 x 10^{-15}) require three components. The best fits were obtained when one of the background components (B_1, centered about 450 x 10^{-15}) was normal while the larger background component (B_2) and the bomb pulse were modeled as lognormal. The cumulative probability distribution function (CDF) of this best fit (hereafter referred to as Model 1) is shown in Figure A-1 as a solid line together with the empirical probability distribution function (EDF) of the data, shown using a dotted line. Although no formal hypothesis testing has been done, the cumulative probability distribution plot shows an excellent match between the fitted mixture model and the data.

Model 1 is diagrammed in Figure A-2. It is a model for the generation of the data, which are shown at the bottom of the figure as the node "ratio(i)", the i^{th} reported $^{36}Cl/Cl$ ratio. Each observation came from one of the three mixture components (background distributions B_1 and B_2 or the bomb-pulse distribution C), but the indicator variable that would tell us which of these three distributions it came from (denoted by $t(i) = 1, 2$ or 3 in Figure A-2) is not observable. Using the EM algorithm, however, we have estimated the fraction of each component present $\pi = (\pi_j, j = 1, 2, 3)$ as well as the parameters $\theta = (\mu_j, \sigma_j, j = 1, 2, 3)$ of each component. (The EM algorithm is based on a model very similar to that of Figure A-2: the expected values of the unobserved indicators $t(i)$ are imputed in the "E" step, and the parameters π and θ are then inferred using maximum likelihood in the "M" step of each iteration.)

There are a number of conceptual problems with Model 1. First of all, it is a purely descriptive model, suggestive but not very amenable to hypothesis testing. The EM algorithm allows us to estimate its parameters but does not provide error estimates for these parameters. Secondly, we are primarily interested in exploring the dependence of π on covariates such as infiltration rate, thickness of the overlying PTn unit, or proximity to faults intersecting the PTn. However, π in Model 1 has no such dependence, although estimates of the expected values $Pr\{z[i] = j\}$ are available as one of the outputs of the EM algorithm.

Examination of Figure 4-1 suggests that the bomb-pulse signal, if present in the south end of the ESF, is not so strong as in the north end, but once the difference in background levels is taken into account, the bomb pulse might be no less significant. However, until the difference in background levels is separated out, the candidates for bomb pulse in the south end appear very similar to the higher background levels of the north end, and a simple mixture model such as Model 1 cannot separate them. A more natural model for this situation, if the hypothesis of two distinct background components is accepted, would take the form

$$\text{ratio}_i \sim \zeta(x_i)^* B_1 + (1-\zeta(x_i))^* B_2 + \omega(i)^*[\,\zeta(x_i)^* S_1 + (1-\zeta(x_i))^* S_2] \qquad \text{(A-4)}$$

where $\zeta(x_i)$ is the probability that the background distribution at the location x_i of the i^{th} observation is B_1, and $\omega(i)$ is the probability that bomb pulse is present in the i^{th} sample. Two distributions for the bomb pulse, corresponding to the two background distributions, are also allowed in this model. This model is diagrammed in Figure A-3.

Notice that Eq. (A-4) can be rewritten as a four-component mixture model in the form of Eq. (A-1) if we set

$$\pi_1 = (1-\omega(x_i))^*\zeta(x_i) \quad \text{and} \quad F_1 = B_1 \qquad \text{(A-5)}$$

$$\pi_2 = (1-\omega(x_i))^*(1-\zeta(x_i)) \quad \text{and} \quad F_2 = B_2$$

$$\pi_3 = \omega(x_i)^*\zeta(x_i) \quad \text{and} \quad F_3 = C_1 = B_1 + S_1$$

$$\pi_4 = \omega(x_i)^*(1-\zeta(x_i)) \quad \text{and} \quad F_4 = C_2 = B_2 + S_2$$

This set of equations is, in fact, the form of the model whose parameters can conveniently be estimated by the method described below.

Predictive mixture modeling using Bayesian updating

The four-component mixture model illustrated in Figure A-3 has as parameters to be estimated the parameters $\theta = (\mu_j, \sigma_j, j = 1, 2, 3, 4)$ and as many $\zeta(x_i)$'s and $\omega(i)$'s as there are distinct sample locations x_i and samples, respectively. There are now independent hidden indicator variables $z(i)$ for the first baseline distribution and $w(i)$ for bomb-pulse presence. The total number of parameters exceeds the number of available observations; the problem is ill-posed. Like other ill-posed problems, however, it can be solved if some regularization constraints are imposed, and effectively, this constraint is what recasting the problem in a Bayesian format accomplishes.

To "recast the problem in a Bayesian format" means to assume that the model parameters listed above are themselves drawn from probability distributions. Independently of the data, prior probability distributions are specified for each parameter. Sometimes these prior distributions can be noninformative, or nearly noninformative, placing almost no constraints on the parameters except those that are implicit in their definitions (e.g., by definition, σ_j is positive.) For example, a uniform prior on (0, 1) can be specified for each of the $\omega(i)$'s. The Bayesian equivalent of parameter estimation consists of using the observations to update the prior distributions to obtain posterior distributions for each parameter. Point estimates of parameters may be obtained as the means of these posterior distributions, whereas their variance or spread is indicative of how precisely they are determined by the data, that is, how much "information" about the parameters is provided by the observations, over and above what was assumed in the prior probability distributions and also imposed by the assumed form of the model.

(Bayesian statistics is the subject of hundreds of papers, books, and monographs; the monograph by Carlin and Louis (1996) is one of the most accessible and is explicitly oriented towards data analysis problems such as the one being considered here.)

Computationally, the updating is accomplished using Markov Chain Monte Carlo (MCMC) simulation. Specifically, the computations in this report were done with a publicly available software package known as BUGS (Bayesian inference Using Gibbs Sampling) (Best et al., 1996; Spiegelhalter et al., 1995.) The output of one run of this program is a sample drawn from the joint posterior distribution of all the parameters (including the hidden variables), which can be used to approximate the means of the posterior distributions of individual parameters as well as other quantities.

Modeling baseline dependence on PTn thickness

Selecting prior distributions on all of the $\zeta(x_i)$'s and $\omega(x_i)$'s is not, unfortunately, enough to regularize the ill-posed problem posed by Model 2. An additional constraint, in the form of a more informative prior, is necessary for at least one of these two sets of parameters. Such a constraint can be imposed by explicitly modeling the dependence of $\zeta(x)$ in Eqs. (A-4, A-5) on a covariate $T(x)$. For a variable like $\zeta(x_i)$, constrained to lie between 0 and 1 because it is a probability, it is convenient to take the form of the dependence to be

$$\text{logit}(\zeta(x_i)) = \log(\zeta(x_i)/(1-\zeta(x_i))) = \alpha_0 + \alpha_1 * (T(x_i) - \langle T(x_i) \rangle) . \qquad \text{(A-6)}$$

As $\zeta(x_i)$ varies between zero and one, $\text{logit}(\zeta(x_i))$ ranges over the entire real line. ($\langle T(x_i) \rangle$ represents the average value of the covariate, included for computational convenience.) Model 3, constrained by a relationship of the form of Eq. (A-6), is illustrated in Figure A-4.

Among the covariates available (see Figure 4-2), PTn thickness appears to be best correlated with the baseline distributions. So, for the initial trial of the Bayesian updating method, we let $T(x_i)$ be this thickness in Eq. (A-6). (This approach will be referred to as Model 3(PTn).) The distributions B_k and C_k are assumed to be lognormal. The prior and posterior distributions of the parameters θ and α are shown in Table A-1. (Posterior distributions from a second version of Model 3—Model 3(TT), which uses a mean travel time estimate for $T(x_i)$—are also shown in the last two columns of Table A-1 and discussed below.) Figures A-5 through A-7 illustrate some of these results. For example, Figure A-6 shows that by comparison with the broad prior distribution on the log-means of the baseline distributions B_k, the posterior distributions are much more concentrated. This effect shows up in the third and fifth rows of Table A-1 as a reduction by a factor of almost 5 between the standard deviations of the prior and posterior distributions. The concentration of other posterior distributions is less striking but still significant; the data provide a good deal of information for the parameters of this model.

Table A-1. Prior and Posterior Distributions for Model 2

Parameter	Prior distribution		Posterior distribution, Model 2(PTn)		Posterior distribution, Model 2(TT)	
	Mean	Standard deviation	Mean	Standard deviation	Mean	Standard deviation
α_0	0.00	2.00	1.57	1.76	0.42	0.58
α_1	-1.00	1.00	-1.48	0.79	-2.55	0.71
μ_1	6.00	0.20	6.16	0.026	6.14	0.045
σ_1	0.39	0.19	0.18	0.022	0.21	0.039
μ_2	6.50	0.30	6.49	0.050	6.38	0.076
σ_2	0.39	0.19	0.25	0.031	0.24	0.048
μ_3	7.00	0.40	6.46	0.071	6.49	0.087
σ_3	1.24	0.64	0.59	0.052	0.51	0.057
μ_4	7.00	0.40	7.27	0.111	7.20	0.156
σ_4	1.24	0.64	0.66	0.072	0.72	0.084

Figure A-8 translates the estimates of θ into samples from each of the four components. The second of these four plots illustrates a continuing unsatisfactory feature of this mixture model (shared by the four-component EM-estimated model), namely, the distribution that is identified as belonging to distributions $B_1 + S_1$ (corresponding to subscript 3 in Table A-1 and Eq. (A-5)) is not strictly greater than the distribution B_1, even though physically S_1 must be non-negative. This model still knows nothing about physics and is using this component to capture some of the very low ^{36}Cl/Cl observations in the south end of the ESF as well as excursions above what appears to be the baseline level in this part of the tunnel. If we could fit the model of Eq. (A-4) directly, this unrealistic result would not occur, but unfortunately the BUGS software is unable to work with the model of Eq. (A-4) for technical reasons. Another consequence of fitting Eq. (A-5) instead of Eq. (A-4) is that $E(w(i))$, the probability that bomb pulse is detected in a sample, is not zero but rather usually about 0.2 for samples that are in the middle of the background distribution (see Figure 4-5), because the background distribution overlaps the bomb-pulse distribution.

Because $B_1 + S_1$ includes some very low ^{36}Cl/Cl values that are unlikely to belong to the background population B_1, as estimated, the model estimates $E(w(i))$ as large for these very low values. In subsequent plots, and in use for hypothesis testing in Section 4, $E(w(i))$ is set equal to 0.18 (the median value of $E(w(i))$ for background observations) when the reported ^{36}Cl/Cl ratio is less than 420×10^{-15}. Although the model still knows nothing about physics, it has captured a unique set of data that fall well below present-day background due to the process of radioactive decay of ^{36}Cl. The other distributions represent samples that either have bomb-pulse signatures due to very fast travel, modern-day background due to travel times of 10,000 years or less, or elevated signals due to travel times of 10,000 years or more but less than about 50,000 years so that decay is not significant.

Although $\zeta(x_i)$ is determined given a realization of α (in any one realization produced by the MCMC simulation), it does not follow that $z(i)$ is constrained to be distributed like a binomial

with parameter $\zeta(x_i)$. "Learning" is possible for $z(i)$, particularly when $\zeta(x_i)$ is not too close to zero or one. In the fitted Model 3(PTn), however, it turns out that $\zeta(x_i)$ is actually quite close to zero or one over much of the range of estimated PTn thicknesses, because in fact PTn thickness discriminates quite well between the two background levels, so that Eq. (A-6) represents a very strong prior constraint on the $z(i)$'s, that is, $E(z(i))$ is also close to zero or one over most of the range. The transition comes in the range of PTn thickness between about 27 and 30 m. In particular, the north/south split used in Section 4 was determined by observing that $E(z(i)) < 0.5$ for locations to the north of this point (except for a few initial observations above the PTn), while $E(z(i)) > 0.5$ for locations to the south.

A second choice for $T(x_i)$ was explored to see how this choice of covariate affects the convergence of the analysis toward a conceptually meaningful result. For this second run, $T(x_i)$ was taken to be the common logarithm of the mean travel time at a sample location as estimated using a model that included both advection and diffusion. The results for the main parameters are shown in the last two columns of Table A-1. The coefficients α are different, of course, but what is reasonably satisfactory is the overall agreement among the remaining parameters describing the four components of the mixture model.

In the fitted Model 3(TT), $\zeta(x_i)$ is never close to zero and is close to one only for the shortest travel times, because the modeled travel time does not discriminate between the two background levels nearly as well as PTn thickness does. As a result, Eq. (A-6) represents a less strong prior constraint than for Model 3(PTn), and the $E(z(i))$ vary much more around $\zeta(x_i)$. The correlation between the $E(z(i))$'s estimated under the two models is not too large (about 0.53, see Figure A-9). Of more importance, however, given their use in hypothesis testing in Section 4 is the result that the correlation among the $E(w(i))$'s is almost 0.9, and we can expect the results of Section 4 to be fairly robust to this choice. Figure A-10 should be compared with Figure 4-6 in the text.

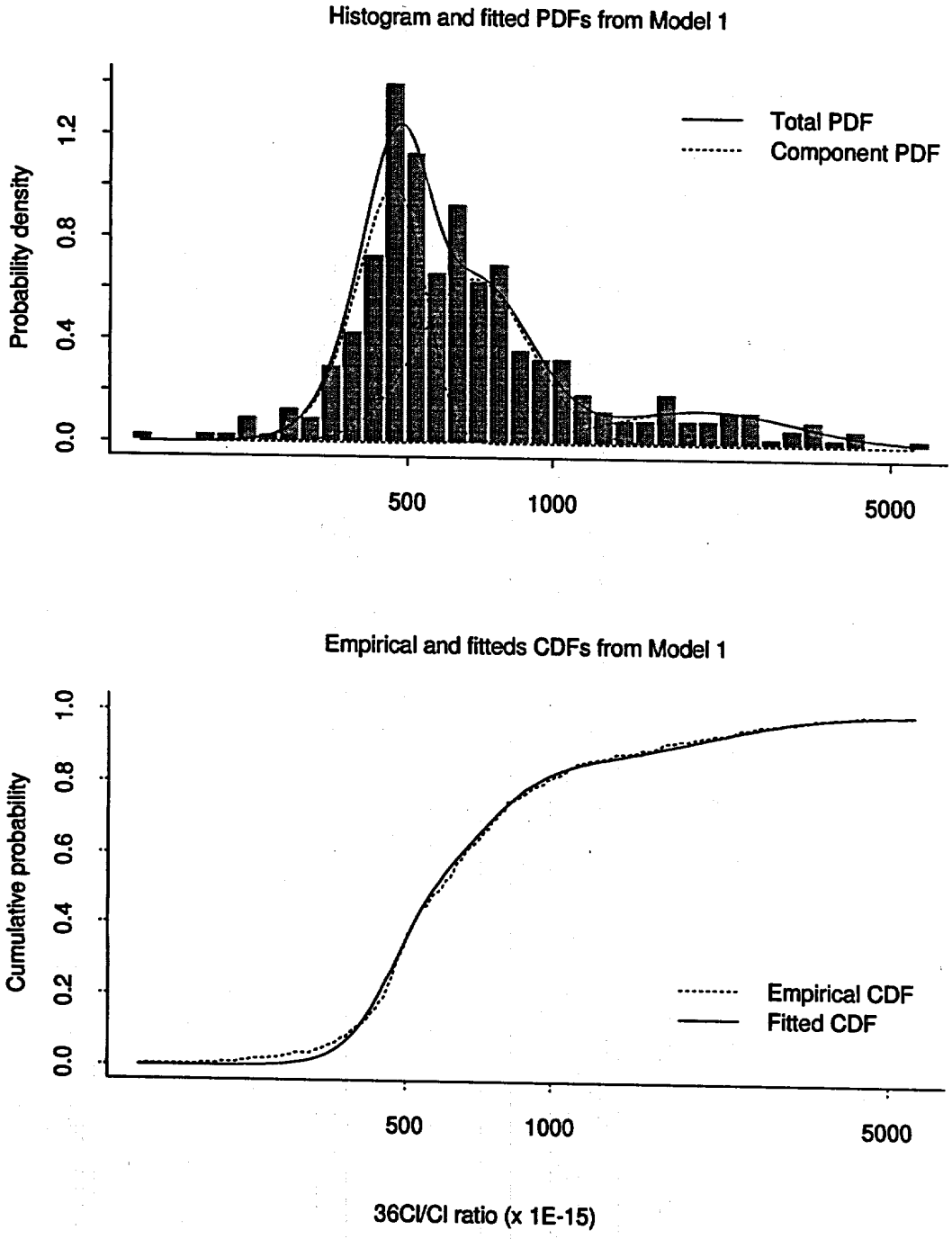

Figure A-1. Fitted distributions for the three-component mixture model for $^{36}Cl/Cl$ ratio data

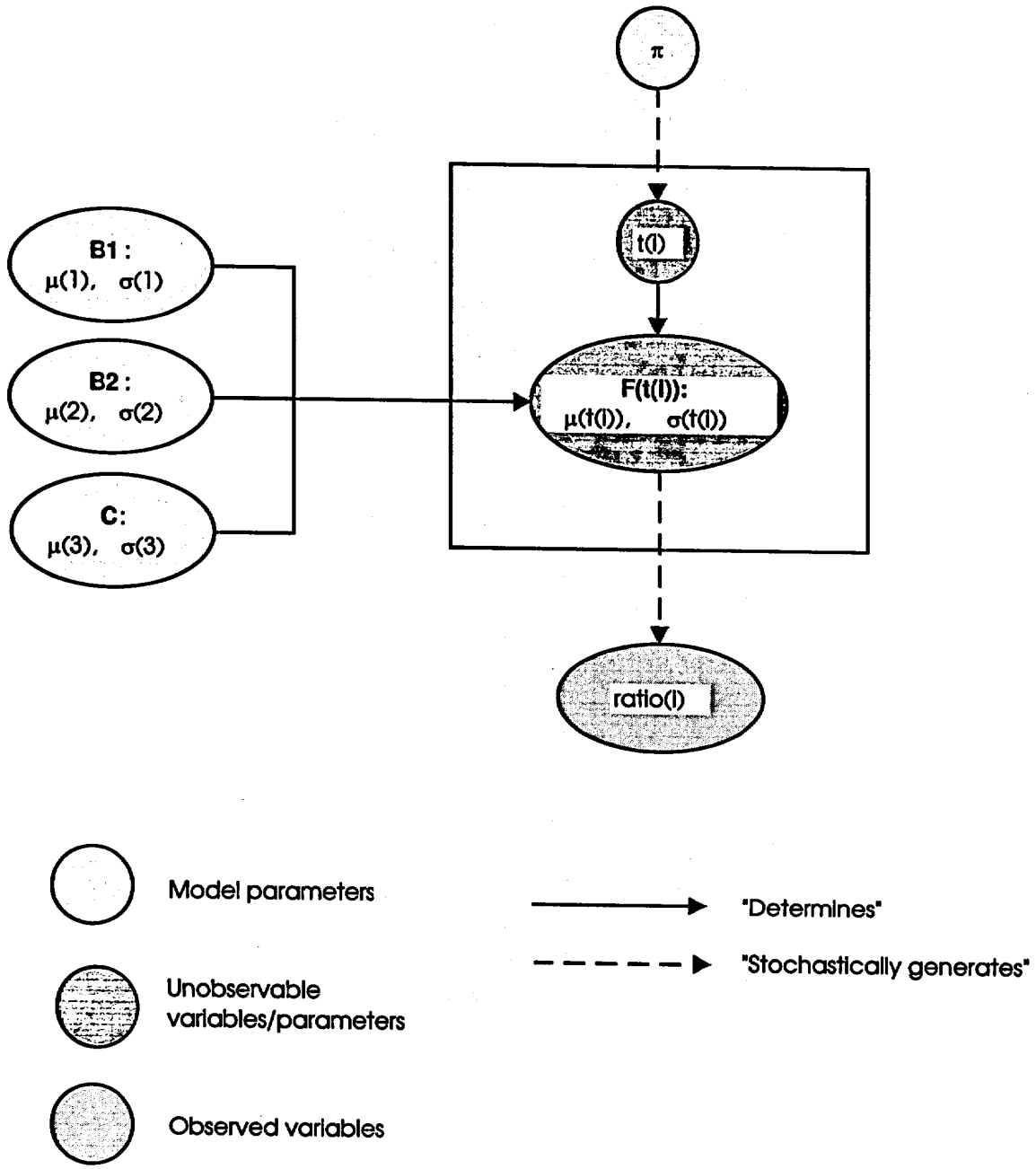

Figure A-2. Model 1, a mixture model for the $^{36}Cl/Cl$ ratio data with two background components and one bomb-pulse component

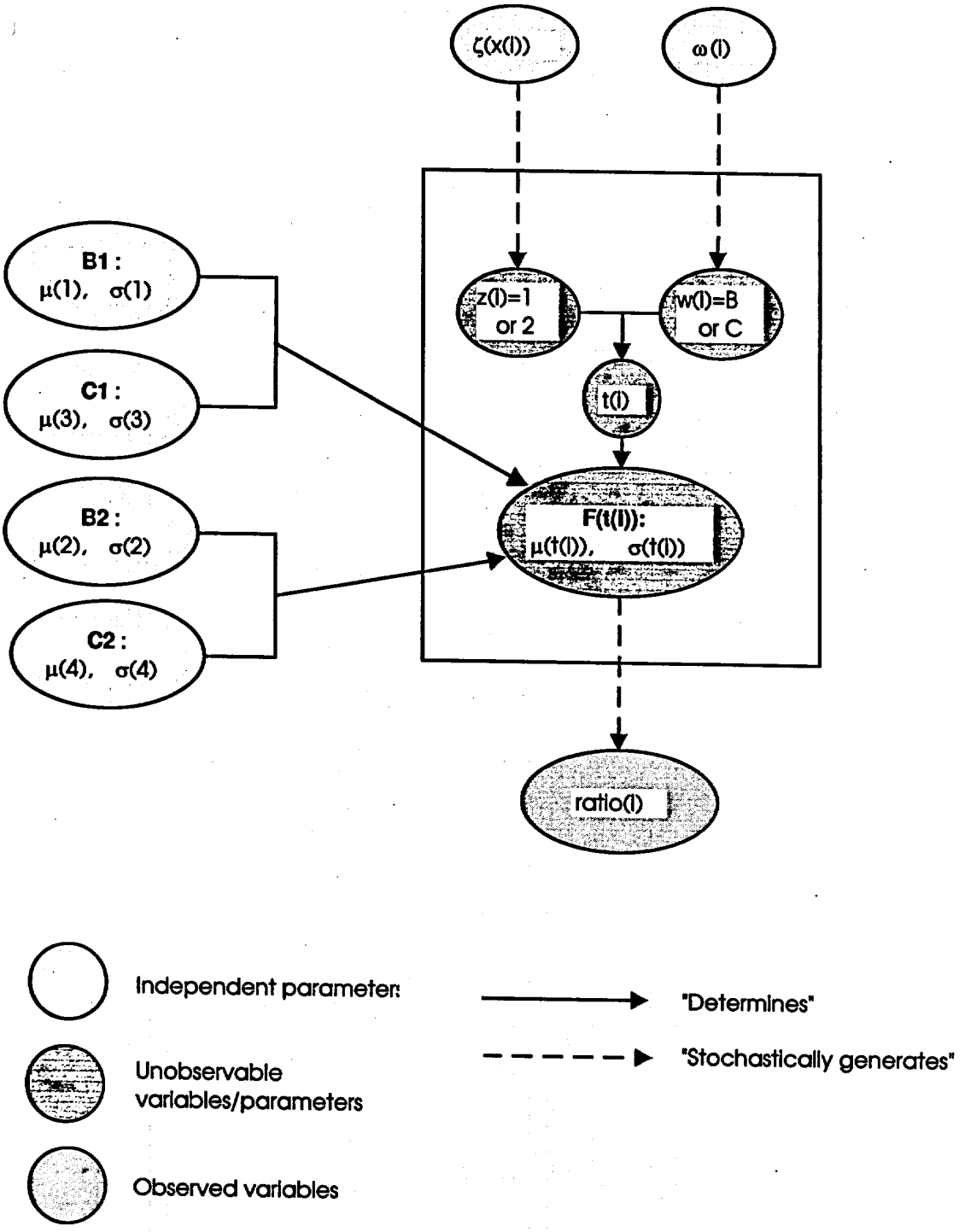

Figure A-3. Model 2, a four-component mixture model for the $^{36}Cl/Cl$ ratio data with spatially varying parameters

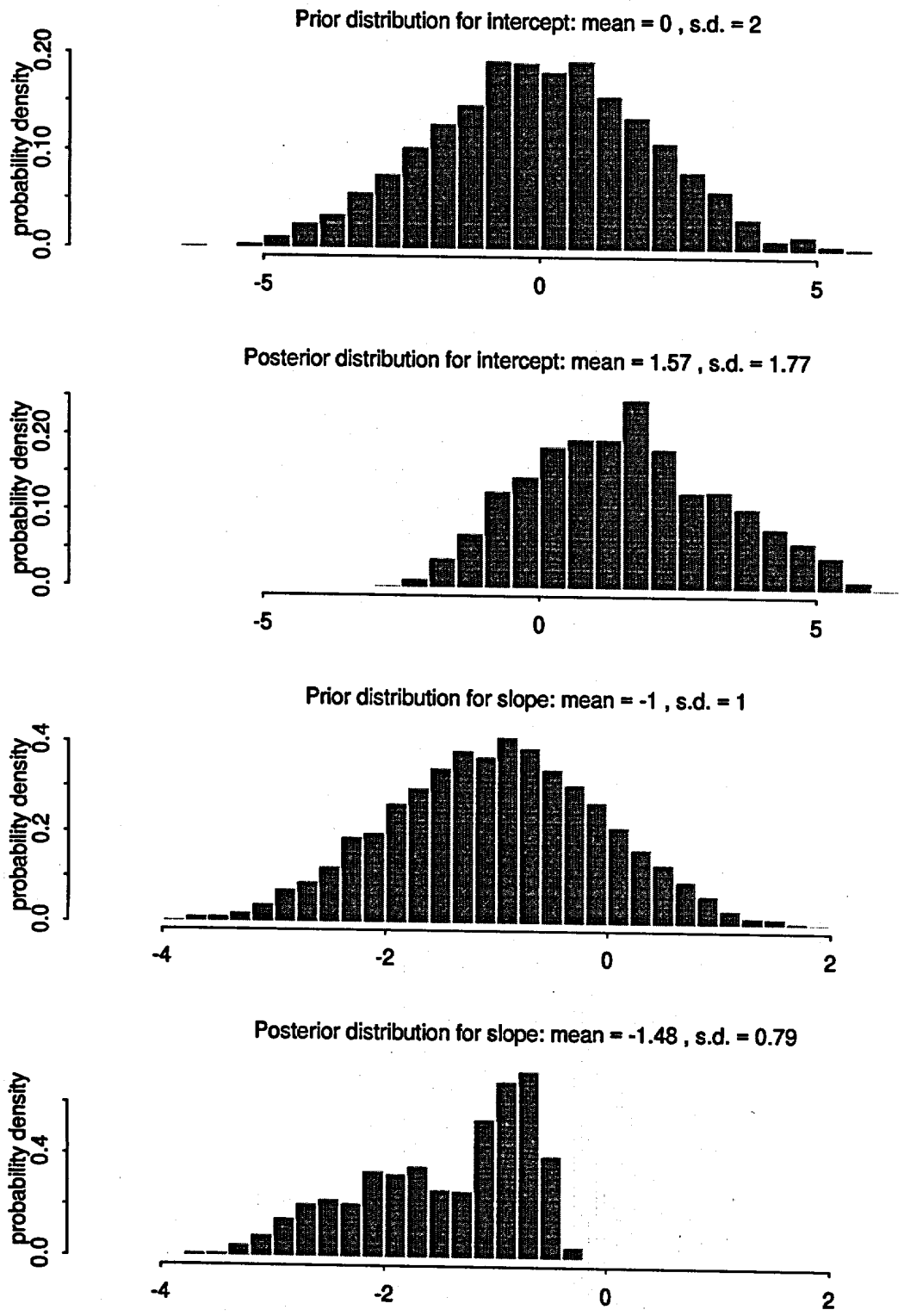

Figure A-5. Prior and posterior means for coefficients of PTn thickness in Model 3(PTn)

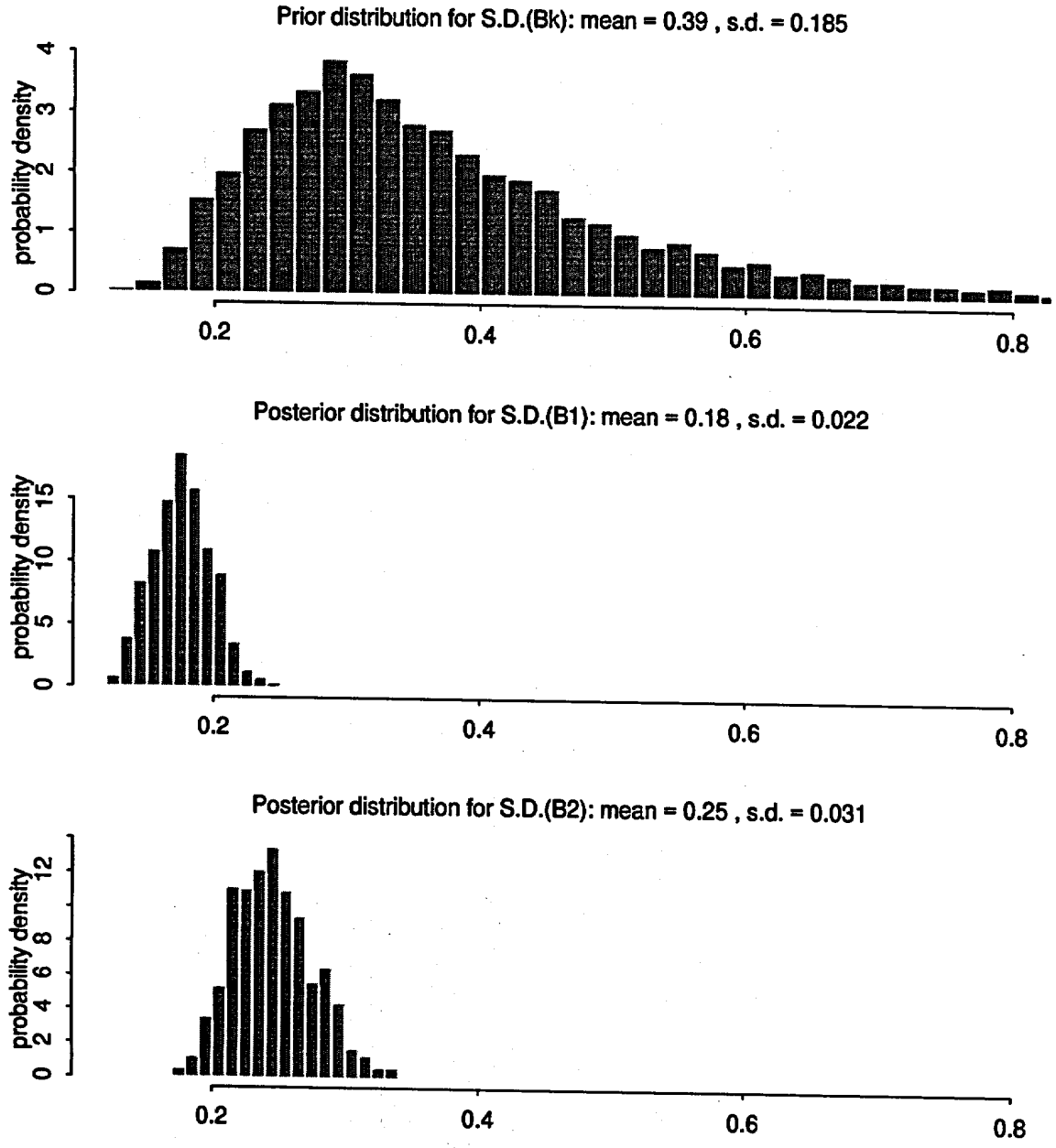

Figure A-7. Prior and posterior means for log-standard deviations of two background distributions in Model 3(PTn)

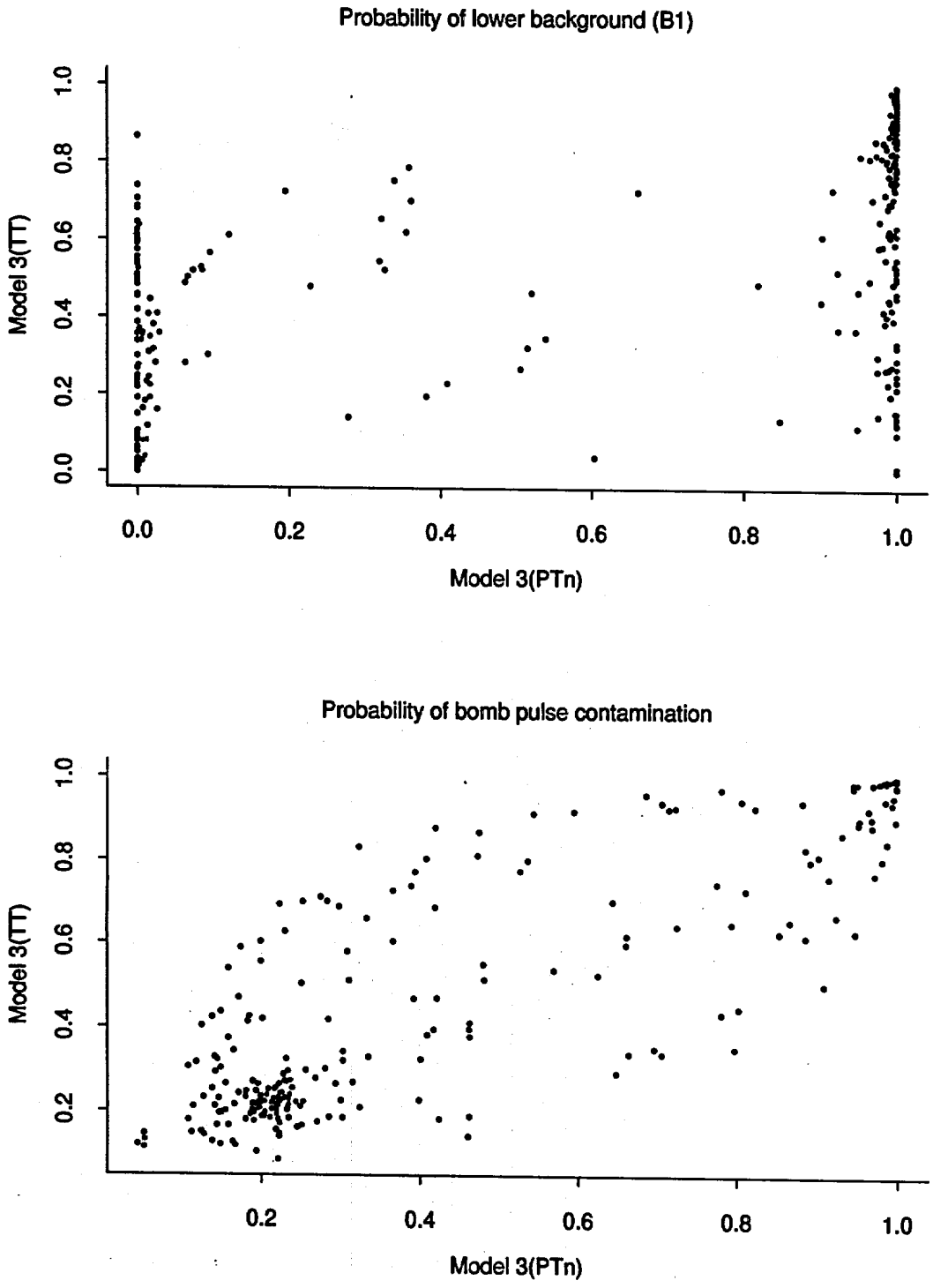

Figure A-9. Comparison of background and bomb pulse probabilities estimated by Models 3(PTn) and 3(TT)

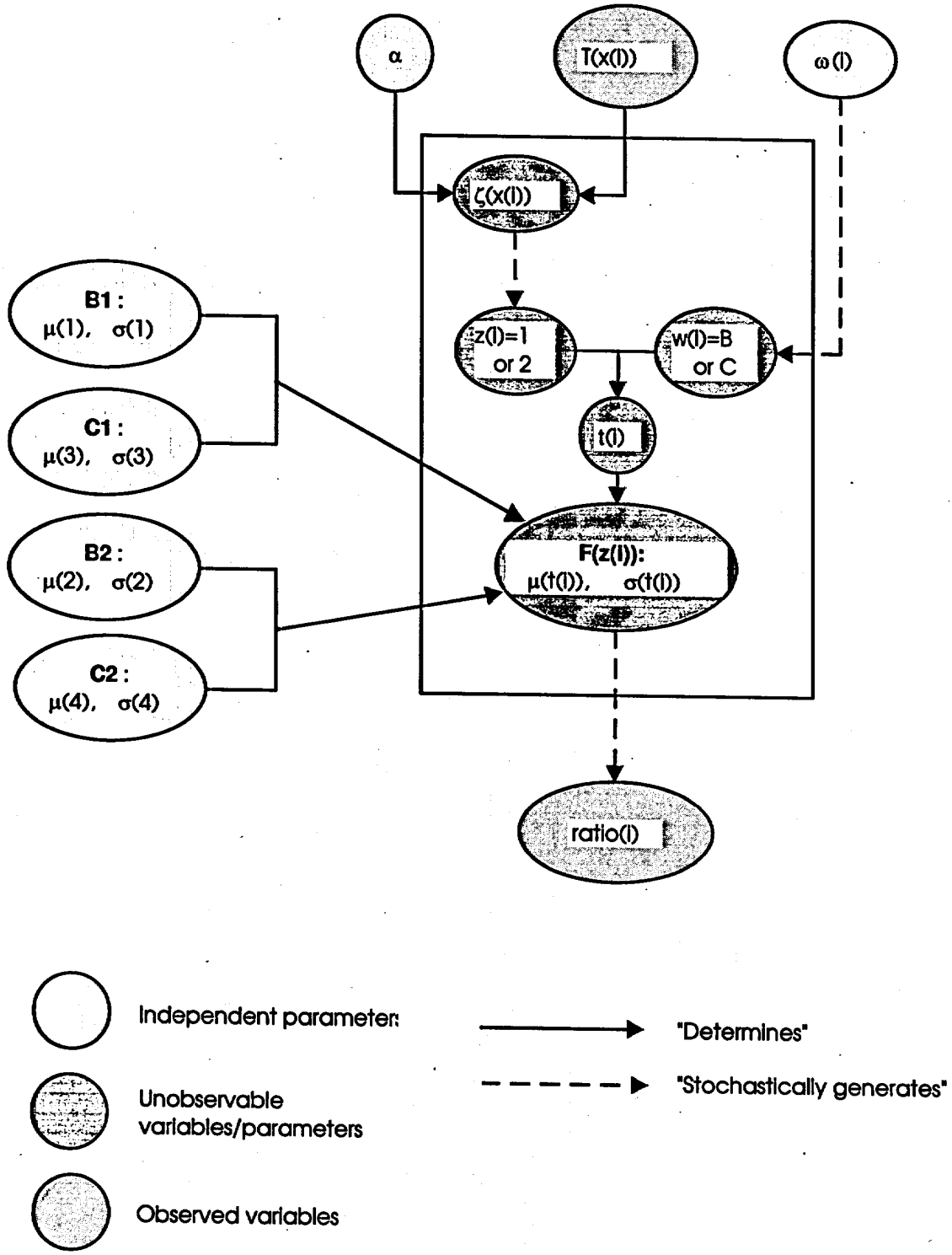

Figure A-4. Model 3, a four-component mixture model in which $\zeta(x)$ is a function of a covariate

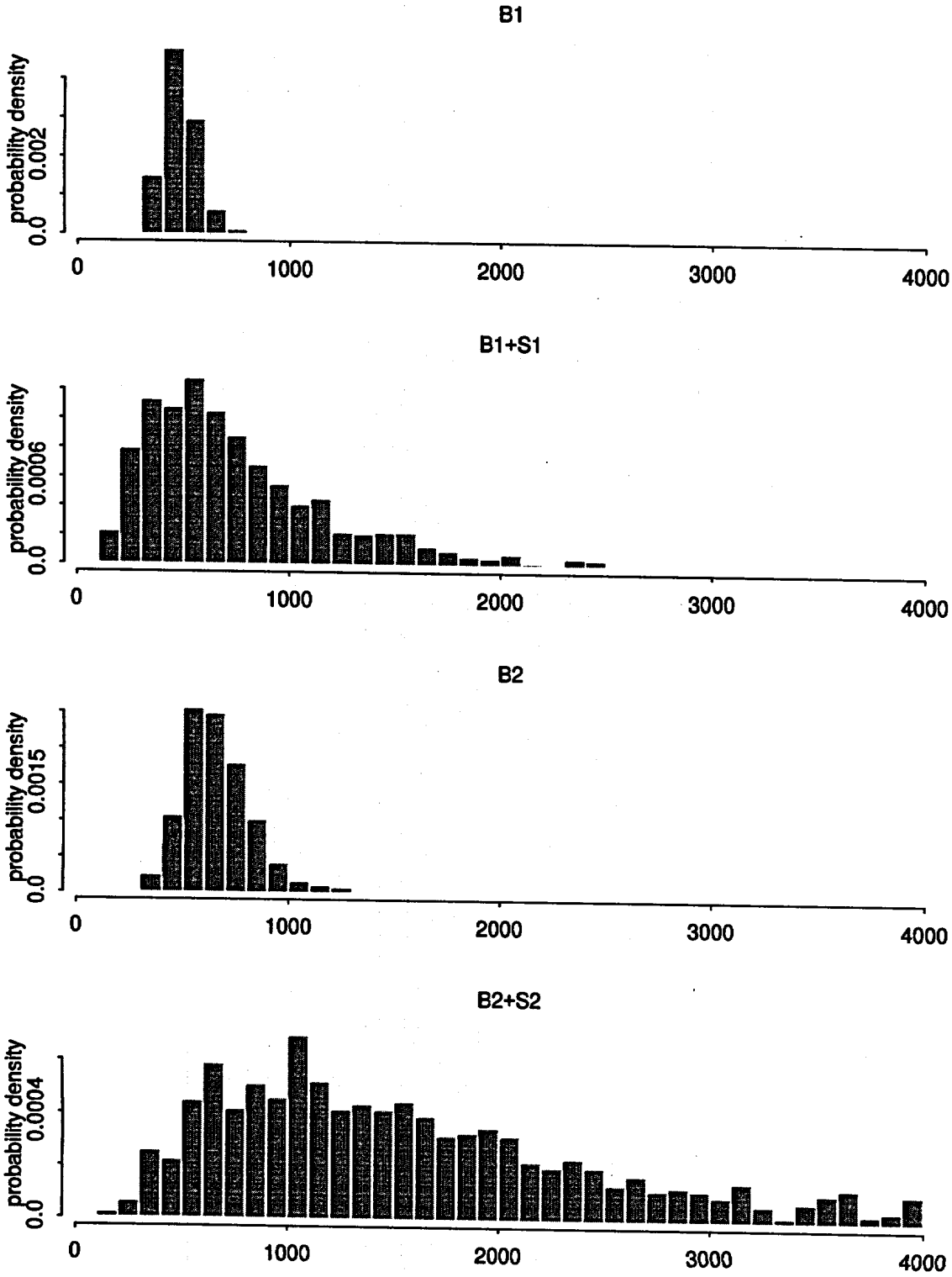

Figure A-8. Samples from the four component distributions of Model 3(PTn)

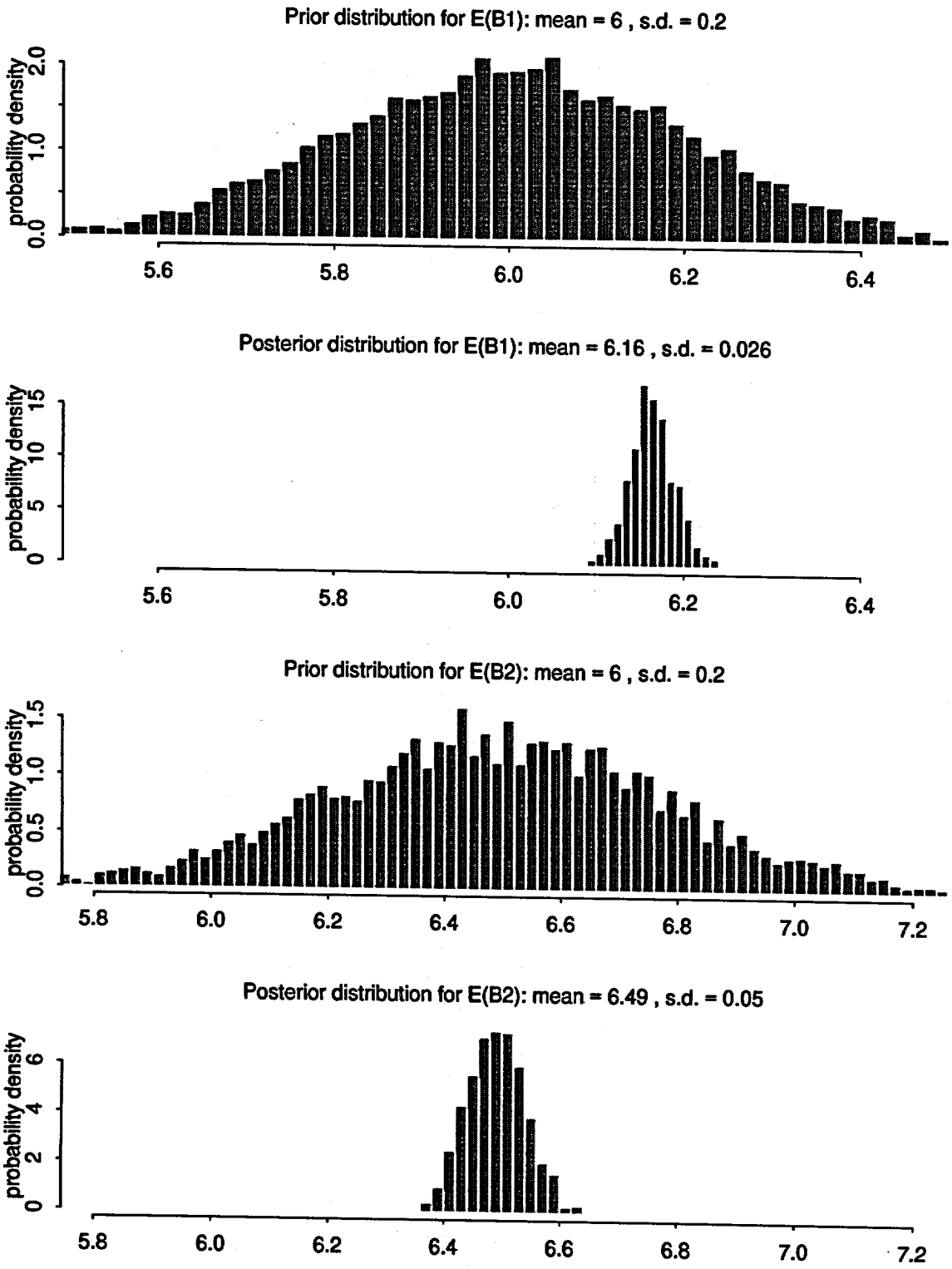

Figure A-6. Prior and posterior means for log-means of two background distributions in Model 3(PTn)

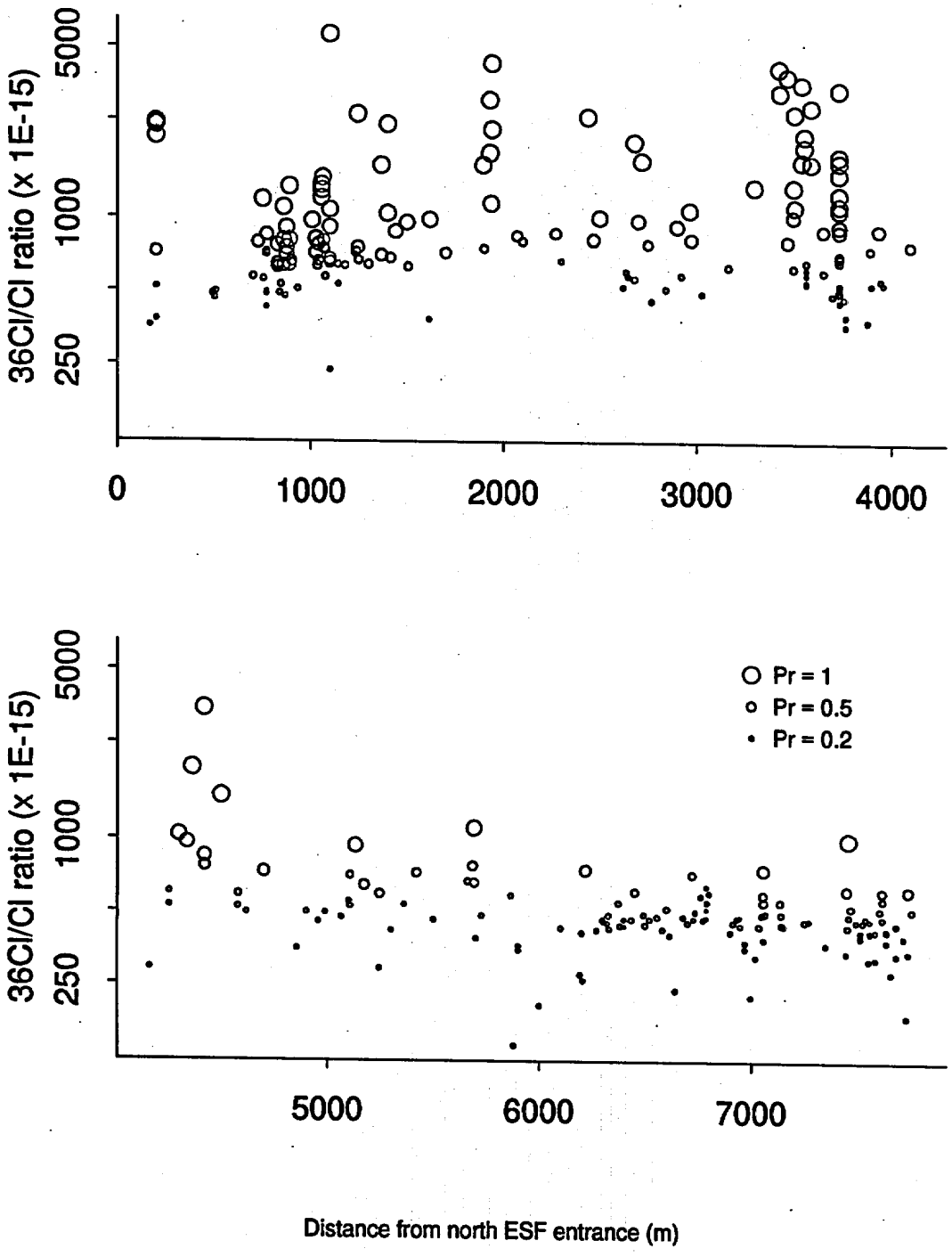

Figure A-10. Probability classification of $^{36}Cl/Cl$ ratio data using Model 3(TT)

APPENDIX B

Q STATUS AND DATA TRACEABILITY OF DATA CITED IN THIS REPORT

DTN or YMP Notebook Identifier*	Title of Data Package	Location in report
LAJF831222AQ98.003	Chloride, bromide, sulfate and chlorine-36 analyses of construction water	Table 7-1 Section 7.2.1
LAJF831222AQ98.004	Chloride, bromide, sulfate and chlorine-36 analyses of salts leached from ESF rock samples	Table 3-1 Table 3-2 Figure 3-1 Section 3.4.2
LAJF831222AQ98.005	Chloride, bromide, sulfate and chlorine-36 analyses of soils collected above the ESF South Ramp	Table 3-5 Section 3.4.3
LAJF831222AQ98.006	Chloride, bromide and sulfate analyses of salts leached from USW WT-24 drillcore	Table 9-2 Section 9.2
LAJF831222AQ98.007	Chloride, bromide and sulfate analyses of salts leached from ECRB-CWAT#1, #2 and #3 drillcore	Figure 7-2 Figure 7-3 Section 7.2.2
LAJF831222AQ98.008	Chloride, bromide and sulfate analyses of salts leached from ECRB-CS, ECRB-TZ#1 and ECRB-TZ#2 drillcore	Table 7-2 Section 7.2.5
LAJF831222AQ98.009	Chlorine-36 analyses of salts leached from ESF Niche 3566 (Niche #1) drillcore	Table 3-4 Section 3.4.2
LAJF831222AQ98.010	Chloride, bromide, sulfate and chlorine-36 analyses of ESF porewaters	Table 2-1 Table 2-2 Fig. 2-2 to 2-6 Section 2.4, 2.5
LAJF831222AQ98.011	Chloride, bromide, sulfate and chlorine-36 analyses of springs, groundwater, porewater, perched water and surface runoff	Table 3-6 Tables 9-1, 9-3 Sections 3.4.3 and 9
LAJF831222AQ98.012	Chloride, bromide, sulfate and chlorine-36 analyses of seeps from the ESF Alcove #1 infiltration experiment	Table 8-1 Figure 8-2 Section 8
LAJF831222AN98.013	Chloride, bromide, sulfate and chlorine-36 analyses of groundwater from USW UZ-1, UE#25-p1, UE25 UZN#2 and USW VH-1	Table 9-1 Section 9
LAJF831222AQ98.014	Chloride, bromide, sulfate and chlorine-36 analyses of salts leached from ESF-NR-MOISTSTDY drillcore	Figure 7-4 Section 7.2.3

DTN or YMP Notebook Identifier*	Title of Data Package	Location in report
LAJF831222AQ98.015	Chloride, bromide and sulfate analyses of porewater extracted from ESF Niche 3566 (Niche #1) drillcore	Table 2-1 Sections 2.4, 2.5
LAJF831222AN98.016	Chloride, bromide and sulfate analyses of shotcrete from ESF Alcove #1	Section 8
LAJF831222AN98.017	Classification of ESF chlorine-36 samples by lithology, feature, and proximity to faults	Section 4
LASL831222AQ98.002	Mineralogic data for chlorine-36 studies	Section 6

* The designator 'AQ" contained as part of the DTN identifier indicates that the data were generated following YMP QA procedures, have been technically reviewed, and have been submitted to the Records Processing Center (RPC). The designator 'AN' indicates that the data were not generated following YMP QA procedures. For example, ONC#1 data were generated following YMP QA procedures but are considered non-Q for YMP purposes because this borehole was not drilled under YMP/QA procedures.

Traceability of the Solute Transport Code, FEHM

The code (FEHM) used to perform the transport calculations in section 8 has been certified in accordance with LANL YMP procedures. The Los Alamos software QA program is a rigorous, life-cycle-based approach in which QA and user documents are reviewed during each of the phases of development, including the requirements phase, the design phase, and the implementation phase. The following documents are available:

- Software Requirements Specifications,
- Models and Methods Summary,
- Software Design Document,
- Verification and Validation Plan and Procedures,
- Verification and Validation Report, and
- User's Manual.

APPENDIX C

DESCRIPTION OF MILESTONE COMPLETION CRITERIA FOR MILESTONE SP33DDM4 AND A SUMMARY OF THEIR LOCATION FOR THE U.S. DEPARTMENT OF ENERGY

Criteria	Text, table or figure location
Include new porewater chemistry data and chlorine-36 data collected between 9/1/97 and 8/31/98 from the ESF and E-W Drift and their associated niches, alcoves and boreholes, as well as from surface-based boreholes.	Sections 2.4, 3.4, 7.2, 8, 9 Tables 2-1, 2-2, 3-1 to 3-4, 7-2, 8-1, 9-1 to 9-3 Figures 2-3 to 2-6, 3-1, 3-2, 7-2, 7-4, 8-1
Characterize 36Cl and Cl porewater sample locations with respect to lithology, mineralogy, and structural settings	Sections 4 and 6 Tables 2-1, 3-2, 3-3, 3-4
Summarize results of statistical and qualitative trend analyses to assess these data in terms of identification of fast paths and stagnant zones, correlation of signals with structural features and surface infiltration patterns, and comparison with other environmental tracers.	Section 4
Evaluate 36Cl and porewater Cl results with respect to UZ flow and transport process models, including consistency of the tracer data with hydrologic properties, fracture-matrix interactions, flow paths and solute transport rates in the nonwelded and welded units, and structural controls on flow paths.	Section 5
Compare data from the EW Drift to the predicted distributions from the EW Drift Predictive Report, and discuss the implications for the validity of existing conceptual models the distribution of fast paths, fracture/matrix interactions, and travel times.	Section 5
Evaluate the implications of data from the ESF and EW Drift for: (a) the influence of construction water on the quality of geochemical or isotopic data, and (b) the extent to which the current geochemical and isotopic data base for samples acquired from subsurface samples is representative of repository block conditions.	Sections 2.4, 5, 7, 10
This deliverable will be prepared in accordance with OCRWM approved quality assurance procedures implementing requirements of the QARD.	Entire document

Verification of technical data submittal compliance will be demonstrated by including as part of the deliverable: 1) a copy of the Technical Data Information Form generated identifying the data in the Automated Technical Data Tracking System, and 2) a copy of the transmittal letter attached to the technical data transmittal to the GENISES Administrator. Record accession numbers and Automated Tracking numbers will be included, as appropriate, for all data used and/or cited in this deliverable.	Verification of technical data submittal has been included with the transmittal letter for this report. Record accession numbers are indicated in the Reference list.